

Kinetics of the chiral phase transition in a quark-meson σ -model

Alex Meistrenko^a, Hendrik van Hees^a, Carsten Greiner^a

^a*Institut für Theoretische Physik, Goethe-Universität Frankfurt am Main, Max-von-Laue-Straße 1, D-60438 Frankfurt am Main, Germany*

Abstract

In this study an effective description in the 2PI effective-action formalism for systems of quarks and mesons in and out of equilibrium within a numerical approach is developed, allowing to approximate the complexity of QCD by taking only the lightest and most relevant degrees of freedom into account. In particular the temporarily building up of fluctuations of the net-baryon number encoded by the fourth-order cumulant (or the rescaled kurtosis) for lower momenta is being demonstrated when the phase transition occurs near the critical point, or even stronger when the phase transition is of first order, although the initial system is prepared with purely Gaussian fluctuations in the net baryon number. This is the result of the evolving slow and critical order parameter, i.e., the σ -field. On the other hand, depending on the speed of the (Hubble-)expansion scale, the final dissipative evolution due to the collisions among the mesons, the quarks and anti-quarks and the order field weakens the final fluctuations considerably.

Keywords: off-equilibrium dynamics, heavy-ion collisions, baryon-number fluctuations

1. Introduction

The experimental approach for studying fundamental properties of quantum chromodynamics (QCD) is based on heavy ion physics at relativistic energies, requiring large accelerating facilities like the Conseil Européen pour la Recherche Nucléaire (CERN) and the Relativistic Heavy Ion Collider (RHIC) as well as much smaller but more specialized facilities like the Gesellschaft für Schwerionenforschung (GSI), the Facility for Antiproton and Ion Research (FAIR) as well as the Nuclotron-based Ion Collider fAcility (NICA), where highly ionized atoms are accelerated to almost the speed of light. Nowadays, it is well-established, that there exists a numerous number of different phases within QCD, which are characterized by different effective degrees of freedom. Besides the hadronic phase, there is a second highly prominent phase, known as the quark gluon plasma (QGP) [1], denoting a quasi-free state of quarks and gluons at high energy and/or particle densities several times higher compared to the usual values of nuclear matter. The existence of a QGP can be expected in the inner core of neutron stars as well as in the early Universe during the first few μs after the Big Bang. However, those conditions are not accessible for experimental physics. The only possible way of studying QGP properties on Earth is encoded into the dynamical evolution of an expanding fireball created in a heavy-ion collision as described before, suggesting that the created medium of quarks and gluons exists only for a very short period of time $\Delta t \approx 10 \text{ fm}/c \sim 10^{-23} \text{ s}$.

For small values of the chemical potential μ_B it has been found within lattice QCD, that there is a smooth crossover between the quark-gluon plasma and the hadronic phase at a relatively high temperature of $T_c \approx 155 \text{ MeV}$ [2, 3], resulting in the limit of vanishing light-quark masses in a second-order phase transition with $O(4)$ as the underlying universality class. Depending on the quark masses one expects different orders of phase transitions for strongly interacting matter (see e.g. Ref. [4]). However, the connection between the most interesting symmetry groups, being responsible for deconfinement and chiral symmetry restoration, remains a subject of study. Based on effective models like the Nambu-Jona-Lasinio (NJL), quark-meson (QM) model with constituent quarks [5, 6, 7, 8] and their Polyakov-loop extended versions (PNJL), (PQM) [9, 10, 11, 12] as well as universality arguments, for high values of the baryon chemical potential one expects a first-order chiral phase transition, ending in a critical point of second

Email addresses: alex.meistrenko@googlemail.com (Alex Meistrenko), hees@itp.uni-frankfurt.de (Hendrik van Hees), Carsten.Greiner@th.physik.uni-frankfurt.de (Carsten Greiner)

order [13, 14, 15, 16]. The exploration of the QCD phase diagram is one of the most important goals for relativistic heavy-ion experiments.

In the vicinity of a critical point the relaxation time diverges, due to growing correlation lengths, leading probably to a phase transition out of equilibrium. Assuming then a static medium in a stationary condition of equilibrium could be a crude and insufficient approximation, resulting in overestimated or significantly false predictions in case of most promising observables [17]. Even a first-order boundary with a coexistence of two different phases could require a non-equilibrium description, when the system is driven out of the equilibrium state during the evolution process of a heavy-ion collision. Furthermore, a heavy-ion collision forms a finite volume of the medium, expanding rapidly in time and thus leading to a limited formation of long-range correlations. In detail, the size of correlated domains cannot significantly exceed a scale of $\xi \sim 5$ fm, comparable with the initial radius of a heavy-ion collision.

Consequently, those effects could drastically modify predicted observables for the phase transition, which have been derived from thermodynamic quantities. Such observables of interest are mainly the cumulants and cumulant ratios of conserved quantities [18, 19], which are directly related to thermodynamic susceptibilities via the correlation length of the system [20, 21, 22]. The net-baryon number as well as the net-charge number are the most prominent and promising examples of conserved quantities. A recent calculation shows the behaviour of fluctuations encoded in cumulant ratios for the net-quark (respectively net-baryon) number within a functional renormalization group (FRG) approach (see Refs. [23, 24, 25]) of a Polyakov-loop extended quark-meson model [26]. In particular, the results show a critical behavior of higher-order cumulant ratios¹ for several choices of the quark chemical potential to temperature μ_q/T , standing for linear trajectories in the T - μ_q plane. Analogously, different choices of the ratio between the entropy and the net-quark density refer to non-linear trajectories in the T - μ_q plane, being more related to the expansion process in a heavy-ion collision. The ratio $R_{4,2} = c_4/c_2 \equiv \kappa\sigma_{q,\text{net}}^2$ for generalized susceptibilities (see Ref. [26] for scaling behavior at finite chemical potential),

$$c_n(T) = \frac{\partial^n [p(T, \mu_q)/T^4]}{\partial (\mu_q/T)^n},$$

$$c_1 = \frac{N_{q,\text{net}}}{VT^3}, \quad c_2 = \frac{1}{VT^3} \left\langle \left(N_{q,\text{net}} - \langle N_{q,\text{net}} \rangle \right)^2 \right\rangle \equiv \frac{1}{VT^3} \sigma_{q,\text{net}}^2,$$

$$c_3 = \frac{1}{VT^3} \left\langle \left(N_{q,\text{net}} - \langle N_{q,\text{net}} \rangle \right)^3 \right\rangle, \quad c_4 = \frac{1}{VT^3} \left[\left\langle \left(N_{q,\text{net}} - \langle N_{q,\text{net}} \rangle \right)^4 \right\rangle - 3\sigma_{q,\text{net}}^4 \right],$$

shows an oscillatory behavior and changes its sign below a certain value of the temperature, denoted with T_c in the following. Thereby, different choices for μ_q/T refer to different and experimentally accessible center-of-mass energies, motivating the energy-beam scan at RHIC. Similar studies of cumulants are also known from lattice-QCD calculations, where due to the sign problem of fermions in MC-based path-integral formulations a Taylor expansion in powers of the thermodynamic potential² is required to compute cumulants of conserved quantities for non-vanishing chemical potentials. Thereby, one introduces thermodynamic bulk quantities (i.e., pressure, energy and entropy densities), which depend on the chemical potentials of baryon number, strangeness and electric charge³ (see [2, 27, 28] and references therein).

An experimental confirmation of the critical point would be crucial to understand fundamental properties of QCD in form of the present symmetries. Furthermore, it would significantly help to confirm and improve effective models. Following that, from first experimental data it seems to be unlikely that the critical point can be found below $\mu_B \equiv 3\mu_q \sim 200$ MeV [29], being in full agreement with lattice-QCD calculations. More interesting are the net-proton number fluctuations⁴ in terms of cumulants, skewness and kurtosis as presented by the STAR Collaboration at RHIC and summarized in [30]. The preliminary results on the fourth order cumulant ratio, encoded in terms of the rescaled kurtosis $\kappa\sigma^2$, show a non-trivial dependence on the center-of-mass energy in central Au+Au collisions, which to date cannot be completely explained by established transport models (see [31] and references therein), even though some

¹With increasing order of cumulants the dependence on the correlation length becomes more prominent.

²Note, that a Taylor expansion with a finite number of terms would break down in case of a critical point, requiring a careful analysis of the convergence radius.

³Often simple referred to as equation of state (EoS) with non-vanishing chemical potentials.

⁴Due to high statistics net-proton number fluctuations are used for estimating the overall net-baryon number fluctuations.

of the observed features are present in the quark-meson model of Ref. [26]. The remarkable drop of the rescaled kurtosis from ~ 1 to even negative values within the error bars with a subsequent increase of this observable for decreasing center of mass energies could indicate a critical point near a center of mass energy of $\sqrt{s_{NN}} = 20$ GeV.

Such a behavior is expected in a similar way for the order parameter σ in an effective description of QCD [32]. For the fourth-order cumulant $\kappa_4(\sigma_V) := \langle (\delta\sigma_V)^4 \rangle - 3 \langle (\delta\sigma_V)^2 \rangle^2$, where σ_V denotes the volume-averaged order parameter for the zero mode $\sigma_V = \int d^3 \vec{x} \sigma(x)$ and $(\delta\sigma_V)^n$ stands for the centralized moment of order n . Here, the cumulant of fourth order is calculated as a function of the Ising parameters $t = (T - T_c)/T_c$ (reduced temperature) and H (magnetic field), which can be analytically mapped to the relevant parameters T and μ_B of the QCD phase diagram. This calculation requires a specification of the universal equation of state around the critical point [32]. The analysis shows that the fourth-order cumulant is negative along the crossover line with $t > 0$ and strongly positive in the region of the first-order phase transition $t < 0$ for all values of $H \neq 0$. Qualitatively, this can be understood by considering the probability distribution of the volume-averaged order parameter σ_V , having a Gaussian distribution in the crossover region (negative kurtosis), which is a direct consequence of the central limit theorem. With decreasing t the Gaussian distribution function develops to a broader probability distribution alongside with a further decrease of the kurtosis. Below $t = 0$ the probability distribution of σ_V has a two-peak structure in the mixed phase of the first order, resulting for $t < 0$ in a positive kurtosis around the dominant peak for all values of $H \neq 0$.

The density plot for the cumulant κ_4 of the volume averaged order parameter σ_V can be transformed in a similar behavior of the cumulants of conserved quantities, which can be motivated by considering for instance the fluctuation of the proton distribution function due to fluctuations of the order parameter and pure statistical fluctuations around the equilibrium distribution function f_p^{eq} :

$$\delta f_p = \delta f_p^{\text{stat}} + \frac{\partial f_p^{\text{eq}}}{\partial m} g \delta \sigma,$$

where the second term follows from the mass relation $m = g\sigma$ with g denoting the coupling constant of the linear σ model. Integrating over the phase space results in

$$\delta N_p = \delta N_p^{\text{stat}} + \delta \sigma_V g d \int \frac{d^3 \vec{p}}{(2\pi)^3} \frac{\partial f_p^{\text{eq}}}{\partial m}$$

with d denoting the degeneracy factor. Assuming that δN_p^{stat} and $\delta \sigma_V$ are stochastically independent variables and focusing on most singular terms near the critical point, leads to the following expression:

$$\begin{aligned} \kappa_4(N_p) &= \kappa_4(N_p^{\text{stat}}) + \kappa_4(\sigma_V) \left(g d \int \frac{d^3 \vec{p}}{(2\pi)^3} \frac{\partial f_p^{\text{eq}}}{\partial m} \right)^4 + \dots \\ &= \langle N_p \rangle + \kappa_4(\sigma_V) \left(\frac{g d}{T} \int \frac{d^3 \vec{p}}{(2\pi)^3} \frac{\partial E_p}{\partial m} f_p^{\text{eq}} \right)^4 + \dots, \end{aligned}$$

where E_p denotes the dispersion relation and the last equality follows from the reasonable assumption of Poisson statistics for δN_p^{stat} . Following that, a negative value of $\kappa_4(\sigma_V)$ leads to a reduction of the corresponding fourth-order cumulant of the proton distribution function in comparison to the Poisson value $\langle N_p \rangle$ (analogously for net protons), leading to an effective mechanism for the experimentally observed behavior with a significant deviation from the cumulants of the expected Skellam distribution function for net-protons.

For a discovery of the QCD critical point it is crucial to develop dynamical models for fluctuations of the net-baryon number that can be embedded in simulations of heavy-ion collisions: Recently it has been emphasized that the relation of the higher-order cumulants being proportional to some higher power in the correlation length being valid at ideal thermodynamical equilibrium close to the critical point can not truly be established in a non-equilibrium situation envisaged in relativistic heavy ion collisions. The diffusion of the conserved net-baryon number is typically understood by elastic collisions of the quarks or protons, whereas the order parameter and thus the potential onset of correlated domains obeys a generalized wave equation [17]. The crucial step is thus to develop a nonequilibrium description of transport equations of the quarks and the coupled chiral fields in order to learn and understand the possible formation of (critical) fluctuations in the net-baryon number and thus the build up of higher order cumulants.

In addition, it requires improved theoretical, dynamical predictions and experiments with highly increased statistics to measure the overall net-baryon fluctuations and to exclude also possible technical issues, concerning, for instance, a limited detector acceptance. Last but not least, also physical effects due to finite-volume fluctuations have to be taken into account carefully.

With all this said, the central point of this paper is an effective description of the chiral phase transition by means of the quark-meson model, resulting from an approximate realization of the chiral symmetry. Thereby, the chiral phase transition is studied for systems of quarks and mesons in and out of equilibrium within a numerical approach of the coupled transport and wave equations. We are interested in investigating critical phenomena at the phase transition and the critical point, where time-dependent long-range correlations can arise. In particular, this work focuses on the restoration of the chiral symmetry within the linear σ model with constituent quarks. Its first-order phase transition ends in a critical point of second order, and non-equilibrium effects near the phase transition can significantly modify the critical behavior, such as the fluctuation of the net-baryon number (density), being the most important observable for the phase transition in this model.

The paper is organized as follows: We will start our discussion in Sect. 2 with some fundamental properties of QCD, focusing on the restoration of the chiral symmetry in a quark-meson model at high temperatures, based on the motivation described in Ref. [33]. In Sect. 3 we derive a set of coupled evolution equations by considering a particular truncation and approximate scheme of the underlying 2PI effective quantum action⁵. Therefore, we review main aspects of the so-called real-time Schwinger-Keldysh formalism and focus on the importance of the interaction between soft and hard modes, encoded in a dissipation kernel. After applying reasonable approximations to the effective quantum action and discussing thermodynamic properties of the effective thermodynamic potential as well as effective mass terms, neglecting divergent vacuum contributions, we end up with a set of coupled kinetic Boltzmann-type and dissipative mean-field (wave-type) equations for the interactions among the quarks, the mesons and the chiral fields.

Finally, within this full approach with mean-field and transport equations we show the dynamical study of the chiral phase transition in Sect. 4, where the equations of motion are modified to include an expanding three-dimensional Hubble-geometry for homogeneous and isotropic systems. Here, the cumulants and cumulant ratios of the net-quark number are considered with respect to different momentum bins and different initial truly Gaussian configurations of the net-quark number in large sets of independent runs, allowing to study a time-dependent evolution of cumulants in expanding systems.

To keep the main text readable, more detailed calculations are performed in the appendix.

2. Chiral effective model of QCD

Within the Standard Model of elementary particle physics the strong interaction is described by Quantum Chromodynamics (QCD), which is a gauge theory based on the “color gauge group” $SU(3)_c$. It describes the strong interaction between quarks, anti-quarks, and gluons. One important feature of the theory is that the running gauge coupling of the theory is small at high energy scales (“asymptotic freedom”) and large at low energy scales and thus perturbative methods become invalid in the low-energy range.

Phenomenologically the observed asymptotic free states of the theory are not quarks and gluons but rather hadrons, i.e., bound states of three quarks (baryons) or quark-antiquark pairs (mesons). Correspondingly the absence of observable states carrying color is known as the confinement of quarks and gluons within color-neutral bound states. Thus at low energies it is desirable to develop effective field theories describing hadrons.

A guiding principle for the formulation of such effective models are the symmetries of the QCD Lagrangian [36],

$$\mathcal{L} = -\frac{1}{4}F_{\mu\nu}^a F^{a\mu\nu} + \bar{\psi}(i\not{D} - \hat{M})\psi. \quad (1)$$

⁵A more phenomenological study, motivated by the Langevin equation, is discussed in Ref. [34], where a novel statistical approach for the scattering effects between quarks as quasi particles and mean fields is introduced. Very recently a similar representation of the 2PI of the quark-meson model is given in [35]. Here the full Kadonoff-Baym evolution equations are derived and solved for a static, non-equilibrium situation in the crossover at net baryon density being zero and to demonstrate the appearance of full thermal equilibrium and spectral properties of the mesons and quarks.

Here the fields $\psi \equiv \psi_{ia}$ are Dirac fields for the 6 quark flavors i (up, down, charm, strange, top, and bottom) and 3 colors a . The mass matrix $M = \text{diag}(m_u, m_d, m_c, m_s, m_t, m_b)$ acts in flavor space.

The $SU_c(3)$ gluon field $A^\mu = T^a A^{a\mu}$ with the hermitean matrices $T^a = \lambda^a/2$ (λ^a : Gell-Mann matrices) acting in color space define the covariant derivative,

$$D_\mu = \partial_\mu - igA_\mu. \quad (2)$$

The field-strength tensor $F_{\mu\nu}$ is defined by

$$F_{\mu\nu}^a = \partial_\mu A_\nu^a - \partial_\nu A_\mu^a - gf^{abc}A_\mu^a A_\nu^b. \quad (3)$$

In the light-quark sector (up and down quarks) the most important symmetry in the context of effective hadronic theories is the chiral symmetry in the limit of massless light quarks. The assumption of this approximate symmetry is justified by the observation that the ‘‘current masses’’ of the light up- and down-quarks are around a few MeV, which is small compared to a typical hadronic mass scale of around 1 GeV and can thus be treated as a perturbation. Since from now on we are interested only in the lightest quarks, we understand that the flavor index runs only over $i \in \{\text{up, down}\}$.

As it turns out, besides the weak explicit breaking of the chiral symmetry the symmetry is also explicitly broken by the formation of a non-vanishing quark condensate, i.e., the vacuum-expectation value $\langle 0|\bar{\psi}\psi|0\rangle \neq 0$. This leads to the spontaneous breaking of the $SU(2)_L \times SU(2)_R$ chiral symmetry (acting on the left- and right-handed parts, $\psi_{R/L} = (1 \pm \gamma_5)/2\psi$ of the doublet formed by the up- and down-quark fields) to the approximate isospin symmetry $SU(2)_V$ with the up- and down-quark fields transforming as a doublet under this transformation. At the hadronic level the spontaneous breaking of the chiral symmetry manifests itself in the mass splitting between chiral-partner hadrons as well as the presence of the very light pions, which are considered to be (pseudo-)Goldstone bosons of the spontaneously broken symmetry.

As detailed in the Introduction in the following we are interested in the understanding of the phase transition from the deconfined phase of strongly interacting matter, where at high temperatures and/or net-baryon densities quark- and gluon-like quasiparticles rather than hadrons become the relevant degrees of freedom. As lattice-QCD calculations show, at vanishing net-baryon density, i.e., vanishing baryo-chemical potential $\mu_B = 0$, this transition is a cross-over transition occurring at a ‘‘pseudo-critical temperature’’ $T_c \simeq 155$ MeV. The deconfinement transition is characterized by a strong increase in the thermodynamical variables (energy density, entropy, pressure, etc.). In the same temperature region also the quark condensate drops quite rapidly to 0. As the order parameter of the approximate chiral symmetry this indicates the restoration of this symmetry.

In the following we thus use an effective chiral model, a linear- σ model with (constituent) quarks, σ -mesons and pions as a model to investigate the phase structure of strongly interacting matter. This model is then used, applying the real-time formalism of off-equilibrium quantum field theory, to derive a transport equation with the goal to study the dynamics of the chiral transition at various net-baryon densities for an expanding fireball of strongly interacting matter. Of particular interest in the context of heavy-ion collisions are the fluctuations of conserved charges like the net-baryon number or the electric charge as possible observables related to different types of phase transitions (cross-over, first-order, and second-order in the region of a critical endpoint of the first-order transition line in the phase diagram).

2.1. Chiral symmetry

In the following we denote by $\psi = (\psi_u, \psi_d)$ the iso-spinor for the up- and down-quarks with usual Dirac-spinor fields ψ_u and ψ_d , which we decompose into left- and right-handed parts,

$$\psi_L = \frac{1 - \gamma_5}{2}\psi, \quad \psi_R = \frac{1 + \gamma_5}{2}\psi. \quad (4)$$

In the limit of massless quarks, the QCD-Lagrangian is invariant under the chiral $SU(2)_L \times SU(2)_R$ symmetry, or equivalently under the vector and axialvector iso-spin transformations with Pauli matrices τ^k being the generators of

isospin rotations:

$$\begin{aligned}\Lambda_V &:= \exp\left(-i \frac{\vec{\tau} \cdot \vec{\theta}}{2}\right), \quad \psi \longrightarrow \left(1 - i \frac{\vec{\tau} \cdot \vec{\theta}}{2}\right)\psi, \quad \bar{\psi} \longrightarrow \bar{\psi} \left(1 + i \frac{\vec{\tau} \cdot \vec{\theta}}{2}\right), \\ \Lambda_A &:= \exp\left(-i \gamma_5 \frac{\vec{\tau} \cdot \vec{\theta}}{2}\right), \quad \psi \longrightarrow \left(1 - i \gamma_5 \frac{\vec{\tau} \cdot \vec{\theta}}{2}\right)\psi, \quad \bar{\psi} \longrightarrow \bar{\psi} \left(1 - i \gamma_5 \frac{\vec{\tau} \cdot \vec{\theta}}{2}\right).\end{aligned}\tag{5}$$

According to Nother's theorem these symmetries lead to the following conserved vector and axial-vector currents,

$$V_\mu^k = \bar{\chi} \gamma_\mu \frac{\tau^k}{2} \chi, \quad A_\mu^k = \bar{\chi} \gamma_\mu \gamma_5 \frac{\tau^k}{2} \chi.\tag{6}$$

The invariance with respect to vector and axial-vector transformations $SU_V(2) \times SU_A(2)$ is called chiral symmetry.

Introducing massive quarks breaks the axial-vector symmetry explicitly and therefore also the chiral symmetry, meaning that the axial-vector current A_μ^k is only partially conserved as can be directly seen by transforming the mass term of the Lagrangian $\mathcal{L}_m = -\bar{\psi} \hat{M} \psi$. With the quark-mass matrix in isospin space, $\hat{M} = \text{diag}(m_u, m_d)$. However, as mentioned before the masses of light quarks are small compared to Λ_{QCD} , therefore it is reasonable to assume that the chiral symmetry should be still a good candidate for an approximate symmetry with observable realization in nature.

Applying vector and axial-vector transformations to pseudo-scalar iso-vector pion-like states $\pi^k = i\bar{\psi} \tau^k \gamma_5 \psi$, forming the lightest mesons of QCD and the scalar iso-scalar $\sigma = i\bar{\psi} \psi$ -like state, leads to the following rotations in isospin-space⁶:

$$\begin{aligned}\Lambda_V : \quad \vec{\pi} &= i\bar{\psi} \vec{\tau} \gamma_5 \psi \longrightarrow i\bar{\psi} \vec{\tau} \gamma_5 \psi + \vec{\theta} \times (i\bar{\psi} \vec{\tau} \gamma_5 \psi) = \vec{\pi} + \vec{\theta} \times \vec{\pi}, \\ \Lambda_V : \quad \sigma &= i\bar{\psi} \psi \longrightarrow i\bar{\psi} \psi = \sigma, \\ \Lambda_A : \quad \vec{\pi} &= i\bar{\psi} \vec{\tau} \gamma_5 \psi \longrightarrow i\bar{\psi} \vec{\tau} \gamma_5 \psi + \vec{\theta} (i\bar{\psi} \psi) = \vec{\pi} + \vec{\theta} \sigma, \\ \Lambda_A : \quad \sigma &= i\bar{\psi} \psi \longrightarrow i\bar{\psi} \psi - i\vec{\theta} \cdot \bar{\psi} \gamma_5 \vec{\tau} \psi = \sigma - \vec{\theta} \cdot \vec{\pi}.\end{aligned}\tag{7}$$

Thus the vector and axial-vector transformations are realized as an $SO(4)$ symmetry on the fields $(\sigma, \vec{\pi})$. Analogous relations hold also for ρ - and a_1 -like states of QCD (see Ref. [37]). The rotations in isospin-space (7) explain the existence of the isospin triplet of pions with almost equal masses $m_\pi \sim 140$ MeV. However, it is not true for the σ -like state, which is believed to have a mass of about $m_\sigma \sim 500$ MeV based on experimental data [38].⁷ Consequently, the symmetry $SU_L(2) \times SU_R(2)$ is not realized in the real world and it seems unrealistic to explain the absolute values and the mass splitting of m_σ and m_{π^k} by taking only the explicit breaking of the chiral symmetry into account, since the quark masses $m_u \approx m_d$ are by two orders of magnitude smaller compared with the lightest mesons. The solution of this problem is the spontaneous breaking of chiral symmetry at low temperatures. For quantum chromodynamics the origin of the broken chiral symmetry is encoded in a finite value for the quark condensate in vacuum, which can be summarized in the so-called Gell-Mann-Oakes-Renner relation [39]:

$$-\langle 0 | m \bar{\psi} \psi | 0 \rangle = -\frac{m_u + m_d}{2} \langle 0 | \bar{\psi}_u \psi_u + \bar{\psi}_d \psi_d | 0 \rangle = m_\pi^2 f_\pi^2 \neq 0\tag{8}$$

with $f_\pi = 93$ MeV denoting the pion decay constant. This condensate dissolves with increasing temperature and the chiral symmetry becomes restored for $T \gtrsim 150$ MeV up to the explicit breaking of the chiral symmetry. Due to a σ -like structure of the quark condensate (8), it is reasonable to construct a mesonic model with σ being the order parameter of the chiral phase transition, which mimics the most important properties of the chiral symmetry in QCD as discussed in more detail in the following sections.⁸ Since m_u and m_d are both small one can assume

⁶The σ -meson is usually identified with the $f^0(500)$ -state.

⁷The vector mesons ρ and a_1 show also a huge mass gap of about 500 MeV. Naively, one would just expect that those vector mesons are degenerate states with equal masses.

⁸Note that extending the system of light quarks by the inclusion of the strange quark breaks the chiral symmetry significantly, explaining large mass splits for multiplets of more massive mesons in the real world. Consequently, beyond the low-energy limit the chiral symmetry loses its importance.

$m_u \simeq m_d$, which explains that the $SU_V(2)$ transformations is an approximate symmetry of the ground state. This explains the low mass of the pions, which in the chiral limit of massless quarks are the Nambu-Goldstone modes of the spontaneous chiral-symmetry breaking due to the formation of the quark condensate. In the mesonic description this implies that the σ -meson field provides also the order parameter of this spontaneous chiral-symmetry breaking, i.e., at low temperatures and densities $\langle 0|\sigma|0\rangle \neq 0$.

2.2. Effective description of spontaneously and explicitly broken chiral symmetry

We consider the $SO(N)$ -Lagrangian of a field theory with a field $\Phi = (\Phi_1, \dots, \Phi_N) \in \mathbb{R}^N$, including quadratic and quartic self-interactions,

$$\mathcal{L} = \frac{1}{2} (\partial_\mu \Phi) (\partial^\mu \Phi) + \frac{1}{2} \mu^2 \Phi^2 - \frac{\lambda}{4} (\Phi^2)^2. \quad (9)$$

From defining the last two terms as an effective potential

$$V := -\frac{1}{2} \mu^2 \Phi^2 + \frac{\lambda}{4} (\Phi^2)^2, \quad (10)$$

it becomes obvious, that the symmetry of the Lagrangian with the origin as global minimum can be broken for $\mu^2 > 0$, meaning that V has a minimum at $\Phi^2 \neq 0$,

$$\frac{\partial V}{\partial \Phi^2} = -\frac{1}{2} \mu^2 + \frac{\lambda}{2} \Phi^2 \stackrel{!}{=} 0 \quad \Rightarrow \quad \Phi_0^2 = \frac{\mu^2}{\lambda} =: v_0^2. \quad (11)$$

More precisely, there is an infinite number of possible minima with respect to different configurations of the components for the field Φ . The quantity v_0^2 is related to the length of the vector Φ_0 , which defines the global minimum of the potential V and denotes the degenerate ground states of the interacting system (9). By expanding the Lagrangian (9) around the global minimum it becomes⁹,

$$\mathcal{L} = \frac{1}{2} (\partial_\mu \Phi)^2 - \frac{\lambda}{4} (\Phi^2 - v_0^2)^2. \quad (12)$$

A certain realization for the global minimum is called spontaneous symmetry breaking in favor of a specified direction for the chiral field.

Switching to the $SO(4)$ linear sigma model the chiral field becomes $\Phi = (\sigma, \vec{\pi})$. Historically this model has been widely used to describe the chiral symmetry in the low-energy limit of hadron physics. Here, large values of nucleon mass require a mechanism for breaking the chiral symmetry without destroying the underlying chiral invariance of the Lagrangian. In case of the linear sigma model the spontaneous symmetry breaking concerns directly the σ -direction and can be achieved by setting the global minimum (11) in σ -direction. Consequently, the σ -component obtains a finite vacuum expectation value $\langle \sigma \rangle_0$, whereas the vacuum expectation values of pions vanish

$$\langle \sigma \rangle_0 = v_0 := f_\pi \quad \text{and} \quad \langle \vec{\pi} \rangle_0 = 0. \quad (13)$$

The $\vec{\pi}$ -direction is given by a rotation in the potential minimum around the origin. Due to a vanishing curvature in every partial direction of $\vec{\pi}$, one obtains well-known relations for the effective mass of sigma and pions

$$m_\sigma^2 := \left. \frac{\partial^2 V}{\partial \sigma^2} \right|_{\sigma=\langle \sigma \rangle_0, \pi=\langle \vec{\pi} \rangle_0} = 2\lambda f_\pi^2, \quad m_\pi^2 := \left. \frac{\partial^2 V}{\partial \pi^2} \right|_{\sigma=\langle \sigma \rangle_0, \pi=\langle \vec{\pi} \rangle_0} = 0, \quad (14)$$

with pions becoming massless modes as described by the Goldstone theorem [40].

By introducing a term linear in the σ -field component an explicit symmetry breaking can be taken into account. With identical vacuum expectation values from the previous calculation, one obtains the following relation for the

⁹Note that constant terms with respect to the chiral field do not change the physics, described by the Lagrangian.

parameter	value	description
λ	20	coupling constant for σ and $\vec{\pi}$
g	2 – 5	coupling constant between $\sigma, \vec{\pi}$ and ψ_i
f_π	93 MeV	pion decay constant
m_π	138 MeV	pion mass
v^2	$f_\pi^2 - m_\pi^2/\lambda$	field shift term
U_0	$m_\pi^4/(4\lambda) - f_\pi^2 m_\pi^2$	ground state

Table 1: Parameters of the quark-meson model with the Lagrangian (17).

ground state of the system:

$$\begin{aligned}
U &:= \frac{\lambda}{4} (\sigma^2 + \vec{\pi}^2 - v^2)^2 - h_q \sigma \quad \Rightarrow \quad v^2 = -\frac{h_q}{\lambda f_\pi} + f_\pi^2, \\
U_0 &:= U \Big|_{\substack{\sigma=\langle\sigma\rangle_0 \\ \pi=\langle\vec{\pi}\rangle_0}} = \frac{1}{4} \frac{h_q^2}{\lambda f_\pi^2} - h_q f_\pi.
\end{aligned} \tag{15}$$

Obviously, the parameters of the theory have to be specified by matching to observables, given here by the pion mass m_π and the pion decay constant f_π (see Tab. 1). The parameter h_q follows directly from the modified mass terms:

$$m_\sigma^2 := \frac{\partial^2 U}{\partial \sigma^2} \Big|_{\substack{\sigma=\langle\sigma\rangle_0 \\ \pi=\langle\vec{\pi}\rangle_0}} = 2\lambda f_\pi^2 + m_\pi^2, \quad m_\pi^2 := \frac{\partial^2 U}{\partial \pi^2} \Big|_{\pi=\langle\pi\rangle_0} = \frac{h_q}{f_\pi}. \tag{16}$$

Additionally, the linear sigma model can be extended to include constituent quarks for an effective description of the low-energy limit of QCD. This full version of the SO(4)-model [41] is suited for studying the chiral phase transition. Because of the spontaneously and explicitly broken chiral symmetry the mesonic part of this theory consists of a massive scalar σ field and three isoscalar pion fields (for a more detailed discussion see [37]). Now, the σ field represents the order parameter for the chiral phase transition and mimics the properties of the quark condensate in QCD from Sec. 2.1, since both transform equally under chiral transformation. Without explicit symmetry breaking an $SU_L(2) \times SU_R(2)$ symmetry transformation would let the full Lagrangian invariant:

$$\mathcal{L} = \sum_{i=1} \bar{\psi}_i [i\cancel{\partial} - g(\sigma + i\gamma_5 \vec{\pi} \cdot \vec{\tau})] \psi_i + \frac{1}{2} (\partial_\mu \sigma \partial^\mu \sigma + \partial_\mu \vec{\pi} \partial^\mu \vec{\pi}) - \frac{\lambda}{4} (\sigma^2 + \vec{\pi}^2 - v^2)^2 + f_\pi m_\pi^2 \sigma + U_0, \tag{17}$$

where $i \in \{u, d\}$. The field-shift term as well as the zero potential constant follow from (15) and (16), resulting in $v^2 = f_\pi^2 - m_\pi^2/\lambda$, $U_0 = m_\pi^4/(4\lambda) - f_\pi^2 m_\pi^2$. Thereby, all parameters (see also Tab. 1) are adjusted to match the vacuum values of the pion decay constant $f_\pi = 93$ MeV and the pion mass $m_\pi = 138$ MeV, leading to an estimated value for the sigma mass of $m_\sigma \approx 604$ MeV.

All discussed features of the model are shown schematically in Fig. 1 and Fig. 2 for the projections of the effective potential on one- as well as two-dimensional subspaces. Thereby, the symmetric potential denotes a configuration with a vanishing vacuum expectation value.

2.3. Semiclassical mean-field dynamics

The classical action is formulated with respect to the Lagrangian of the linear sigma model (17):

$$\begin{aligned}
S[\Phi, \bar{\psi}, \psi] &= \int d^4x \left[\sum_i \bar{\psi}_i [i\cancel{\partial} - g(\sigma + i\gamma_5 \vec{\pi} \cdot \vec{\tau})] \psi_i \right. \\
&\quad \left. + \frac{1}{2} (\partial_\mu \sigma \partial^\mu \sigma + \partial_\mu \vec{\pi} \partial^\mu \vec{\pi}) - \frac{\lambda}{4} (\sigma^2 + \vec{\pi}^2 - v^2)^2 + f_\pi m_\pi^2 \sigma + U_0 \right] \\
&:= S_0[\bar{\psi}, \psi] + S_I[\Phi, \bar{\psi}, \psi] + S_0[\Phi] + S_I[\Phi],
\end{aligned} \tag{18}$$

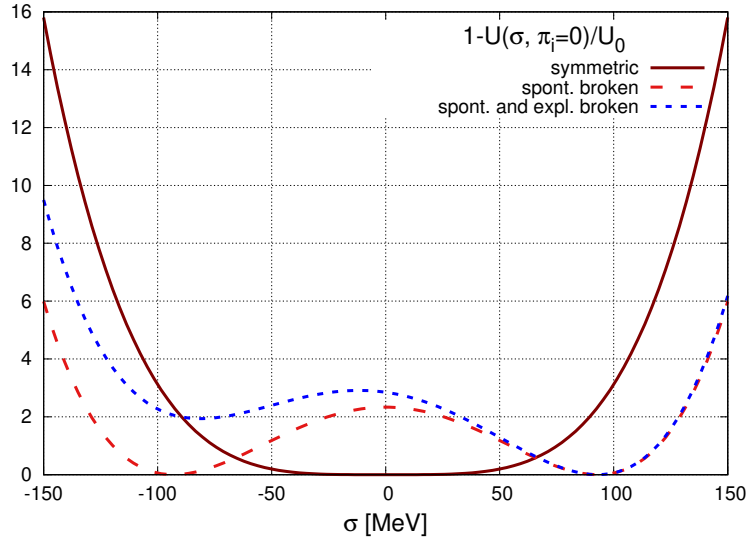


Figure 1: Effective potential of the linear sigma model for symmetric, spontaneously as well as explicitly broken chiral symmetry with respect to σ and $\pi_i = 0$.

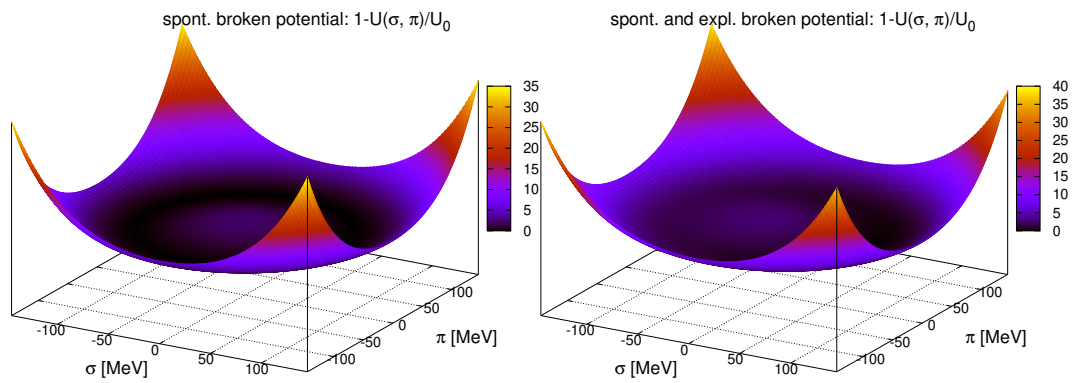


Figure 2: Effective potential of the linear sigma model for spontaneously as well as explicitly broken chiral symmetry with respect to σ and $\pi = |\vec{\pi}|$.

where the last line defines different contributions, given by the free fermionic and bosonic parts:

$$S_0[\bar{\psi}, \psi] = \int d^4x \left[\sum_i \bar{\psi}_i i \not{\partial} \psi_i \right], \quad S_0[\Phi] = \int d^4x \left[\frac{1}{2} (\partial_\mu \sigma \partial^\mu \sigma + \partial_\mu \vec{\pi} \partial^\mu \vec{\pi}) \right] \quad (19)$$

as well as the corresponding interaction parts:

$$S_I[\Phi, \bar{\psi}, \psi] = \int d^4x \left[-g \sum_i \bar{\psi}_i (\sigma + i\gamma_5 \vec{\pi} \cdot \vec{\tau}) \psi_i \right] \quad (20)$$

$$S_I[\Phi] = \int d^4x \left[-\frac{\lambda}{4} (\sigma^2 + \vec{\pi}^2 - v^2)^2 + f_\pi m_\pi^2 \sigma + U_0 \right].$$

The set of inhomogeneous Klein-Gordon equations of motion follow directly from variation of $S[\Phi, \bar{\psi}, \psi]$ with respect to the components σ and $\vec{\pi}$ of the chiral field and treating quarks at one-loop level:

$$\begin{aligned} \partial_\mu \partial^\mu \sigma + \lambda (\sigma^2 + \vec{\pi}^2 - v^2) \sigma - f_\pi m_\pi^2 + g \langle \bar{\psi} \psi \rangle &= 0, \\ \partial_\mu \partial^\mu \vec{\pi} + \lambda (\sigma^2 + \vec{\pi}^2 - v^2) \vec{\pi} + g \langle \bar{\psi} i\gamma_5 \vec{\tau} \psi \rangle &= 0. \end{aligned} \quad (21)$$

Thereby, the scalar and pseudoscalar densities are given by¹⁰:

$$\begin{aligned} \langle \bar{\psi} \psi \rangle(t, \vec{x}) &= g d_\psi \sigma(t, \vec{x}) \int \frac{d^3p}{(2\pi)^3} \frac{f_\psi(t, \vec{x}, \vec{p}) + f_{\bar{\psi}}(t, \vec{x}, \vec{p})}{E(t, \vec{x}, \vec{p})}, \\ \langle \bar{\psi} i\gamma_5 \vec{\tau} \psi \rangle(t, \vec{x}) &= g d_\psi \vec{\pi}(t, \vec{x}) \int \frac{d^3p}{(2\pi)^3} \frac{f_\psi(t, \vec{x}, \vec{p}) + f_{\bar{\psi}}(t, \vec{x}, \vec{p})}{E(t, \vec{x}, \vec{p})}, \end{aligned} \quad (22)$$

with f_ψ and $f_{\bar{\psi}}$ denoting the phase-space distribution functions of quarks and antiquarks with their degeneracy factor $d_\psi = N_c N_s N_f = 12$ for $N_c = 3$ colors, $N_s = 2$ spins and $N_f = 2$ flavors. In a dynamical simulation, one of the most simple descriptions of quarks would be to propagate them according to the Vlasov equation:

$$\left[\partial_t + \frac{\vec{p}}{E(t, \vec{x}, \vec{p})} \cdot \nabla_{\vec{x}} - \nabla_{\vec{x}} E(t, \vec{x}, \vec{p}) \nabla_{\vec{p}} \right] f_{\psi, \bar{\psi}}(t, \vec{x}, \vec{p}) = 0, \quad (23)$$

where the force term is dynamically generated through the effective mass of quarks, depending on the mean-field values,

$$E(t, \vec{x}, \vec{p}) = \sqrt{\vec{p}^2(t) + M_\psi^2(t, \vec{x})}, \quad M_\psi^2(t, \vec{x}) = g^2 [\sigma^2(t, \vec{x}) + \vec{\pi}^2(t, \vec{x})]. \quad (24)$$

With the inverse temperature $\beta = 1/T$ and quark chemical potential μ_ψ the effective thermodynamic potential of the semiclassical approximation is given by:

$$\begin{aligned} \Omega_{\text{eff}}^{\text{MF}}(T, \mu_\psi) &= \frac{\lambda}{4} (\sigma^2 + \vec{\pi}^2 - v^2)^2 - h_q \sigma - U_0 \\ &\quad - d_\psi \frac{1}{\beta} \int \frac{d^3\vec{p}}{(2\pi)^3} \left[\ln(1 + e^{-\beta(E_\psi - \mu_\psi)}) + \ln(1 + e^{-\beta(E_\psi + \mu_\psi)}) \right], \end{aligned} \quad (25)$$

where we introduced the logarithmic terms, since their derivatives with respect to the components of the chiral field reproduces the scalar and pseudoscalar contributions with the densities of Eq. 22 as required:

$$\begin{aligned} \frac{\partial \Omega_{\text{eff}}^{\text{MF}}}{\partial \sigma} &= \lambda (\sigma^2 + \vec{\pi}^2 - v^2) \sigma - f_\pi m_\pi^2 + g \langle \bar{\psi} \psi \rangle \stackrel{!}{=} 0 \\ \frac{\partial \Omega_{\text{eff}}^{\text{MF}}}{\partial \vec{\pi}} &= \lambda (\sigma^2 + \vec{\pi}^2 - v^2) \vec{\pi} + g \langle \bar{\psi} i\gamma_5 \vec{\tau} \psi \rangle \stackrel{!}{=} 0 \end{aligned} \quad (26)$$

¹⁰The exact derivation of scalar and pseudoscalar densities from fermionic one-loop integral can be found in the next section, when the model is extended to a functional approach.

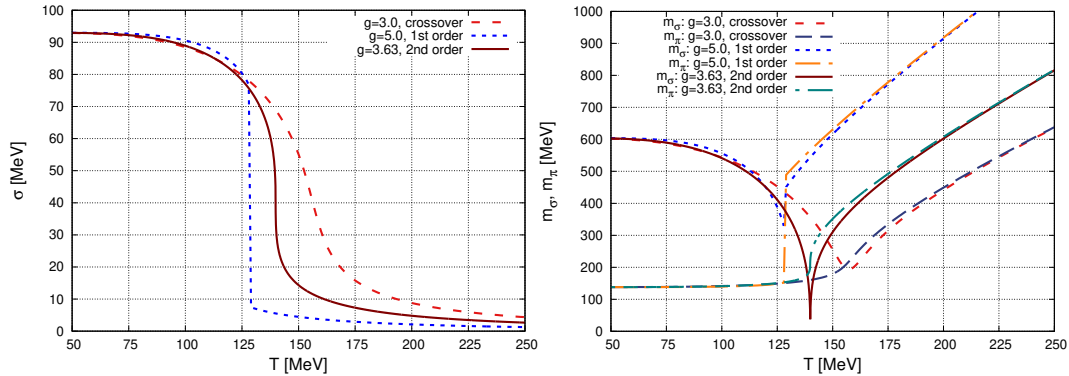


Figure 3: Order parameter, σ and pion mass for the semiclassical approximation as given by Eqs. (21). The coupling constant g is chosen to reproduce different kinds of the chiral phase transition at vanishing chemical potential of quarks.

The chiral phase diagram is obtained by numerically solving self-consistently the first equation in (26) for arbitrary combinations of $T \geq 0$ and μ_q , since the expectation value $\langle \vec{\pi} \rangle$ vanishes in equilibrium. For this purpose, one applies the bisection or Newton's method. In the second step, one computes the numerical derivatives of Eqs. (27) by applying a finite difference method of higher order.

Here, the distribution functions in scalar and pseudoscalar densities are given by the Fermi distribution and the last conditions account for a stationary state. Now, the effective masses follow from the curvature of the effective potential with respect to the chiral components, which are evaluated at equilibrium values of the chiral field:

$$m_\sigma^2 = \left. \frac{\partial^2 \Omega_{\text{eff}}^{\text{MF}}}{\partial \sigma^2} \right|_{\Phi = \langle \Phi \rangle_{\text{eq}}}, \quad m_\pi^2 = \left. \frac{\partial^2 \Omega_{\text{eff}}^{\text{MF}}}{\partial \vec{\pi}^2} \right|_{\Phi = \langle \Phi \rangle_{\text{eq}}}. \quad (27)$$

In case of this semiclassical approach the most crucial and problematic approximation is the fact of neglecting fluctuations around the mean field, being justified only at very low or high temperatures, since these thermal fluctuations can be interpreted as mesonic interactions (see Sec. 3). In the vicinity of the critical point the mass of σ mesons becomes small as seen from the Fig. 3, so that thermal fluctuations due to mesons can significantly contribute to the total rate of interactions between the different components of the chiral field and quarks.

The resulting equilibrium properties of such a semiclassical description are shown in Fig. 3 for the order parameter as well as effective σ and pion masses as a function of the temperature T . Depending on the Yukawa coupling constant g different orders of the chiral-phase transition occur. More results, also with a constant binary cross section for quarks, can be found in [42, 43, 44, 45], where the semiclassical model has been extended to include mean-field fluctuations by introducing a new stochastic formalism for an effective interaction between the σ field and quarks via intermediate mesonic states. In the next section we shall derive a consistent set of equations for the chiral order parameter, $\langle \sigma \rangle$, as well as the fluctuations in terms of a coupled set of (non-Markovian) kinetic equations.

3. Transport equations

The first part of this Sect. briefly introduces fundamental techniques in non-equilibrium quantum field theory by starting from the general concept of the Green's function in the real-time formalism, which has been developed by Schwinger and Keldysh [46, 47]. It is worth to mention, that n -point Green's functions do not fulfill the properties of a physical observable, since they cannot be directly measured. However, they are connected to physical transition amplitudes (see for instance [48]) and contain all accessible information about the system, encoded in the underlying quantum field theory. Based on the real-time technique, we introduce the well-established concept of a generating functional for connected diagrams and discuss the so-called two-particle-irreducible (2PI) quantum effective action. This functional approach acts as a starting point for deriving selfconsistent and exact evolution equations on the

level of one- and two-point functions in quantum field theories out of equilibrium, known as Schwinger-Dyson and Kadanoff-Baym equations.

After applying the gradient expansion to the exact evolution equations for one- and two-point functions of the quark-meson model from Sec. 2.3, one obtains generalized transport equations, allowing to interpret the full dynamics of two-point functions in terms of mesonic interactions. Finally, a truncated version of the 2PI effective action is considered, which still contains the most relevant diagrams, describing also the dissipation with and without memory effects, arising from the interaction between the slowly changing chiral mean-field and mesonic excitations.

3.1. Imaginary and real-time formalisms

The physics of many-body systems in thermal equilibrium can be studied by means of Matsubara's widely used Euclidean-time formalism [49]. This approach is based on the similarity between the partition function and transition amplitudes in the path-integral formalism, allowing to connect both quantities by formally identifying the imaginary time $t = -i\tau$, $\tau \in [0, \beta]$ with the inverse temperature $\beta = 1/T$. For an arbitrary function f we define space-time and energy-momentum integrations by

$$\int_x f(x) = \int_0^{-i\beta} dt \int d^3\vec{x} f(t, \vec{x}), \quad \int_k f(k) = \frac{1}{-i\beta} \sum_{n=-\infty}^{\infty} \int \frac{d^3\vec{k}}{(2\pi)^3} f(i\omega_n, \vec{k}), \quad (28)$$

where the so-called bosonic and fermionic Matsubara frequencies are given by $\omega_n = 2\pi n/\beta$, respectively $\omega_n = 2\pi(n+1)/\beta$ with $n \in \mathbb{Z}$. These discrete frequencies result from the finite time interval and periodic/antiperiodic boundary conditions (see Ref. [50] for more details).

In general, for non-equilibrium systems the initial density matrix ρ_D deviates significantly from the corresponding thermal equilibrium density matrix (for instance $\rho_D^{\text{eq}} \sim e^{-\beta H}$) of the same system. Consequently, the correct treatment of a system out of equilibrium requires to introduce a non-equilibrium effective action and to take the initial correlations via $\rho_D(t_i)$ into account [51]. The exact form of such an effective action and corresponding generating functionals will be discussed in the following (see Sec. 3.2 and Sec. 3.3).

In the Heisenberg picture, the time dependence of a non-equilibrium system is encoded in the field operators, whereas the initial density matrix $\rho_D(t_i)$, for evaluating expectation values, stays constant. Therefore, the full time evolution requires to start from the initial time $t_i \in (-\infty, \infty)$ and propagate the system chronologically on the upper branch C_1 to some maximum value of time $t_f > t_i$ as shown in Fig. 4. From the final time the operator evaluation runs in antichronological order on the lower branch C_2 back to t_i . Finally, the vertical line to $t_i - i\beta$ allows to treat also equilibrium systems within the same framework (compare with Eq. (28)). The full contour line represents the extended real-time contour of the closed-time-path (CTP) method by Schwinger and Keldysh. Consequently, time integrals along the extended real-time contour $C := C_1 \cup C_2 \cup C_3$ can be separated with respect to the upper, lower and vertical branches:

$$\int_C dt = \int_{C_1} dt + \int_{C_2} dt + \int_{C_3} dt = \int_{t_i}^{t_f} dt - \int_{t_i}^{t_f} dt + \int_{t_i}^{t_i - i\beta} dt. \quad (29)$$

A consistent description within the real-time formalism requires only the contour $C = C_1 \cup C_2$, whereas the imaginary-time formalism is based on the contour $C = C_3$ (see Refs. [52, 53]). The functional approach developed in the following sections stays true for equilibrium and non-equilibrium systems and one has only to keep track of the right formalism with its corresponding integration contour. Following that a contour ordered two-point Green's function of a general bosonic or fermionic field $\varphi(x)$ reads

$$G_C(x, y) := \langle \mathcal{T}_C(\varphi(x) \varphi^\dagger(y)) \rangle = \Theta_C(x^0, y^0) \langle \varphi(x) \varphi^\dagger(y) \rangle \pm \Theta_C(y^0, x^0) \langle \varphi^\dagger(y) \varphi(x) \rangle, \quad (30)$$

where an odd number of permutations leads to a sign change for the expectation value of fermionic fields. The time-ordering operator \mathcal{T}_C along the contour can be replaced by using the contour ordered Heaviside function,

$$\Theta_C(x^0, y^0) \equiv \Theta_C(x^0 - y^0) := \begin{cases} \Theta(x^0 - y^0) & \forall x^0, y^0 \in C_1 \\ 0 & \forall x^0 \in C_1, y^0 \in C_2, \\ 1 & \forall y^0 \in C_1, x^0 \in C_2, \\ \Theta(y^0 - x^0) & \forall x^0, y^0 \in C_2. \end{cases} \quad (31)$$

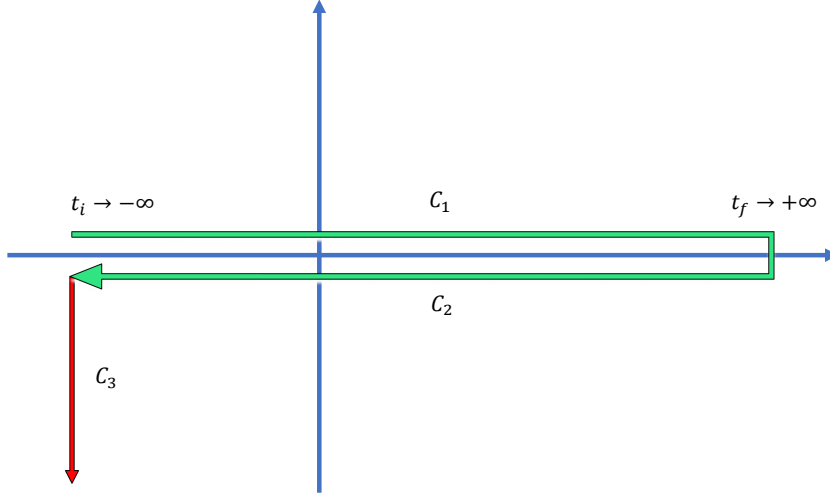


Figure 4: Extended real-time contour of the CPT formalism by Schwinger and Keldysh.

Equivalently, one can introduce a matrix with four components along the contour,

$$\begin{aligned}
G^{11}(x, y) &\equiv iG^c(x, y) := \langle \mathcal{T}_c(\varphi(x)\varphi^\dagger(y)) \rangle \\
&= \Theta(x^0 - y^0) \langle \varphi(x)\varphi^\dagger(y) \rangle \pm \Theta(y^0 - x^0) \langle \varphi^\dagger(y)\varphi(x) \rangle \quad \forall x^0, y^0 \in C_1, \\
G^{22}(x, y) &\equiv iG^a(x, y) := \langle \mathcal{T}_a(\varphi(x)\varphi^\dagger(y)) \rangle \\
&= \Theta(y^0 - x^0) \langle \varphi(x)\varphi^\dagger(y) \rangle \pm \Theta(x^0 - y^0) \langle \varphi^\dagger(y)\varphi(x) \rangle \quad \forall x^0, y^0 \in C_2, \\
G^{12}(x, y) &\equiv iG^<(x, y) := \pm \langle \varphi^\dagger(y)\varphi(x) \rangle \quad \forall x^0 \in C_1, y^0 \in C_2, \\
G^{21}(x, y) &\equiv iG^>(x, y) := \langle \varphi(x)\varphi^\dagger(y) \rangle \quad \forall y^0 \in C_1, x^0 \in C_2.
\end{aligned} \tag{32}$$

Obviously, one of the four Green's functions can be eliminated and instead of (32) one often finds physical expressions in the literature, which are formulated in terms of retarded and advanced Green's functions,

$$\begin{aligned}
iG^{\text{ret}}(x, y) &= G^{11}(x, y) - G^{12}(x, y) = G^{21}(x, y) - G^{22}(x, y) \\
&= \Theta(x^0 - y^0) (iG^>(x, y) - iG^<(x, y)), \\
iG^{\text{adv}}(x, y) &= G^{11}(x, y) - G^{21}(x, y) = G^{12}(x, y) - G^{22}(x, y) \\
&= -\Theta(y^0 - x^0) (iG^>(x, y) - iG^<(x, y)).
\end{aligned} \tag{33}$$

Because of the form (33), one often introduces two additional quantities,

$$\begin{aligned}
A_{B/F} &:= \left\langle \left[\varphi(x), \varphi^\dagger(y) \right]_{\mp} \right\rangle = i(G^>(x, y) - G^<(x, y)), \\
F_{B/F} &:= \left\langle \left[\varphi(x), \varphi^\dagger(y) \right]_{\pm} \right\rangle = i(G^>(x, y) + G^<(x, y)),
\end{aligned} \tag{34}$$

which contain spectral and statistical information about the system.

In equilibrium the real-time propagators depend effectively only on the difference with respect to space-time coordinates and it becomes convenient to represent them in momentum space. Especially, one obtains a dispersion

relation between the retarded Green's function and the spectral function¹¹,

$$G^{\text{ret}}(k) = \int \frac{d\omega}{2\pi} \frac{A_{B/F}(\omega, \vec{k})}{k^0 - \omega + i\epsilon}, \quad (35)$$

which follows directly from the transformation properties for a product of two functions in combination with the regularized form of a θ -function:

$$\theta_\epsilon(x^0) := \theta(x^0) \exp(-\epsilon x^0) \Rightarrow \theta_\epsilon(k^0) = \int_0^\infty dx^0 \exp(ik^0 x^0 - \epsilon x^0) = \frac{i}{k^0 + i\epsilon}. \quad (36)$$

For noninteracting bosonic or fermionic fields with mass m , the Green's functions are solutions of the corresponding homogeneous Klein-Gordon equations. Their explicit form can be derived from analyzing the Kubo-Martin-Schwinger (KMS) boundary conditions¹² of the imaginary-time contour C_3 and by considering the Fourier transform of the Wightman propagators iG^{\gtrless} as shown in Ref. [50]. By introducing the Bose distribution function $f_B(k^0)$ and making use of the general relations (32), (33), (34), one obtains the following relations for bosons:

$$\begin{aligned} A_B(k) &= 2\pi \text{sign}(k^0) \delta(k^2 - m^2), \quad iG^{\text{ret}}(k) = \frac{i}{k^2 - m^2 + i\epsilon \text{sign}(k^0)}, \\ iG^c(k) &= \frac{i}{k^2 - m^2 + i\epsilon} + 2\pi\delta(k^2 - m^2) f_B(|k^0|), \\ iG^a(k) &= \frac{-i}{k^2 - m^2 - i\epsilon} + 2\pi\delta(k^2 - m^2) f_B(|k^0|), \\ iG^<(k) &= 2\pi\delta(k^2 - m^2) (\theta(-k^0) + f_B(|k^0|)), \\ iG^>(k) &= 2\pi\delta(k^2 - m^2) (\theta(k^0) + f_B(|k^0|)). \end{aligned} \quad (37)$$

An analogous calculation for fermions, with f_F standing for the Fermi distribution function and $f_{\bar{F}}$ referring to the corresponding antiparticles, leads to:

$$\begin{aligned} A_F(k) &= 2\pi \text{sign}(k^0) \delta(k^2 - m^2) (\mathbf{k} + m), \quad iD^{\text{ret}}(k) = \frac{i(\mathbf{k} + m)}{k^2 - m^2 + i\epsilon \text{sign}(k^0)}, \\ iD^c(k) &= \left[\frac{i}{k^2 - m^2 + i\epsilon} - 2\pi\delta(k^2 - m^2) (\theta(k^0) f_F(k^0) + \theta(-k^0) f_{\bar{F}}(k^0)) \right] (\mathbf{k} + m), \\ iD^a(k) &= \left[\frac{-i}{k^2 - m^2 - i\epsilon} - 2\pi\delta(k^2 - m^2) (\theta(k^0) f_F(k^0) + \theta(-k^0) f_{\bar{F}}(k^0)) \right] (\mathbf{k} + m), \\ iD^<(k) &= 2\pi\delta(k^2 - m^2) (\theta(-k^0) (1 - f_{\bar{F}}(k^0)) - \theta(k^0) f_F(k^0)) (\mathbf{k} + m), \\ iD^>(k) &= 2\pi\delta(k^2 - m^2) (\theta(k^0) (1 - f_F(k^0)) - \theta(-k^0) f_{\bar{F}}(k^0)) (\mathbf{k} + m). \end{aligned} \quad (38)$$

The expressions for the self-energies¹³ along the contour are similar to the definition of Green's functions (32). However, in general self-energies contain a singular part for diagonal elements (see also Sec. 3.3):

$$\begin{aligned} \Pi^{11}(x, y) &= \delta^4(x - y) \Pi^s(x) + \Theta(x^0 - y^0) \Pi^>(x, y) + \Theta(y^0 - x^0) \Pi^<(x, y), \\ \Pi^{22}(x, y) &= \delta^4(x - y) \Pi^s(x) + \Theta(x^0 - y^0) \Pi^<(x, y) + \Theta(y^0 - x^0) \Pi^>(x, y). \end{aligned} \quad (39)$$

¹¹For non-equilibrium system the Fourier transformation is replaced by the Wigner transformation (see Sec. 3.5).

¹²Periodic for bosons and antiperiodic for fermions.

¹³The connection between self-energies and Green's functions is discussed in Sec. 3.3.

In analogy to (33) one obtains the following relations for the retarded and advanced self-energies:

$$\begin{aligned} i\Pi^{\text{ret}}(x, y) &= \Theta(x^0 - y^0) (i\Pi^>(x, y) - i\Pi^<(x, y)) , \\ i\Pi^{\text{adv}}(x, y) &= -\Theta(y^0 - x^0) (i\Pi^>(x, y) - i\Pi^<(x, y)) . \end{aligned} \quad (40)$$

3.2. 1PI quantum effective action

As discussed before, we prefer not to be restricted to mean-field dynamics, but are interested in deriving transport equations for quantum fluctuations around the mean field, which can be partially interpreted as mesonic interactions. Therefore, we start directly with the commonly used concept of a generating functional for connected diagrams $W[J, \theta, \bar{\theta}]$, formulated here with respect to one-point sources, $J := (J_0, \dots, J_3)$, $\theta := (\theta_1, \theta_2)$, $\bar{\theta} := (\bar{\theta}_1, \bar{\theta}_2)$. The source terms act as auxiliary functions to derive connected diagrams and have to vanish for the physical case, leading to generalized equations of motion. To avoid an overloaded notation, one should just keep in mind, that for systems out of equilibrium all source and field terms carry an additional but hidden index with respect to the upper or lower branch of the real-time contour \mathcal{C} . By introducing the shorthand notation

$$\int_x := \int_C dx^0 \int d^3x, \quad x \equiv (x^0, \vec{x}) \quad (41)$$

and summing up over identical indices for involved fields, the generating functional becomes

$$\begin{aligned} iW[J, \theta, \bar{\theta}] &\equiv \ln \left(Z[J, \theta, \bar{\theta}] \right), \\ Z[J, \theta, \bar{\theta}] &= \mathcal{N} \int \mathcal{D}\Phi \mathcal{D}\bar{\psi} \mathcal{D}\psi \exp \left(i \left[S[\Phi, \bar{\psi}, \psi] + \int_x J_a(x) \Phi_a(x) + \int_x \bar{\psi}_i(x) \theta_i(x) + \int_x \bar{\theta}_i(x) \psi_i(x) \right] \right), \end{aligned} \quad (42)$$

with \mathcal{N} denoting a normalization constant, which does not depend on the source terms and will be skipped in the following without loss of generality. The relevant expectation values of the quantum field theory follow from the generating functional by taking functional derivatives with respect to the corresponding source terms,

$$\begin{aligned} \langle \Phi_a(x) \rangle &= \frac{\delta W[J, \theta, \bar{\theta}]}{\delta J_a(x)} = \phi_a(x) , \\ \langle \bar{\psi}_i(x) \rangle &= -\frac{\delta W[J, \theta, \bar{\theta}]}{\delta \theta_i(x)} \stackrel{!}{=} 0, \quad \langle \psi_i(x) \rangle = \frac{\delta W[J, \theta, \bar{\theta}]}{\delta \bar{\theta}_i(x)} \stackrel{!}{=} 0, \\ G_{\Phi_a \Phi_b}(x, y) &= \langle \mathcal{T}_{\mathcal{C}}(\Phi_a(x) \Phi_b(y)) \rangle = -i \frac{\delta^2 W}{\delta J_a(x) \delta J_b(y)} , \\ D_{\psi_i \bar{\psi}_j}(x, y) &= \langle \mathcal{T}_{\mathcal{C}}(\psi_i(x) \bar{\psi}_j(y)) \rangle = -i \frac{\delta^2 W}{\delta \theta_j(y) \delta \bar{\theta}_i(x)} , \end{aligned} \quad (43)$$

where we exploit the physical condition of vanishing fermionic mean fields due to Lorentz invariance¹⁴. Obviously, the name ‘‘generating functional’’ of (42) refers to the possibility of deriving arbitrary n -point Green’s functions by subsequent functional differentiation with respect to the external sources.

With the properties (43) one can introduce an effective action by performing a functional Legendre transformation with respect to one-point sources of the chiral field,

$$\Gamma[\langle \Phi \rangle, \theta, \bar{\theta}] := W[J, \theta, \bar{\theta}] - \int_x J_a(x) \phi_a(x) , \quad (44)$$

allowing to specify the source terms via the functional derivative,

$$J_a(x) = -\frac{\delta \Gamma[\langle \phi_a \rangle]}{\delta \phi_a(x)} . \quad (45)$$

¹⁴Physical observables have to be bilinear in fermionic fields.

Furthermore, this relation defines dynamical mean-field equations for the physical case of $J_a(x) \stackrel{!}{=} 0$. Making use of the path transformation $\Phi \rightarrow \langle \Phi \rangle + \varphi$ in Eq. (42), results in:

$$\begin{aligned}
W[J, \theta, \bar{\theta}] &= -i \ln \left[\int \mathcal{D}\varphi \mathcal{D}\bar{\psi} \mathcal{D}\psi \exp \left(i \left[S[\langle \Phi \rangle + \varphi, \bar{\psi}, \psi] \right. \right. \right. \\
&\quad \left. \left. \left. + \int_x J_a(x) (\langle \Phi_a(x) \rangle + \varphi_a(x)) + \int_x \bar{\psi}_i(x) \theta_i(x) + \int_x \bar{\theta}_i(x) \psi_i(x) \right] \right) \right] \\
&= -i \ln \left[\int \mathcal{D}\varphi \mathcal{D}\bar{\psi} \mathcal{D}\psi \exp \left(i \left[S[\langle \Phi \rangle + \varphi, \bar{\psi}, \psi] - S[\langle \Phi \rangle] \right. \right. \right. \\
&\quad \left. \left. \left. + \int_x J_a(x) \varphi_a(x) + \int_x \bar{\psi}_i(x) \theta_i(x) + \int_x \bar{\theta}_i(x) \psi_i(x) \right] \right) \right] \\
&\quad + S[\langle \Phi \rangle] + \int_x J_a(x) \phi_a(x) .
\end{aligned} \tag{46}$$

With the definition,

$$\Gamma_1[\langle \Phi \rangle, \theta, \bar{\theta}] := W[J, \theta, \bar{\theta}] - \int_x J_a(x) \phi_a(x) - S[\langle \Phi \rangle] = \Gamma[\langle \Phi \rangle, \theta, \bar{\theta}] - S[\langle \Phi \rangle] , \tag{47}$$

we obtain a new relation for the effective action, where $\Gamma_1[\langle \Phi \rangle, \theta, \bar{\theta}]$ contains one- and multi-loop diagrams, as can be seen in the following.

Before proceeding with the further analysis of Eq. (46), we rewrite the purely bosonic part $S[\Phi]$ of the classical action (18), evaluated at $\langle \Phi \rangle + \varphi$, by expanding it around the mean-field $\langle \Phi \rangle$ in the functional sense,

$$S[\langle \Phi \rangle + \varphi] = S[\langle \Phi \rangle] + S_I[\langle \Phi \rangle, \varphi^3] + \int_x \varphi_a(x) \frac{\delta S[\varphi]}{\delta \varphi_a(x)} \Big|_{\varphi=\langle \Phi \rangle} + \frac{1}{2} \int_{x,y} \varphi_a(x) \frac{\delta^2 S[\varphi]}{\delta \varphi_a(x) \delta \varphi_b(y)} \Big|_{\varphi=\langle \Phi \rangle} \varphi_b(y) , \tag{48}$$

where $S_I[\langle \Phi \rangle, \varphi^3]$ includes only terms with at least cubic interaction with respect to the fluctuation φ .

For notational reasons, we introduce the so-called ‘‘classical’’ or modified form of the free inverse propagator, defined by the second functional derivative of the bosonic part of the classical action (18) as given in the second integral of Eq. (48):

$$\begin{aligned}
iG_{0,\varphi_a\varphi_b}^{-1}(x,y) &:= \frac{\delta^2 S[\varphi]}{\delta \varphi_a(x) \delta \varphi_b(y)} \Big|_{\varphi=\langle \Phi \rangle} = \frac{\delta^2 S[\langle \Phi \rangle]}{\delta \phi_a(x) \delta \phi_b(y)} \\
&= - \left[\partial_\mu \partial^\mu + \lambda (\phi_c(x) \phi_c(x) - v^2) \right] \delta_{ab} \delta_C(x-y) \\
&\quad - 2\lambda \phi_a(x) \phi_b(x) \delta_C(x-y) .
\end{aligned} \tag{49}$$

This representation allows to profit from the Gaussian form of path integrals as will be seen in the following. In particular, we obtain for the diagonal elements

$$\begin{aligned}
iG_{0,\sigma\sigma}^{-1}(x,y) &= - \left(\partial_\mu \partial^\mu + \lambda \left(3\sigma^2 + \sum_i \pi_i^2 - v^2 \right) \right) \delta_C(x-y) , \\
iG_{0,\pi_i\pi_i}^{-1}(x,y) &= - \left(\partial_\mu \partial^\mu + \lambda \left(\sigma^2 + 3\pi_i^2 + \sum_{j \neq i} \pi_j^2 - v^2 \right) \right) \delta_C(x-y) .
\end{aligned} \tag{50}$$

For massive fermions the usual definition of an inverse free propagator,

$$iD_{0,\psi_i\psi_j}^{-1}(x,y) := (i\hat{\not{D}} - M_{\psi_i}) \delta_{ij} \delta_C(x-y) , \tag{51}$$

is used, where $M_{\psi_i} = \sigma + i\gamma_5 \vec{\pi} \cdot \vec{\tau}$ acts as a mass matrix¹⁵.

Now, we are equipped to reformulate Eq. (46) in a more convenient form. By making use of relations (48)-(51) and applying them to the full expression of the classical action, we can introduce a shifted action,

$$\begin{aligned} \hat{S}[\langle\Phi\rangle, \varphi, \bar{\psi}, \psi] &:= S[\langle\Phi\rangle + \varphi, \bar{\psi}, \psi] - S[\langle\Phi\rangle] - \int_x \varphi_a(x) \left. \frac{\delta S[\varphi]}{\delta \varphi_a(x)} \right|_{\varphi=\langle\Phi\rangle} \\ &= \frac{1}{2} \int_{x,y} \varphi_a(x) iG_{0,\varphi_a\varphi_b}^{-1}(x,y) \varphi_b(y) + S_I[\langle\Phi\rangle, \varphi^3] \\ &\quad + \int_{x,y} \bar{\psi}_i(x) iD_{0,\psi_i\psi_j}^{-1}(x,y) \psi_j(y) + S_I[\langle\Phi\rangle + \varphi, \bar{\psi}, \psi]. \end{aligned} \quad (52)$$

For (47)

$$\begin{aligned} \Gamma_1[\langle\Phi\rangle, \theta, \bar{\theta}] &= -i \ln \left[\int \mathcal{D}\varphi \mathcal{D}\bar{\psi} \mathcal{D}\psi \exp \left(i \left[\hat{S}[\langle\Phi\rangle, \varphi, \bar{\psi}, \psi] \right. \right. \right. \\ &\quad \left. \left. + \int_x \left(\left. \frac{\delta S[\varphi]}{\delta \varphi_a(x)} \right|_{\varphi=\langle\Phi\rangle} + J_a(x) \right) \varphi_a(x) \right. \right. \\ &\quad \left. \left. + \int_x \bar{\psi}_i(x) \theta_i(x) + \int_x \bar{\theta}_i(x) \psi_i(x) \right) \right] \end{aligned} \quad (53)$$

follows Comparing (53) with (42) leads to the statement that $\Gamma_1[\langle\Phi\rangle, \theta, \bar{\theta}]$ can be understood as a generating functional of connected diagrams for a theory with the classical action $\hat{S}[\langle\Phi\rangle, \varphi, \bar{\psi}, \psi]$, where $J_{1,a}(x) := \left(\left. \frac{\delta S[\varphi]}{\delta \varphi_a(x)} \right|_{\varphi=\langle\Phi\rangle} + J_a(x) \right)$ act as source terms for the components of the chiral field. In case of scalar fields an explicit calculation for this property can be found in Ref. [54].

We can explicitly evaluate the effective action to one-loop order for bosons by exploiting Gaussian integration in (53) over bosonic as well as fermionic fields with Grassmann algebra:

$$\begin{aligned} \int \mathcal{D}\varphi \exp \left[-\frac{1}{2} \int_{x,y} \varphi_a(x) G_{0,\varphi_a\varphi_b}^{-1}(x,y) \varphi_b(y) \right] &= \sqrt{2\pi} \det(G_{0,\varphi_a\varphi_b}^{-1})^{-\frac{1}{2}} \\ \int \mathcal{D}\bar{\psi} \mathcal{D}\psi \exp \left[-\int_{x,y} \bar{\psi}_i(x) D_{0,\psi_i\psi_j}^{-1}(x,y) \psi_j(y) \right] &= \det(D_{0,\psi_i\psi_j}^{-1}) \end{aligned} \quad (54)$$

and employing the property $\text{Tr} \ln(M) = \ln(\det(M))$ for a diagonalizable matrix M , where traces are taken with respect to field and Dirac (for fermions) indices¹⁶. Finally, we arrive at

$$\Gamma[\langle\Phi\rangle, \theta, \bar{\theta}] = S[\langle\Phi\rangle] + \frac{i}{2} \text{Tr} \ln(G_{0,\varphi_a\varphi_b}^{-1}) - i \text{Tr} \ln(D_{0,\psi_i\psi_j}^{-1}) + \Gamma_2[\langle\Phi\rangle, \theta, \bar{\theta}], \quad (55)$$

where all connected and diagrams with two or more purely bosonic loops are absorbed in the last term. The bosonic part $S_I[\langle\Phi\rangle, \varphi^3]$ of the shifted action (52) has no vertices with respect to only one fluctuating field φ , meaning that different parts of purely bosonic diagrams in $\Gamma_2[\langle\Phi\rangle, \theta, \bar{\theta}]$ are connected by at least two propagators. Consequently, those diagrams cannot be separated by cutting one inner line and $\Gamma[\langle\Phi\rangle, \theta, \bar{\theta}]$ becomes the 1PI effective action for the chiral field, since also contributions from zero- and one-loop order are one particle-irreducible.

3.3. 2PI quantum effective action

One of the most successful approaches for describing non-equilibrium systems is based on Baym's Φ -functionals (see Ref. [55] for more details) and is known as the 2PI effective action, which is a technique to sum large classes of

¹⁵Even though the Lagrangian has no explicit mass dependence, an effective mass term is generated via interactions with the chiral field.

¹⁶In this final form all constant contributions are skipped, since they do not change the evolution equations, resulting from the effective action.

perturbative 1PI diagrams in and out of equilibrium, closely related to the well-known Cornwall–Jackiw–Tomboulis (CJT) formalism at zero and finite temperature [56, 57]. In more detail, the 2PI effective is a generating functional Γ for connected diagrams with fully dressed propagators as internal lines, allowing to derive self-consistent off-shell evolution equations with respect to the mean fields and Green’s functions (32) of the theory. These evolution equations preserve global symmetries of the original theory and can be renormalized with vacuum counter terms [58, 59]. They also guarantee thermodynamic consistency [60] and recover the correct equilibrium limit. Furthermore, the functional approach allows for a systematic inclusion of collisional memory effects [61, 62, 63, 64]. The abbreviation 2PI stands for two-particle irreducible, which means that diagrams from the corresponding functional do not become disconnected by cutting 2 inner lines.

With the knowledge from the previous section, we are prepared to extend the concept of the 1PI effective action to the 2PI generating functional for connected diagrams with respect to one- (J_a) and two-point ($K_{a,b}, L_{i,j}$) sources. Thereby, we directly exploit the property of vanishing expectation values for the fermionic fields and start with the general form,

$$\begin{aligned} iW[J, K, L] &\equiv \ln(Z[J, K, L]), \\ Z[J, K, L] &= \mathcal{N} \int \mathcal{D}\Phi \mathcal{D}\bar{\psi} \mathcal{D}\psi \exp\left(i\left[S^{K,L}[\Phi, \bar{\psi}, \psi] + \int_x J_a(x) \Phi_a(x)\right]\right), \end{aligned} \quad (56)$$

where the modified expression for the classical action is given by

$$S^{K,L}[\Phi, \bar{\psi}, \psi] := S[\Phi, \bar{\psi}, \psi] + \frac{1}{2} \int_{x,y} \Phi_a(x) K_{a,b}(x,y) \Phi_b(y) + \int_{x,y} \bar{\psi}_i(x) L_{i,j}(x,y) \psi_j(y). \quad (57)$$

After performing a functional Legendre transformation of (56) with respect to the source J ,

$$\Gamma^{K,L}[\langle\Phi\rangle] = W[J, K, L] - \int_x J_a(x) \phi_a(x), \quad (58)$$

the generating functional (58) can be formally identified as the 1PI effective action for a theory with the modified classical action (57). Thereby, the quadratic field contributions with two-point sources act as effective time- and space-dependent mass terms (see also Ref. [51] for scalar field theory).

In analogy to Eq. (47), we write beyond the zero-loop part:

$$\Gamma_1^{K,L}[\langle\Phi\rangle] = \Gamma^{K,L}[\langle\Phi\rangle] - S^{K,L}[\langle\Phi\rangle]. \quad (59)$$

According to expressions (53) and (55), one obtains:

$$\Gamma_1^{K,L}[\langle\Phi\rangle] := -i \ln \left[\int \mathcal{D}\varphi \mathcal{D}\bar{\psi} \mathcal{D}\psi \exp\left(i\left[\hat{S}^{K,L}[\langle\Phi\rangle, \varphi, \bar{\psi}, \psi] - \int_x \frac{\delta\Gamma_1^{K,L}[\langle\Phi\rangle]}{\delta\phi_a} \varphi_a(x)\right]\right) \right], \quad (60)$$

where the modified and shifted classical action follows directly from comparing with the relation (52):

$$\begin{aligned} \hat{S}^{K,L}[\langle\Phi\rangle, \varphi, \bar{\psi}, \psi] &= S_I[\langle\Phi\rangle, \varphi^3] + S_I[\langle\Phi\rangle + \varphi, \bar{\psi}, \psi] \\ &+ \int_{x,y} \bar{\psi}_i(x) i \left(D_{0,\psi_i\psi_j}^{-1}(x,y) - iL_{i,j}(x,y) \right) \psi_j(y) \\ &+ \frac{1}{2} \int_{x,y} \varphi_a(x) i \left(G_{0,\varphi_a\varphi_b}^{-1}(x,y) - iK_{a,b}(x,y) \right) \varphi_b(y). \end{aligned} \quad (61)$$

Before performing Gaussian integrals over field configurations, by replacing the inverse classical propagators by modified expressions of (61), we apply a second functional Legendre transformation with respect to the two-point sources

$$\Gamma[\langle\Phi\rangle, G, D] := \Gamma^{K,L}[\langle\Phi\rangle] - \int_{x,y} K_{b,a}(y,x) \frac{\delta\Gamma^{K,L}[\langle\Phi\rangle]}{\delta K_{b,a}(y,x)} - \int_{x,y} L_{j,i}(y,x) \frac{\delta\Gamma^{K,L}[\langle\Phi\rangle]}{\delta L_{j,i}(y,x)}. \quad (62)$$

With the requirement of independent one- and two-point sources, the functional derivatives with respect to two-point sources lead to the following relations:

$$\begin{aligned}
\frac{\delta \Gamma^{K,L}[\langle \Phi \rangle]}{\delta K_{b,a}(y,x)} &= \frac{\delta W[J,K,L]}{\delta K_{b,a}(y,x)} \\
&= \langle \mathcal{T}_C(\Phi_b(y)\Phi_a(x)) \rangle = \frac{1}{2}(\phi_a(x)\phi_b(y) + G_{\varphi_a\varphi_b}(x,y)), \\
\frac{\delta \Gamma^{K,L}[\langle \Phi \rangle]}{\delta L_{j,i}(y,x)} &= \frac{\delta W[J,K,L]}{\delta L_{j,i}(y,x)} \\
&= \langle \mathcal{T}_C(\bar{\psi}_j(y)\psi_i(x)) \rangle = -D_{\psi_i\psi_j}(x,y).
\end{aligned} \tag{63}$$

Consequently, we conclude that derivatives with respect to two-point sources generate the full propagators for the chiral field, which include also products of the mean-fields.

Now, without loss of generality we introduce a parametrization for inverse propagators:

$$\begin{aligned}
G_{\varphi_a\varphi_b}^{-1}(x,y) &= G_{0,\varphi_a\varphi_b}^{-1}(x,y) - iK_{a,b}(x,y) - \Pi_{\varphi_a\varphi_b}(x,y), \\
D_{\psi_i\psi_j}^{-1}(x,y) &= D_{0,\psi_i\psi_j}^{-1}(x,y) - iL_{i,j}(x,y) - \Sigma_{\psi_i\psi_j}(x,y),
\end{aligned} \tag{64}$$

where the source contributions vanish in physical cases, leading to the general form of dressed propagators with $\Pi_{\varphi_a\varphi_b}(x,y)$ and $\Sigma_{\psi_i\psi_j}(x,y)$ denoting the proper self-energies.

Combining (62), (63), (64) and exploiting Gaussian integration in analogy to (54), (55), results in

$$\begin{aligned}
\Gamma[\langle \Phi \rangle, G, D] &= S^{K,L}[\langle \Phi \rangle] + \Gamma_1^{K,L}[\langle \Phi \rangle] \\
&\quad - \frac{1}{2} \int_{x,y} K_{b,a}(y,x) [\phi_a(x)\phi_b(y) + G_{\varphi_a\varphi_b}(x,y)] \\
&\quad + \int_{x,y} L_{j,i}(y,x) D_{\psi_i\psi_j}(x,y) \\
&= S[\langle \Phi \rangle] - \frac{1}{2} \text{Tr} [K_{b,a}G_{\varphi_a\varphi_b}] + \text{Tr} [L_{j,i}D_{\psi_i\psi_j}] + \Gamma_1^{K,L}[\langle \Phi \rangle] \\
&= S[\langle \Phi \rangle] + \frac{i}{2} \text{Tr} \ln(G_{\varphi_a\varphi_b}^{-1}) - i \text{Tr} \ln(D_{\psi_i\psi_j}^{-1}) \\
&\quad + \frac{i}{2} \text{Tr} [G_{0,\varphi_b\varphi_a}^{-1}G_{\varphi_a\varphi_b}] - i \text{Tr} [D_{0,\psi_j\psi_i}^{-1}D_{\psi_i\psi_j}] \\
&\quad - \frac{i}{2} \text{Tr} [\Pi_{\varphi_b\varphi_a}G_{\varphi_a\varphi_b}] + \text{Tr} [\Sigma_{\psi_j\psi_i}D_{\psi_i\psi_j}] + \text{const.} \\
&\quad + \left(\Gamma_1^{K,L}[\langle \Phi \rangle] - \frac{i}{2} \text{Tr} \ln(G_{\varphi_a\varphi_b}^{-1}) + i \text{Tr} \ln(D_{\psi_i\psi_j}^{-1}) \right) \\
&=: S[\langle \Phi \rangle] + \frac{i}{2} \text{Tr} \ln(G_{\varphi_a\varphi_b}^{-1}) - i \text{Tr} \ln(D_{\psi_i\psi_j}^{-1}) \\
&\quad + \frac{i}{2} \text{Tr} [G_{0,\varphi_b\varphi_a}^{-1}G_{\varphi_a\varphi_b}] - i \text{Tr} [D_{0,\psi_j\psi_i}^{-1}D_{\psi_i\psi_j}] + \Gamma_2[\langle \Phi \rangle, G, D] + \text{const.}
\end{aligned} \tag{65}$$

For the final result, we adjust the expression for the 2PI effective action (65) to a simplified and more usual notation, which will be regularly used in the following:

$$\Gamma[\sigma, \vec{\pi}, G, D] = S[\sigma, \vec{\pi}] + \frac{i}{2} \text{Tr} \ln G^{-1} + \frac{i}{2} \text{Tr} G_0^{-1}G - i \text{Tr} \ln D^{-1} - i \text{Tr} D_0^{-1}D + \Gamma_2[\sigma, \vec{\pi}, G, D]. \tag{66}$$

Here, the mean-fields and propators stand for

$$\begin{aligned}
(\sigma, \vec{\pi}) &= \langle \Phi(x) \rangle, & G_0^{-1} &= G_{0,\varphi_a\varphi_b}^{-1}(x,y), & D_0^{-1} &= D_{0,\psi_i\psi_j}^{-1}(x,y), \\
G &= G_{\varphi_a\varphi_b}(x,y), & D &= D_{\psi_i\psi_j}(x,y).
\end{aligned} \tag{67}$$

Taking functional derivatives of (65) with respect to the full propagators,

$$\begin{aligned}
\frac{\delta\Gamma[\langle\Phi\rangle, G, D]}{\delta G_{\varphi_b\varphi_a}(y, x)} &= -\frac{i}{2} \left[G_{\varphi_a\varphi_b}^{-1}(x, y) - G_{0, \varphi_a\varphi_b}^{-1}(x, y) + 2i \frac{\delta\Gamma_2[\langle\Phi\rangle, G, D]}{\delta G_{\varphi_b\varphi_a}(y, x)} \right] \\
&= -\frac{1}{2} K_{a,b}(x, y), \\
\frac{\delta\Gamma[\langle\Phi\rangle, G, D]}{\delta D_{\psi_j\psi_i}(y, x)} &= i \left[D_{\psi_i\psi_j}^{-1}(x, y) - D_{0, \psi_i\psi_j}^{-1}(x, y) - i \frac{\delta\Gamma_2[\langle\Phi\rangle, G, D]}{\delta D_{\psi_j\psi_i}(y, x)} \right] \\
&= L_{i,j}(x, y),
\end{aligned} \tag{68}$$

where the last equalities follow from comparing with expression (62), allows to define the proper self-energies of Eqs. (64) within the functional approach:

$$\Pi_{\varphi_a\varphi_b}(x, y) = 2i \frac{\delta\Gamma_2[\langle\Phi\rangle, G, D]}{\delta G_{\varphi_b\varphi_a}(y, x)}, \quad \Sigma_{\psi_i\psi_j}(x, y) = -i \frac{\delta\Gamma_2[\langle\Phi\rangle, G, D]}{\delta D_{\psi_j\psi_i}(y, x)}. \tag{69}$$

Since the self-energies consist of one-particle irreducible diagrams, the functional Γ_2 cannot contain two independent parts in the same diagram, which are only connected by two propagators of type G or D . To be more specific, deriving of Γ_2 with respect to one of the fully dressed propagators is equivalent to opening the corresponding propagator line in the diagrammatic representation. Consequently, the functional Γ_2 stands for the sum of all connected two-particle irreducible diagrams, which can be constructed from vertices of the shifted classical action (61), connected by bosonic G as well as fermionic D propagators. Indeed, in case of the 2PI effective action Γ_2 denotes the two-loop and higher order for bosonic as well as fermionic diagrams, when the local part of the fermionic self-energy Σ is absorbed in the free inverse propagator as an effective mass contribution¹⁷.

So, the final form (65) is a significant simplification of the original and rather formal expression (62). In case of vanishing source terms, the relations in (68) define evolution equations for the propagators G and D , fulfilling the corresponding Schwinger-Dyson equations¹⁸:

$$\begin{aligned}
G_0^{-1}G - \Pi G &= \mathbb{1} \quad \Rightarrow \quad G = G_0 + G_0\Pi G, \\
D_0^{-1}D - \Sigma D &= \mathbb{1} \quad \Rightarrow \quad D = D_0 + D_0\Sigma D.
\end{aligned} \tag{70}$$

Because of the recursive structure of these differential equations, all internal lines G , D are indeed fully dressed propagators, which can be expressed as infinite series with respect to the classical propagators G_0 , D_0 as well as self-energies Π , Σ . Consequently, every diagram from the 2PI effective action resums an infinite number of 1PI diagrams from Sec. (3.2).

3.4. Exact evolution equations from 2PI effective action

Based on the previous section, we are prepared to recover exact evolution equations on the level of fully dressed propagators, which fulfill the Schwinger-Dyson equations (70) as well as self-consistent mean-field equations. Therefore, we explicitly derive the 2PI effective action (66) with respect to the relevant mean fields of the chiral components and propagators, where the spatial coordinates are taken on the upper or lower branch, denoted with latin indices $a, b, c \in \{1, 2\}$.¹⁹ From this, we obtain stationary conditions, leading then to equations of motion with traces running

¹⁷The local part of the fermionic self-energy arises from the interaction between the fermions and the chiral mean field, resulting in an effective mass contribution for fermions.

¹⁸Here, a symbolic matrix notation is used.

¹⁹Note, that off-diagonal branch elements do not contribute to mean-field equations.

over flavor and Dirac indices:

$$\begin{aligned}
\frac{\delta\Gamma}{\delta\sigma^c} &= -J_0^c \stackrel{!}{=} 0 \\
&\Rightarrow \left(\partial_\mu \partial^\mu + \lambda \left((\sigma^c)^2 + (\vec{\pi}^c)^2 - v^2 \right) + 3\lambda G_{\sigma\sigma}^{cc} + \lambda \sum_i G_{\pi_i\pi_i}^{cc} \right) \sigma^c \\
&= f_\pi m_\pi^2 + g \operatorname{Tr} \left(D_{\psi_i\psi_i}^{cc} \right) + \frac{\delta\Gamma_2}{\delta\sigma^c}, \\
\frac{\delta\Gamma}{\delta\pi_i^c} &= -J_i^c \stackrel{!}{=} 0 \\
&\Rightarrow \left(\partial_\mu \partial^\mu + \lambda \left((\sigma^c)^2 + (\vec{\pi}^c)^2 - v^2 \right) + 3\lambda G_{\pi_i\pi_i}^{cc} + \lambda \sum_{j \neq i} G_{\pi_j\pi_j}^{cc} + \lambda G_{\sigma\sigma}^{cc} \right) \pi_i^c \\
&= g \operatorname{Tr} \left(i\gamma_5 \tau_i D_{\psi_i\psi_i}^{cc} \right) + \frac{\delta\Gamma_2}{\delta\pi_i^c}.
\end{aligned} \tag{71}$$

In the following the two quark flavors will be often treated as degenerate states with equal masses, allowing to skip the explicit dependence on the flavor index,

$$\begin{aligned}
\frac{\delta\Gamma}{\delta G_{\sigma\sigma}^{a,b}} &= -\frac{1}{2} K_{\sigma\sigma}^{a,b} \stackrel{!}{=} 0 \\
&\Rightarrow -\left(\partial_\mu \partial^\mu + \lambda \left(3\sigma^2 + \sum_i \pi_i^2 - v^2 \right) \right) G_{\sigma\sigma}^{a,b}(x, y) \\
&= i \int_z \Pi_{\sigma\sigma}^{a,c}(x, z) G_{\sigma\sigma}^{c,b}(z, y) + i\delta_C^{a,b}(x - y), \\
\frac{\delta\Gamma}{\delta G_{\pi_i\pi_i}^{a,b}} &= -\frac{1}{2} K_{\pi_i\pi_i}^{a,b} \stackrel{!}{=} 0 \\
&\Rightarrow -\left(\partial_\mu \partial^\mu + \lambda \left(\sigma^2 + 3\pi_i^2 + \sum_{j \neq i} \pi_j^2 - v^2 \right) \right) G_{\pi_i\pi_i}^{a,b}(x, y) \\
&= i \int_z \Pi_{\pi_i\pi_i}^{a,c}(x, z) G_{\pi_i\pi_i}^{c,b}(z, y) + i\delta_C^{a,b}(x - y), \\
\frac{\delta\Gamma}{\delta D_{\psi_i\psi_i}^{a,b}} &= L_{\psi_i\psi_i}^{a,b} \stackrel{!}{=} 0, \\
&\Rightarrow \left(i\rlap{/}\partial - M_{\psi_i} \right) D_{\psi_i\psi_i}^{a,b}(x, y) = i \int_z \Sigma_{\psi_i\psi_i}^{a,c}(x, z) D_{\psi_i\psi_i}^{c,b}(z, y) + i\delta_C^{a,b}(x - y).
\end{aligned} \tag{72}$$

Thereby, the integro-differential evolution equations for propagators can be reformulated in a rather usual way by explicitly evaluating the time arguments on the contour line, leading to the famous Kadanoff-Baym equations. In case

of the important Wightman functions, one obtains following expressions:

$$\begin{aligned}
(\partial_\mu \partial^\mu + M_\sigma^2(x)) iG_{\sigma\sigma}^{\leq}(x, y) &= - \int_{t_0}^{t_1} dz_0 \int d^3z [\Pi_{\sigma\sigma}^>(x, z) - \Pi_{\sigma\sigma}^<(x, z)] iG_{\sigma\sigma}^{\leq}(z, y) \\
&\quad + \int_{t_0}^{t_2} dz_0 \int d^3z \Pi_{\sigma\sigma}^{\leq}(x, z) [iG_{\sigma\sigma}^>(z, y) - iG_{\sigma\sigma}^<(z, y)] , \\
(\partial_\mu \partial^\mu + M_{\pi_i}^2(x)) iG_{\pi_i\pi_i}^{\leq}(x, y) &= - \int_{t_0}^{t_1} dz_0 \int d^3z [\Pi_{\pi_i\pi_i}^>(x, z) - \Pi_{\pi_i\pi_i}^<(x, z)] iG_{\pi_i\pi_i}^{\leq}(z, y) \\
&\quad + \int_{t_0}^{t_2} dz_0 \int d^3z \Pi_{\pi_i\pi_i}^{\leq}(x, z) [iG_{\pi_i\pi_i}^>(z, y) - iG_{\pi_i\pi_i}^<(z, y)] , \\
(i\cancel{\phi} - M_{\psi_i}(x)) iD_{\psi_i\psi_i}^{\leq}(x, y) &= + \int_{t_0}^{t_1} dz_0 \int d^3z [\Sigma_{\psi_i\psi_i}^>(x, z) - \Sigma_{\psi_i\psi_i}^<(x, z)] iD_{\psi_i\psi_i}^{\leq}(z, y) \\
&\quad - \int_{t_0}^{t_2} dz_0 \int d^3z \Sigma_{\psi_i\psi_i}^{\leq}(x, z) [iD_{\psi_i\psi_i}^>(z, y) - iD_{\psi_i\psi_i}^<(z, y)] ,
\end{aligned} \tag{73}$$

where we introduced a shorthand notation for the effective mass terms, depending on the local part of the self-energy (compare with (A.6)):

$$\begin{aligned}
M_\sigma^2(x) &:= \lambda \left(3\sigma^2 + \sum_i \pi_i^2 - v^2 \right) + \Pi_{\sigma\sigma}^{\text{loc.}}(x) , & \Pi_{\sigma\sigma}^{\text{loc.}}(x) &:= i\Pi_{\sigma\sigma}^{11}(x, x) , \\
M_{\pi_i}^2(x) &:= \lambda \left(\sigma^2 + 3\pi_i^2 + \sum_{j \neq i} \pi_j^2 - v^2 \right) + \Pi_{\pi_i\pi_i}^{\text{loc.}}(x) , & \Pi_{\pi_i\pi_i}^{\text{loc.}}(x) &:= i\Pi_{\pi_i\pi_i}^{11}(x, x) , \\
M_{\psi_i}^2(x) &:= M_{\psi_i}^\dagger M_{\psi_i} = g^2 (\sigma - i\gamma_5 \vec{\pi} \cdot \vec{\tau}) (\sigma + i\gamma_5 \vec{\pi} \cdot \vec{\tau}) \equiv g^2 \left(\sigma^2 + \sum_i \pi_i^2 \right) .
\end{aligned} \tag{74}$$

The evolution equations for retarded and advanced propagators can be derived in full analogy to Eqs. (73).

For the rest of this section, we will consider a truncated version of the 2PI effective action to simplify the dynamics encoded in the exact evolution equations (71) and (72). The Γ_2 -part of the truncated version is given by its representation in Fig. 5, consisting only of one- and two-point diagrams. For those diagrams a first order gradient expansion of Kadanoff-Baym equations in Wigner space reduces to a Markov-like collisional dynamics without memory effects [61, 62, 63, 64]. However, since we are interested in describing dissipation phenomena from the mean-fields to mesons, it becomes necessary to go beyond the simple gradient expansion by partially including memory effects at least for the bosonic sunset diagram. Thereby, one has to emphasize and keep in mind that all finite truncations of the 2PI effective action cause serious difficulties, concerning the Ward-Takahashi-identities of global and local symmetries, which are violated in the first neglected order of the expansion parameter. This violation of the symmetries is a direct consequence of the resummation in the two-point function and it even follows, that also the Goldstone theorem is violated [65, 66], leading to a non-vanishing and temperature dependent mass of pions in the broken phase of the linear sigma model, even when the chiral symmetry is not explicitly broken. We refer to Ref. [67], where the authors discuss some possible modifications for a symmetry-improved 2PI effective action.

3.5. Generalized Boltzmann Equation

From a numerical point of view a direct solution of the Kadanoff-Baym equations (72) is a costly task, since all relevant two-point functions have to be stored over the time, requiring a rapidly increasing amount of memory even for a moderately growing number of space-time grid points. Furthermore, with every additional time step the computational time for this step increases due to the memory aspect of Kadanoff-Baym equations²⁰. It is also worth to

²⁰In numerical computations one usually introduces a maximum value for the difference between two time points, which is chosen to be large compared to the relaxation time of memory effects.

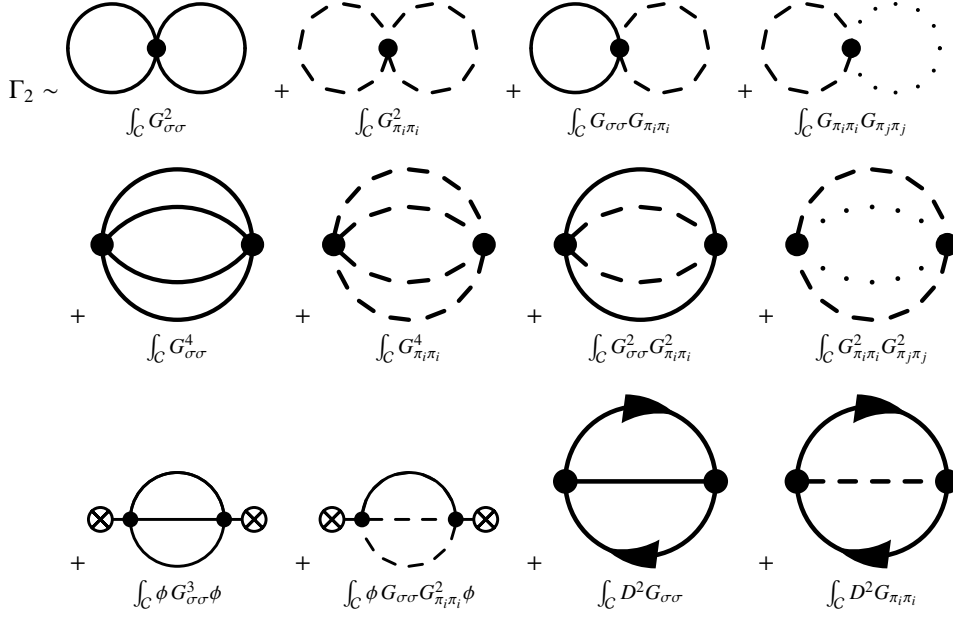


Figure 5: Included 2PI part of the effective action with 1st line: Hartree diagrams, 2nd line: basketball diagrams, 3rd line: sunset diagrams, where solid lines stand for the σ propagator, dashed and pointed lines for the pion propagators and solid lines with arrows for the fermion propagator. The circle with a cross represents a mean-field. For all diagrams a schematic integral representation in terms of formal expressions for the propagators is shown.

mention, that from a physical point of view a direct and exact solution of the Kadanoff-Baym equations is difficult to interpret, since the dynamics is encoded in abstract two-point functions. Of course, the propagators allow to extract various physical observables, but they offer only a limited insight to the physics in terms of elementary scattering processes, which allow to understand the underlying transport effects as long as the system is not too far away from the equilibrium state. Because of these reasons, we will simplify the Kadanoff-Baym equations by deriving transport evolution equations for quasi-particle distribution functions. Thereby, the convolutions of propagators and self-energies can be interpreted in terms of collisional integrals for quasi-particle distribution functions. For this approach, it is suitable to switch to the Wigner transform with respect to the difference of space-time positions $\Delta x := x - y$ and the averaged space-time variable $X := \frac{x+y}{2}$.

Denote $B(x, y)$ an arbitrary two-point function, its Wigner transform and the inverse are given by

$$\begin{aligned}
\mathcal{F}_W[B(x, y)] &:= \int d^4\Delta x e^{ip^\mu\Delta x_\mu} B\left(X + \frac{\Delta x}{2}, X - \frac{\Delta x}{2}\right) \\
&\equiv \int d^4\Delta x e^{ip^\mu\Delta x_\mu} B(X, \Delta x) = \tilde{B}(X, p), \\
\mathcal{F}_W^{-1}[\tilde{B}(X, p)] &= \int \frac{d^4p}{(2\pi)^4} e^{-ip^\mu\Delta x_\mu} \tilde{B}(X, p).
\end{aligned} \tag{75}$$

For products of two-point functions, one obtains a convolution in momentum space, as known from the usual Fourier transform

$$\mathcal{F}_W[B(x, y)C(x, y)] = \int \frac{d^4k}{(2\pi)^4} \tilde{B}(X, p+k) \tilde{C}(X, k) = (\tilde{A} * \tilde{B})(X, p). \tag{76}$$

Transforming the Kadanoff-Baym equations (72), (73) requires also to evaluate spatial convolutions of the form:

$$D(x, y) := \int d^4z B(x, z) C(z, y). \tag{77}$$

This can be done by expanding the formal expressions (compare with Eq. (75) and see [68, 69] for further details),

$$B(x, z) \equiv B\left(X + \frac{z-y}{2}, x-z\right), \quad C(z, y) \equiv C\left(X + \frac{z-x}{2}, z-y\right), \quad (78)$$

in a Taylor series with respect to the first variable and making use of the property, that ∂_X is a generator of translations. To be more precise, for an arbitrary function $f(X)$

$$f(X+a) = e^{a\partial_X} f(X). \quad (79)$$

After applying this relation to Eq. (78), one obtains the following expression for the convolution:

$$D(x, y) = \int d^4 z \left[e^{\frac{z-y}{2}\partial_X^B} B(X, x-z) \right] \left[e^{\frac{z-x}{2}\partial_X^C} C(X, z-y) \right] = A' * B', \quad (80)$$

$$B'(X, x-z) := B(X, x-z) e^{-\frac{x-z}{2}\partial_X^C}, \quad C'(X, z-y) := C(X, z-y) e^{\frac{z-y}{2}\partial_X^B},$$

where the operators act to the left or right side, flagged by the corresponding superscript. A Fourier transform of this expression results then in:

$$\mathcal{F}[B' * C'] = \mathcal{F}[B'] \mathcal{F}[C'],$$

$$\mathcal{F}[B'] = \int d^4 u e^{ip_\mu u^\mu} B(X, u) e^{-\frac{u}{2}\partial_X^C} = B'(X, p) = \tilde{B}(X, p) e^{\frac{1}{2}\partial_X^C \partial_p^B}, \quad (81)$$

$$\mathcal{F}[C'] = \int d^4 u e^{ip_\mu u^\mu} C(X, u) e^{\frac{u}{2}\partial_X^B} = C'(X, p) = \tilde{C}(X, p) e^{-\frac{1}{2}\partial_X^B \partial_p^C},$$

where the last relation follows from the general property:

$$\mathcal{F}[e^{au} f(u)] = f(p-ia) = e^{-ia\partial_p} f(p). \quad (82)$$

Finally, after introducing the diamond operator,

$$\diamond\{\cdot\}\{\cdot\} := \frac{1}{2} \left(\partial_X^{(1)} \partial_p^{(2)} - \partial_p^{(1)} \partial_X^{(2)} \right) \{\cdot\}\{\cdot\}, \quad (83)$$

the Wigner transform of a spatial convolution (77) reads

$$\tilde{D}(X, p) := \int d^4 \Delta x e^{ip^\mu \Delta x_\mu} \int d^4 z B(x, z) C(z, y) = e^{-i\diamond} \{\tilde{B}(X, p)\} \{\tilde{C}(X, p)\}. \quad (84)$$

In transport theory one usually assumes that all relevant two-point functions change slowly with respect to the averaged coordinate, allowing to skip higher-order derivatives,

$$\tilde{D}(X, p) = \tilde{B}(X, p) \tilde{C}(X, p) - i\diamond\{\tilde{B}(X, p)\} \{\tilde{C}(X, p)\} + \mathcal{O}\left(\partial_X^2\right). \quad (85)$$

Now, we start with rewriting the left-hand side of the Kadanoff-Baym equations²¹ for Wightman functions in terms of the Wigner transform and its coordinates $\Delta x, X$:

$$\begin{aligned} \mathcal{F}_W \left[\partial_\mu \partial^\mu iG^{\leq}(x, y) \right] &= \int d^4 \Delta x e^{ip\Delta x} \partial_\mu \partial^\mu iG^{\leq}(x, y) \\ &= \int d^4 \Delta x e^{ip\Delta x} \left(\frac{1}{4} \partial_X^2 + \partial_X \partial_{\Delta x} + \partial_{\Delta x}^2 \right) iG^{\leq}(x, y) \\ &= \left(\frac{1}{4} \partial_X^2 - ip\partial_X - p^2 \right) i\tilde{G}^{\leq}(X, p), \end{aligned} \quad (86)$$

²¹Here, the flavor indices are skipped, also in the following, to avoid an overloaded notation as well as formally equal calculations for sigma and pion propagators.

$$\begin{aligned}
\mathcal{F}_W [M^2(x) iG^{\lessgtr}(x, y)] &= \int d^4 \Delta x e^{ip\Delta x} M^2(x) iG^{\lessgtr}(x, y) \\
&= \int d^4 \Delta x e^{ip\Delta x} \int d^4 z \delta(x-z) M^2(z) iG^{\lessgtr}(z, y) \\
&= e^{-i\Diamond} \{M^2(X)\} \{i\tilde{G}^{\lessgtr}(X, p)\},
\end{aligned} \tag{87}$$

$$\begin{aligned}
\mathcal{F}_W [(i\phi - M_\psi(x)) iD^{\lessgtr}(x, y)] &= \int d^4 \Delta x e^{ip\Delta x} \left(i\frac{1}{2}\phi_X + i\phi_{\Delta x} - M_\psi(x) \right) iD^{\lessgtr}(x, y) \\
&= \left(i\frac{1}{2}\phi_X + \not{p} \right) i\tilde{D}^{\lessgtr}(X, p) - e^{-i\Diamond} \{M_\psi(X)\} \{i\tilde{D}^{\lessgtr}(X, p)\}.
\end{aligned} \tag{88}$$

The Wigner transform of the right-hand side follows from a straightforward calculation by extending the time contour from $-\infty$ to $+\infty$ and taking into account the final time by a theta function, leading to retarded and advanced expressions inside the memory integrals:

$$\begin{aligned}
\left(p^2 + ip\partial_X - \frac{1}{4}\partial_X^2 \right) i\tilde{G}^{\lessgtr}(X, p) - e^{-i\Diamond} \{M^2(X) + \tilde{\Pi}^{\text{ret}}\} \{i\tilde{G}^{\lessgtr}\} &= e^{-i\Diamond} \{\tilde{\Pi}^{\lessgtr}\} \{i\tilde{G}^{\text{adv}}\}, \\
\left(\not{p} + i\frac{1}{2}\phi_X \right) i\tilde{D}^{\lessgtr}(X, p) - e^{-i\Diamond} \{M_\psi(X) + \tilde{\Sigma}^{\text{ret}}\} \{i\tilde{D}^{\lessgtr}(X, p)\} &= e^{-i\Diamond} \{\tilde{\Sigma}^{\lessgtr}\} \{i\tilde{D}^{\text{adv}}\}.
\end{aligned} \tag{89}$$

To first order in gradient expansion, it follows

$$\begin{aligned}
\left(p^2 + ip\partial_X - M^2 - \tilde{\Pi}^{\text{ret}} \right) i\tilde{G}^{\lessgtr} + i\Diamond \{M^2 + \tilde{\Pi}^{\text{ret}}\} \{i\tilde{G}^{\lessgtr}\} &= \tilde{\Pi}^{\lessgtr} i\tilde{G}^{\text{adv}} - i\Diamond \{\tilde{\Pi}^{\lessgtr}\} \{i\tilde{G}^{\text{adv}}\}, \\
\left(\not{p} + i\frac{1}{2}\phi_X - M_\psi - \tilde{\Sigma}^{\text{ret}} \right) i\tilde{D}^{\lessgtr} + i\Diamond \{M_\psi + \tilde{\Sigma}^{\text{ret}}\} \{i\tilde{D}^{\lessgtr}\} &= \tilde{\Sigma}^{\lessgtr} i\tilde{D}^{\text{adv}} - i\Diamond \{\tilde{\Sigma}^{\lessgtr}\} \{i\tilde{D}^{\text{adv}}\}
\end{aligned} \tag{90}$$

Since real and imaginary parts are independent, it is convenient to separate them, by exploiting the property of $i\tilde{G}^{\lessgtr}$, $i\tilde{\Pi}^{\lessgtr}$ being real functions in Wigner space. Furthermore, one should decompose the retarded and advanced propagators as well as corresponding self-energies with respect to the real and imaginary parts in Wigner space. For bosons one obtains following relations²²:

$$\begin{aligned}
\tilde{G}^{\text{ret,adv}} &= \text{Re}\{\tilde{G}^{\text{ret}}\} \pm i \text{Im}\{\tilde{G}^{\text{ret}}\} =: \text{Re}\{\tilde{G}^{\text{ret}}\} \mp i\tilde{A}/2, \\
\tilde{\Pi}^{\text{ret,adv}} &= \text{Re}\{\tilde{\Pi}^{\text{ret}}\} \pm i \text{Im}\{\tilde{\Pi}^{\text{ret}}\} =: \text{Re}\{\tilde{\Pi}^{\text{ret}}\} \mp i\tilde{\Gamma}/2.
\end{aligned} \tag{91}$$

For instance, the Wigner transform of the retarded self-energy is given by:

$$\begin{aligned}
\tilde{\Pi}^{\text{ret}}(X, k) &= \int d^4 \Delta x e^{ik\Delta x} \Theta(x^0 - y^0) (\Pi^>(x, y) - \Pi^<(x, y)) \\
&= \int \frac{dk^{0'}}{2\pi} \frac{i\tilde{\Pi}^>(X, k') - i\tilde{\Pi}^<(X, k')}{k^0 - k^{0'} + i\epsilon}.
\end{aligned} \tag{92}$$

²²Corresponding expressions for fermions can be introduced analogously, keeping only in mind, that the real and imaginary parts are considered with respect to each Lorentz component.

Decomposing the retarded self-energy with respect to the real and imaginary parts, leads to:

$$\begin{aligned}
\text{Im} \left[\tilde{\Pi}^{\text{ret}}(X, k) \right] &= \int \frac{dk^{0'}}{2\pi} \frac{-\epsilon}{(k^0 - k^{0'})^2 + \epsilon^2} \left(i\tilde{\Pi}^>(X, k') - i\tilde{\Pi}^<(X, k') \right) \\
&\xrightarrow{\epsilon \rightarrow 0} -\frac{1}{2} \left(i\tilde{\Pi}^>(X, k) - i\tilde{\Pi}^<(X, k) \right), \\
\text{Re} \left[\tilde{\Pi}^{\text{ret}}(X, k) \right] &= \int \frac{dk^{0'}}{2\pi} \frac{k^0 - k^{0'}}{(k^0 - k^{0'})^2 + \epsilon^2} \left(i\tilde{\Pi}^>(X, k') - i\tilde{\Pi}^<(X, k') \right) \\
&\xrightarrow{\epsilon \rightarrow 0} \mathcal{P} \int \frac{dk^{0'}}{2\pi} \frac{-2 \text{Im} \left[\tilde{\Pi}^{\text{ret}}(X, k') \right]}{k^0 - k^{0'}} = \mathcal{P} \int \frac{dk^{0'}}{2\pi} \frac{\tilde{\Gamma}}{k^0 - k^{0'}},
\end{aligned} \tag{93}$$

where the last relation is known as the Kramers–Kronig relation, which defines an analytic connection between the real and imaginary part.

Inserting the decomposition (91) into (90) leads then to a set of two equations for every particle species. In detail, one obtains from the imaginary parts the so-called generalized transport equations (see also Ref. [70] for scalar field theory),

$$\begin{aligned}
2p_\mu \partial_X^\mu i\tilde{G}^{\leq} + 2\Diamond \{M^2 + \text{Re}\{\tilde{\Pi}^{\text{ret}}\}\} i\tilde{G}^{\leq} + 2\Diamond \{i\tilde{\Pi}^{\leq}\} \{\text{Re}\{\tilde{G}^{\text{ret}}\}\} &= i\tilde{\Pi}^<i\tilde{G}^> - i\tilde{\Pi}^>i\tilde{G}^<, \\
\phi_X i\tilde{D}^{\leq} + 2\Diamond \{M_\psi + \text{Re}\{\tilde{\Sigma}^{\text{ret}}\}\} i\tilde{D}^{\leq} + 2\Diamond \{i\tilde{\Sigma}^{\leq}\} \{\text{Re}\{\tilde{D}^{\text{ret}}\}\} &= i\tilde{\Sigma}^<i\tilde{D}^> - i\tilde{\Sigma}^>i\tilde{D}^<,
\end{aligned} \tag{94}$$

whereas the real parts lead to the generalized mass-shell equations,

$$\begin{aligned}
(p^2 - M^2 - \text{Re}\{\tilde{\Pi}^{\text{ret}}\}) i\tilde{G}^{\leq} &= i\tilde{\Pi}^{\leq} \text{Re}\{\tilde{G}^{\text{ret}}\} + \frac{1}{2} \Diamond \{i\tilde{\Pi}^<\} \{i\tilde{G}^>\} - \frac{1}{2} \{i\tilde{\Pi}^>\} \{i\tilde{G}^<\}, \\
(p - M_\psi - \text{Re}\{\tilde{\Sigma}^{\text{ret}}\}) i\tilde{D}^{\leq} &= i\tilde{\Sigma}^{\leq} \text{Re}\{\tilde{D}^{\text{ret}}\} + \frac{1}{2} \Diamond \{i\tilde{\Sigma}^<\} \{i\tilde{D}^>\} - \frac{1}{2} \{i\tilde{\Sigma}^>\} \{i\tilde{D}^<\}.
\end{aligned} \tag{95}$$

In Wigner space the propagator structure becomes more obvious by writing $i\tilde{G}^{\leq}$ as a product of the spectral function $\tilde{A}(X, p)$ and the generalized quasi-particle distribution function $\tilde{N}^{\leq}(X, p)$. This separation method is known as the Kadanoff-Baym ansatz, which generalizes the KMS condition for propagators in equilibrium to systems out of equilibrium. With the identity $i\tilde{G}^<(X, -p) = i\tilde{G}^>(X, p)$ and in accordance with the definition of the spectral function, one obtains the following expressions for bosonic propagators:

$$\begin{aligned}
i\tilde{G}^>(X, p) &= \tilde{A}(X, p) \tilde{N}^>(X, p), \quad \tilde{N}^>(X, p) = \begin{cases} 1 + f(X, \vec{p}), & p^0 = E_p \\ -f(X, -\vec{p}), & p^0 = -E_p, \end{cases} \\
i\tilde{G}^<(X, p) &= \tilde{A}(X, p) \tilde{N}^<(X, p), \quad \tilde{N}^<(X, p) = \begin{cases} f(X, \vec{p}), & p^0 = E_p \\ -(1 + f(X, -\vec{p})), & p^0 = -E_p, \end{cases}
\end{aligned} \tag{96}$$

where $f(X, \vec{p})$ denotes the usual one-particle distribution function. For fermionic Wightman propagators, it follows:

$$\begin{aligned}
i\tilde{D}^>(X, p) &= \tilde{A}_\psi(X, p) \tilde{N}_\psi^>(X, p), \quad \tilde{N}_\psi^>(X, p) = \begin{cases} 1 - f_\psi(X, \vec{p}), & p^0 = E_p, \\ f_\psi(X, -\vec{p}), & p^0 = -E_p, \end{cases} \\
i\tilde{D}^<(X, p) &= -\tilde{A}_\psi(X, p) \tilde{N}_\psi^<(X, p), \quad \tilde{N}_\psi^<(X, p) = \begin{cases} f_\psi(X, \vec{p}), & p^0 = E_p, \\ (1 - f_\psi(X, -\vec{p})), & p^0 = -E_p. \end{cases}
\end{aligned} \tag{97}$$

The spectral functions \tilde{A} , \tilde{A}_ψ with corresponding widths $\tilde{\Gamma}$, $\tilde{\Gamma}_\psi$ follow directly from the first-order gradient expansion of the Kadanoff-Baym equations (72) for retarded and advanced propagators (see also [70, 71]). In detail, one obtains for bosons the well-known Breit-Wigner form (analogously for fermions):

$$\tilde{A} = \frac{\tilde{\Gamma}}{\tilde{\Omega}^2 + \tilde{\Gamma}^2/4}, \quad \tilde{\Omega}^2(X, p) = p^2 - \tilde{M}^2(X) - \text{Re}(\tilde{\Gamma}^{\text{ret}}(X, p)). \quad (98)$$

Since the limit of the Lorentz sequence results in a δ -function,

$$\delta_\epsilon(x) = \frac{1}{\pi} \frac{\epsilon}{x^2 + \epsilon^2} \xrightarrow{\epsilon \rightarrow 0} \delta(x), \quad (99)$$

vanishing widths $\tilde{\Gamma}$, $\tilde{\Gamma}_\psi$ of quasi-particles lead to a simplified form for the spectral functions, known as on-shell approximation,

$$\begin{aligned} \tilde{A} &= 2\pi \text{sign}(p^0) \delta(\tilde{\Omega}^2) = \frac{\pi}{E(X, p)} \left(\delta(p^0 - E(X, p)) - \delta(p^0 + E(X, p)) \right), \\ \tilde{A}_\psi &= 2\pi \text{sign}(p^0) \delta(\tilde{\Omega}_\psi^2) (\not{p} + M_\psi) \\ &= (\not{p} + M_\psi) \frac{\pi}{E(X, p)} \left(\delta(p^0 - E(X, p)) - \delta(p^0 + E(X, p)) \right). \end{aligned} \quad (100)$$

Now, it is straightforward to derive generalized transport equations of Boltzmann type by making use of the decompositions (96), (97) and their on-shell interpretations with (100). Thereby, in the limit of vanishing quasi-particle widths $\tilde{\Gamma}$, $\tilde{\Gamma}_\psi$ the contribution from the real part of the retarded self-energy can be neglected as can be seen from the Kramers-Kronig relation (93). This approximation scheme will also be discussed in the next section. Consequently, the dispersion relation obtains its usual form $E = \sqrt{\vec{p}^2 + \tilde{M}^2(X)}$.

In comparison to the generalized mass-shell equations (95), the generalized transport equations (94) have a rather natural form for transport equations, with a drift term, a Vlasov term from the local part of the self-energy and a mass shift due to the real part of the retarded self-energy. Furthermore, the right side of the equation contains a typical gain and loss structure. The second diamond operator on the left-hand side does not explicitly depend on the quasi-particle distribution functions and thus purely describes the off-shell evolution of the system. This part is of no relevance for Boltzmann like evolutions equations as pointed out in [71] and it is indeed sufficient to solve (94) instead of (95), since the solutions differ only by contributions of higher order in gradients.

3.6. Thermodynamic properties

Before proceeding with non-equilibrium studies, it is convenient to discuss some thermodynamic properties of the effective potential, which is directly related to the effective action:

$$\Omega_{\text{eff}}[\sigma, \vec{\pi}, G, D] = -\frac{1}{\beta V} i\Gamma[\sigma, \vec{\pi}, G, D]. \quad (101)$$

In the following, we firstly focus on the effective bosonic mass, arising from the Hartree approximation of the Γ_2 -part and will then discuss an extension to include quark contributions to the effective mass of bosons. Diagrammatically, the Hartree approximation is given by the first line in Fig. 5 and includes the most relevant contributions to the effective potential of bosons by taking into account all one-point diagrams from the full truncation of the effective action $\Gamma[\sigma, \vec{\pi}, G, D]$. In terms of 1PI diagrams the Hartree approximation sums the so-called daisy diagrams for tree level propagators, which form a large and important class of thermal diagrams. The full 2PI effective action for this approximation reads

$$\begin{aligned} \Gamma^{\text{h}}[\sigma, \vec{\pi}, G, D] &= S[\sigma, \vec{\pi}] + \frac{i}{2} \text{Tr} \ln G^{-1} + \frac{i}{2} \text{Tr} G_0^{-1} G - i \text{Tr} \ln D^{-1} - i \text{Tr} D_0^{-1} D \\ &\quad - \frac{3}{4} \lambda \int_C d^4x G_{\sigma\sigma}^2(x, x) - \frac{1}{2} \lambda \sum_i \int_C d^4x G_{\sigma\sigma}(x, x) G_{\pi_i\pi_i}(x, x) \\ &\quad - \frac{3}{4} \lambda \sum_i \int_C d^4x G_{\pi_i\pi_i}^2(x, x) - \frac{1}{2} \lambda \sum_{i,j \neq i} \int_C d^4x G_{\pi_i\pi_i}(x, x) G_{\pi_j\pi_j}(x, x). \end{aligned} \quad (102)$$

The restriction to one-point diagrams allows to calculate the full expression of the effective potential by simply using the imaginary time formalism with on-shell propagators as will be discussed in the following.

Within the Hartree approximation the general form for fully dressed propagators of the Schwinger-Dyson equation (70) for bosons and fermions reduce to the rather simple expressions

$$\begin{aligned} iG_{\varphi_a\varphi_a}^{-1}(x, y) &= iG_{0,\varphi_a\varphi_a}^{-1}(x, y) - i\Pi_{\varphi_a\varphi_a}(x, y) = \left(-\partial_\mu\partial^\mu - M_{\varphi_a}^2(x)\right)\delta_C(x-y), \\ iD_{\psi_i\psi_i}^{-1}(x, y) &= iD_{0,\psi_i\psi_i}^{-1}(x, y) - i\Sigma_{\psi_i\psi_i}(x, y) = \left(i\cancel{\partial} - M_{\psi_i}(x)\right)\delta_C(x-y), \end{aligned} \quad (103)$$

containing only local self-energy contributions and leading to effective mass terms (compare also with Eq. (74)). As already discussed in Sec. 3.1 the equilibrium propagators as two-point functions depend only on the relative space-time difference, allowing to perform all relevant calculations in momentum space. Furthermore, within the imaginary time formalism with $k = (\omega_n, \vec{k}) =: k_n$

$$\begin{aligned} iG_{\varphi_a\varphi_a}^{-1}(k) = k^2 - M_{\varphi_a}^2 &\Rightarrow G_{\varphi_a\varphi_a}(k) = \frac{i}{k_n^2 - M_{\varphi_a}^2}, \\ iD_{\psi_i\psi_i}^{-1}(k) = \cancel{k} - M_{\psi_i} &\Rightarrow D_{\psi_i\psi_i}(k) = \frac{i}{\cancel{k}_n - M_{\psi_i}}, \end{aligned} \quad (104)$$

where the last step becomes possible as long as the mass terms are positive, since the norm of the Euclidean momentum vector with the metric convention $g^{\mu\nu} = (-1, -1, -1, -1)$ is always spacelike $k_n^2 \leq 0$. This calculation would be incorrect for real-time propagators, where the Minkowski metric leads to the existence of possible poles in the denominator, which have to be taken into account, leading to a form with an explicit vacuum and a thermal part as already known from the thermal propagators of a noninteracting field theory (see relations (37) and (38)).

In Appendix B, we calculate the logarithmic terms as well as the loop integrals for the effective thermodynamic potential (102). With the following definition of a loop integral,

$$Q(M_{\varphi_a}) := \int \frac{d^3\vec{p}}{(2\pi)^3} \frac{1}{E_{\varphi_a}} f_{\varphi_a}(t, \vec{x}, \vec{p}) = \int \frac{d^3\vec{p}}{(2\pi)^3} \frac{1}{E_{\varphi_a}} \frac{1}{e^{\beta E_{\varphi_a}} - 1}, \quad (105)$$

the trace relations at one-loop order in equilibrium lead to

$$\begin{aligned} \frac{i}{2} \text{Tr} G_0^{-1} G &= -\frac{i\beta V}{2} \sum_a \left[M_{\varphi_a}^2 - \lambda \left(3\varphi_a^2 + \sum_{b \neq a} \varphi_b^2 - v^2 \right) \right] Q(M_{\varphi_a}), \\ i \text{Tr} D_0^{-1} D &= \text{const.} \end{aligned} \quad (106)$$

We are then able to give an explicit and rather lengthy result for the effective potential,

$$\begin{aligned} \Omega_{\text{eff}} &= \Omega_{\text{eff}}^{\text{MF}} + \frac{1}{\beta} \int \frac{d^3\vec{p}}{(2\pi)^3} \ln(1 - e^{-\beta E_\sigma}) + \sum_i \frac{1}{\beta} \int \frac{d^3\vec{p}}{(2\pi)^3} \ln(1 - e^{-\beta E_{\pi_i}}) \\ &\quad - \frac{1}{2} \left[M_\sigma^2 - \lambda \left(3\sigma^2 + \sum_i \pi_i^2 - v^2 \right) \right] Q(M_\sigma) \\ &\quad - \frac{1}{2} \sum_i \left[M_{\pi_i}^2 - \lambda \left(\sigma^2 + 3\pi_i^2 + \sum_{j \neq i} \pi_j^2 - v^2 \right) \right] Q(M_{\pi_i}) \\ &\quad + \frac{3}{4} \lambda [Q(M_\sigma)]^2 + \frac{3}{4} \lambda \sum_i [Q(M_{\pi_i})]^2 \\ &\quad + \frac{1}{2} \lambda \sum_i [Q(M_\sigma) Q(M_{\pi_i})] + \frac{1}{2} \lambda \sum_{i,j \neq i} [Q(M_{\pi_i}) Q(M_{\pi_j})] + R_{\text{eff}} \\ &=: \Omega_{\text{eff}}^{\text{MF}} + \Omega_{\text{eff}}^{\varphi_a} + R_{\text{eff}}, \end{aligned} \quad (107)$$

where $\Omega_{\text{eff}}^{\varphi_a}$ contains all mesonic contributions and $\Omega_{\text{eff}}^{\text{MF}}$ is already known from Sec. 2.3 (see Eq. (25)). Finally, divergent integral contributions are absorbed into the term R_{eff} , which require a proper renormalization scheme²³ as discussed in Refs. [72, 73] for a purely mesonic theory. However, we will simply skip those terms, since the renormalization of the mass leads qualitatively to a rather small modification in the vicinity of the phase transition as already known for the mesonic part from Ref. [73].

We also note that a proper renormalization-scheme in this full off-equilibrium situation is very challenging. For the equilibrium case it has been shown in [58, 59, 66, 73, 74] that self-consistent renormalization schemes based on the 2PI/CJT action formalism can be renormalized with vacuum counter terms, but that also ‘‘hidden divergencies’’ have to be properly subtracted involving a self-consistent solution of the corresponding subdiagrams involving overlapping divergences. For that reason it is also not sufficient to simply use a cutoff-regularization since the divergent contributions to the non-perturbative sub-divergencies cannot be controlled. As already stated, we skip the terms R_{eff} containing the divergent contributions to define a feasible set of kinetic equations to study the fluctuations of conserved charges in the medium undergoing a cross-over or phase transition.

In comparison to the effective potential of the semi-classical mean-field approach, which is simply given by the term $\Omega_{\text{eff}}^{\text{MF}}$, the full Hartree approximation leads to a significant modification, extending the model by a large number of resummed mesonic diagrams.

The upper plot of Fig. 6 shows a normalized form of the effective potential Ω_{eff}/T^4 from Eq. (107) for several values of the temperature T and a fixed quark chemical potential $\mu = 157 \text{ MeV}$. The effective potential has a very flat form for $T = 108 \text{ MeV}$, being also supported by the plot below, showing equipotential lines in the σ - T -plane, which become almost parallel to the σ -axis in the range of $T = 108 - 110 \text{ MeV}$. In the following we consider also the derivatives of the effective potential to confirm more precisely the position of the critical point.

Now, we derive explicit expression for the stationary value of the chiral field $\langle \Phi \rangle = (\langle \sigma \rangle, \langle \vec{\pi} \rangle)$ as well as effective mass terms of sigma and pions, resulting from partial derivatives of the thermodynamic potential,

$$\begin{aligned}
\frac{\partial \Omega_{\text{eff}}}{\partial \sigma} &= \frac{\partial \Omega_{\text{eff}}^{\text{MF}}}{\partial \sigma} + \frac{\partial \Omega_{\text{eff}}^{\varphi_a}}{\partial \sigma} \stackrel{!}{=} 0 \\
&= \lambda \left[\left(\sigma^2 + \sum_i \pi_i^2 - v^2 \right) + 3Q(M_\sigma) + \sum_i Q(M_{\pi_i}) \right] \sigma - f_\pi m_\pi^2 + g \langle \bar{\psi} \psi \rangle \\
\frac{\partial \Omega_{\text{eff}}}{\partial \pi_i} &= \frac{\partial \Omega_{\text{eff}}^{\text{MF}}}{\partial \pi_i} + \frac{\partial \Omega_{\text{eff}}^{\varphi_a}}{\partial \pi_i} \stackrel{!}{=} 0 \\
&= \lambda \left[\left(\sigma^2 + \sum_i \pi_i^2 - v^2 \right) + Q(M_\sigma) + 3Q(M_{\pi_i}) + \sum_{j \neq i} Q(M_{\pi_j}) \right] \pi_i + g \langle \bar{\psi} i \gamma_5 \tau_i \psi \rangle \\
\frac{\partial^2 \Omega_{\text{eff}}}{\partial \sigma^2} &= \lambda \left[\left(3\sigma^2 + \sum_i \pi_i^2 - v^2 \right) + 3Q(M_\sigma) + \sum_i Q(M_{\pi_i}) \right] \\
&\quad + \left. \frac{\partial}{\partial \sigma} g \langle \bar{\psi} \psi \rangle \right|_{\sigma=\langle \sigma \rangle} =: M_\sigma^2, \\
\frac{\partial^2 \Omega_{\text{eff}}}{\partial \pi_i^2} &= \lambda \left[\left(\sigma^2 + 3\pi_i^2 + \sum_{j \neq i} \pi_j^2 - v^2 \right) + 3Q(M_{\pi_i}) + \sum_{j \neq i} Q(M_{\pi_j}) + Q(M_\sigma) \right] \\
&\quad + \left. \frac{\partial}{\partial \pi_i} g \langle \bar{\psi} i \gamma_5 \tau_i \psi \rangle \right|_{\pi_i=\langle \pi_i \rangle} =: M_{\pi_i}^2,
\end{aligned} \tag{109}$$

with mass terms being evaluated at the stationary value of the chiral field $\langle \Phi \rangle = (\langle \sigma \rangle, \langle \vec{\pi} \rangle)$. We note that with vanishing scalar- and pseudoscalar densities the mass relations of Eq. (109) reduce to purely bosonic expressions, being equal to the effective mass terms from the propagator gap equation of Hartree approximation without quarks (compare also

²³Note that the divergent terms are not purely vacuum contributions, since the effective mass terms are determined self-consistently and depend on the medium properties via the one-particle distribution functions.

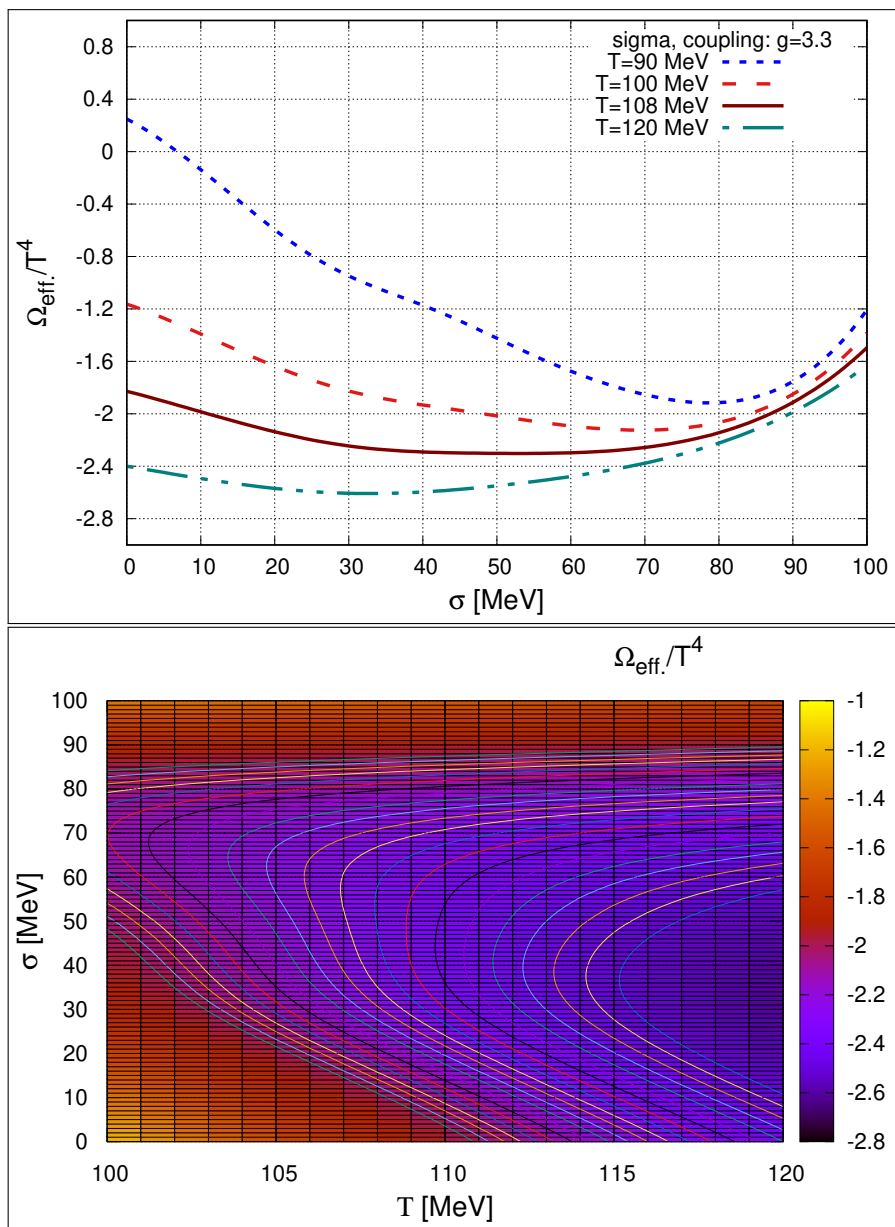


Figure 6: Normalized form of the effective potential from Hartree approximation (107) for a fixed value of the quark chemical potential $\mu = 157$ MeV.

with Ref. [73]). However, additional contributions to the propagator from the fermionic sunset diagrams are crucial to reproduce a phase diagram as expected from a quark-meson model, with the order of the phase transition depending on the chemical potential of quarks²⁴. An inclusion of two-loop diagrams from Fig. 5 makes it necessary to consider the effective mass as a momentum dependent expression, since also the real part of the retarded self-energy has to be taken into account (compare with Eq. (98)), leading to a modification for the propagator gap equations. In numerical calculations we checked for the zero mode, that a contribution from the retarded part of the fermionic sunset diagram to the effective mass in the sense of Kramers-Kronig relation fails to reproduce a phase diagram with a second order phase transition. Consequently, the first gradient expansion with the on-shell ansatz for propagators is not sufficient for our studies and we decided to use effectively derived mass terms of Eq. (109). However, neglecting all two-loop diagrams from Γ_2 in Fig. 5 is a reasonable approximation for the thermodynamic potential as long as the system's effective particle density is small for higher order processes to contribute significantly to the real part of the retarded self-energy.²⁵

For systems out of equilibrium, we simply rewrite the effective mass terms of Eq. (109) by replacing the thermal loop integrals with the general expressions, which are directly calculated in the real-time formalism (compare therefore Eq. (108) with exact evolution equations for the chiral field (71)). Since the loop integrals are local in space and time, the Wigner transform depends effectively only on the variable X and the momentum dependence can be integrated out, leading to the following loop integrals for bosons,

$$\begin{aligned}
iG_{\varphi_a\varphi_a}^c(x, x) &= \frac{1}{2} (iG_{\varphi_a\varphi_a}^>(x, x) + iG_{\varphi_a\varphi_a}^<(x, x)) = \frac{1}{2} \int \frac{d^4 p}{(2\pi)^4} \tilde{F}_{\varphi_a\varphi_a}(X, p) \\
&= \frac{1}{2} \int \frac{d^4 p}{(2\pi)^4} \tilde{A}_{\varphi_a}(X, p) (N_{\varphi_a}^>(X, p) + N_{\varphi_a}^<(X, p)) \\
&= \frac{1}{2} \int \frac{d^3 p}{(2\pi)^3} \frac{1 + 2f^{\varphi_a}(t, \vec{x}, \vec{p})}{E_{\vec{p}}^{\varphi_a}} =: \int \frac{d^3 p}{(2\pi)^3} \frac{f^{\varphi_a}(t, \vec{x}, \vec{p})}{E_{\vec{p}}^{\varphi_a}} + R_{\varphi_a}(x)
\end{aligned} \tag{110}$$

and fermions,

$$\begin{aligned}
\text{Tr}(iD^c(x, x)) &= \frac{1}{2} \text{Tr}(iD^>(x, x) + iD^<(x, x)) = \frac{1}{2} \int \frac{d^4 p}{(2\pi)^4} \text{Tr}(\tilde{F}_{\psi\psi}(X, p)) \\
&= \frac{1}{2} \int \frac{d^4 p}{(2\pi)^4} \text{Tr}(\tilde{A}_{\psi}(X, p) (\tilde{N}_{\psi}^>(X, p) - \tilde{N}_{\psi}^<(X, p))) \\
&= -d_{\psi} g \sigma \int \frac{d^3 \vec{p}}{(2\pi)^3} \frac{1}{E_{\vec{p}}^{\psi}} [f^{\psi}(t, \vec{x}, \vec{p}) + f^{\bar{\psi}}(t, \vec{x}, \vec{p}) - 1] \\
&=: -\langle \bar{\psi}\psi \rangle + R_{\sigma, \psi}(x), \\
\text{Tr}(i\gamma_5 \tau_j iD^c(x, x)) &=: -\langle \bar{\psi} i\gamma_5 \tau_j \psi \rangle + R_{\pi_j, \psi}(x)
\end{aligned} \tag{111}$$

where the traces are evaluated with respect to Dirac and Lorentz indices as well as Pauli indices in isospin-space, $\text{Tr}(\not{p} + M_{\psi}^{\dagger}) = 4g\sigma$ and $\text{Tr}(i\gamma_5 \tau_j (\not{p} + M_{\psi}^{\dagger})) = 4g\pi_j$. The scalar and pseudoscalar densities $\langle \bar{\psi}\psi \rangle$, $\langle \bar{\psi} i\gamma_5 \tau_j \psi \rangle$ are equal to the definitions given in Eq. (22). Finally, $R_{\varphi_a, \psi}(x)$ absorbs divergent contributions, requiring once more a proper renormalization due to the mass dependence of the loop integral. With a similar argument as before we will simply skip these terms in the following. Note that a calculation of logarithmic terms in Eq. (102) within the real-time formalism is more technical and not required for the dynamical evolution equations, since they are not explicitly present in the evolution equations as seen from (71) and (72).

The self-consistent set of equations (108) and (109) is solved for equilibrium one-particle distribution functions by using for instance an improved version of Newton's algorithm for finding minima (respectively roots) of multi-dimensional functions. In case of a problematic initial input vector $(\sigma_0, \vec{\pi}_0, m_{\sigma,0}^2, m_{\pi,0}^2)$ for Newton's algorithm an additional stochastic distortion to the initial guess can be applied.

²⁴Out of equilibrium the phase transition is governed by the effective quark number.

²⁵Such an argument does not hold for the vacuum part of the self-energy and one has to keep this limitation in mind.

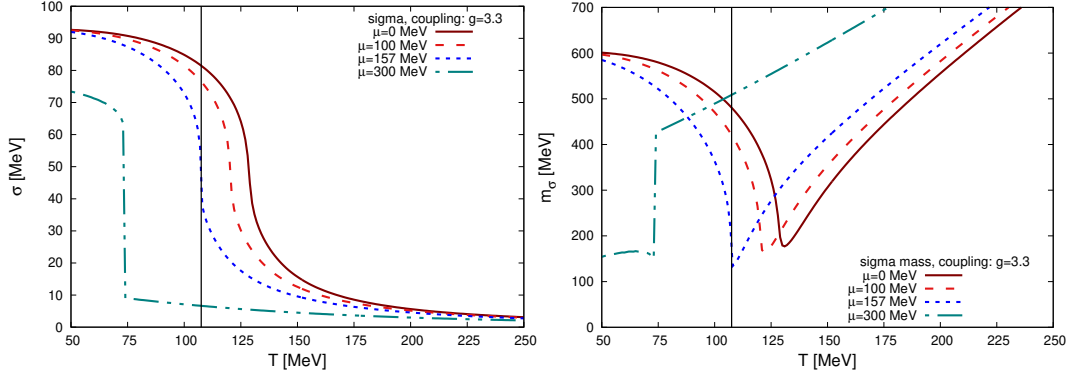


Figure 7: Equilibrium phase diagram of the linear sigma model from self-consistent solving of Eqs. (108) and (109) for the coupling constant $g = 3.3$. Showing the order parameter σ and the effective mass m_σ as a function of the temperature T and several values of the quark chemical potential μ .

Fig. 7 and Fig. 8 show the numerical solution for the order parameter (108) as well as effective mass terms (109) with respect to the temperature and several values of the quark chemical potential μ . Effectively, such a behavior of σ and m_σ is already known from Sec. 2.3, where the variation of the coupling constant g between the chiral field and quarks led to different orders of the phase transition at zero chemical potential (see Fig. 3).

In detail, below $\mu \approx 157$ MeV we find the system in a crossover like state with a smooth structure of the order parameter, which changes for large values of μ to a first-order phase transition with a gap at the corresponding value of the critical temperature. Following that, the phase transition of the first-order has to end up in a critical point of second order with decreasing μ , which is identified in the region of $(T \approx 108$ MeV, $\mu \approx 157$ MeV). Here, it has to be pointed out that the required property of a vanishing sigma mass is not perfectly fulfilled at the critical point, being a consequence of explicit symmetry breaking, renormalization as well as truncation effects of the 2PI action as discussed before, requiring a more detailed study of those contributions in an upcoming work. Note, that the position of the critical point is not a fixed and universal value of the model, more precisely it depends strongly on the value of the coupling constant g to quarks. Therefore, we adjusted the coupling constant in such a way, that the crossover temperature at zero quark chemical potential is still comparable with QCD. Furthermore, the quark chemical potential stays in a range, being still accessible to heavy-ion experiments²⁶ and beyond the region, which is already excluded by experiments and lattice QCD calculations (see Sec. 1).

3.7. Dissipation term

Now, we are prepared to derive a dissipation term, which is consistent with the on-shell approximation of Sec. 3.5, but will partially recover the memory properties of the mean-field and Kadanoff-Baym equations. Doing so, we extend the usual formalism of the inhomogeneous Klein-Gordon as well as Boltzmann-Uehling-Uhlenbeck equation to non-local interactions in time.

As discussed before, for the study of the chiral phase transition we focus on systems with a non-vanishing mean-field for the first component $\phi := \sigma$ of the chiral field $\Phi = (\sigma, \vec{\pi})$ and $\vec{\pi}$ being zero. Thereby, the leading contribution²⁷ to the dissipative part of the mean-field equation follows from the bosonic sunset diagrams:

$$\begin{aligned} \Gamma_2^{\text{b.s.}} = & 3i\lambda^2 \int_C d^4x \int_C d^4y \phi(x) G_{\sigma\sigma}^3(x, y) \phi(y) \\ & + i\lambda^2 \sum_i \int_C d^4x \int_C d^4y \phi(x) G_{\sigma\sigma}(x, y) G_{\pi_i\pi_i}^2(x, y) \phi(y). \end{aligned} \quad (112)$$

²⁶Indeed, it cannot be excluded that the value of the chemical potential for the critical point in QCD, if it exists, is significantly below $T \approx 100$ MeV. In this case it would be hardly possible to find a signal for the phase transition in experimental data.

²⁷Since the coupling constant is large at the phase transition, the relevant parameter is given by the number of involved fields.

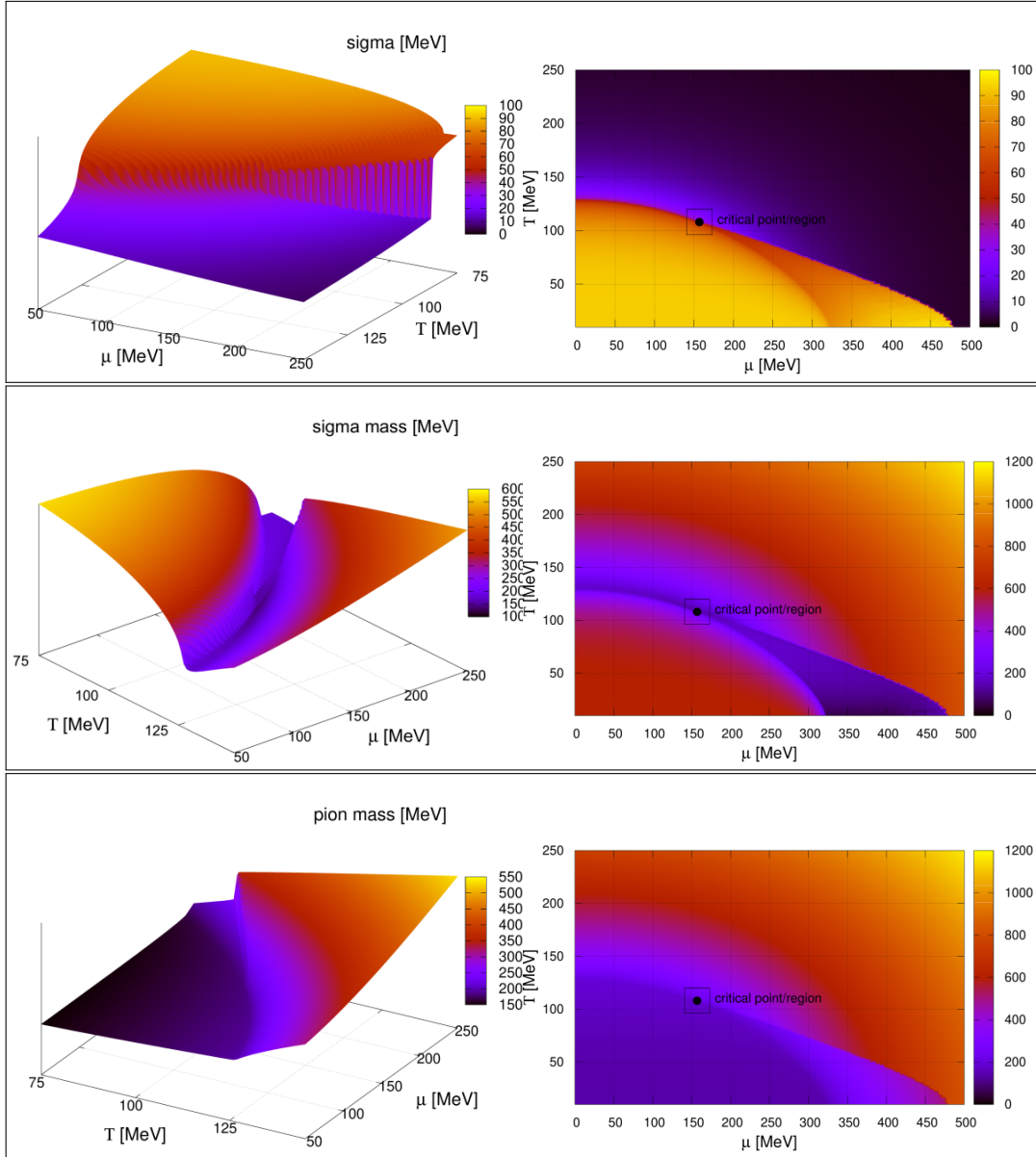


Figure 8: Equilibrium phase diagram of the linear sigma model from self-consistent solving of Eqs. (108) and (109) for the coupling constant $g = 3.3$. The first line shows the order parameter σ as a function of the temperature T and quark chemical potential μ (3-dimensional and 2-dimensional) Analogously, the second and third lines show similar information for the sigma and pion mass.

As shown in the following, this formal expression can be rewritten in terms of a convolution, describing the past-dependent interaction between the mean-field and a memory kernel, which is generated by non-zero modes.

3.8. On-shell approximation of the dissipation term

After taking the functional derivative of (112) with respect to the mean-field evaluated on the upper branch of the real-time contour and splitting the contour integrals, we obtain

$$\begin{aligned}
\frac{\delta\Gamma_2^{\text{b.s.}}}{\delta\phi^1(z)} &= 3i\lambda^2 \int d^4y \left(G_{\sigma\sigma}^{11}(z, y)\right)^3 \phi^1(y) + 3i\lambda^2 \int d^4x \phi^1(x) \left(G_{\sigma\sigma}^{11}(x, z)\right)^3 \\
&\quad - 3i\lambda^2 \int d^4y \left(G_{\sigma\sigma}^{12}(z, y)\right)^3 \phi^2(y) - 3i\lambda^2 \int d^4x \phi^2(x) \left(G_{\sigma\sigma}^{21}(x, z)\right)^3 \\
&\quad + i\lambda^2 \sum_i \int d^4y G_{\sigma\sigma}^{11}(z, y) \left(G_{\pi_i\pi_i}^{11}(z, y)\right)^2 \phi^1(y) \\
&\quad + i\lambda^2 \sum_i \int d^4x \phi^1(x) G_{\sigma\sigma}^{11}(x, z) \left(G_{\pi_i\pi_i}^{11}(x, z)\right)^2 \\
&\quad - i\lambda^2 \sum_i \int d^4y G_{\sigma\sigma}^{12}(z, y) \left(G_{\pi_i\pi_i}^{12}(z, y)\right)^2 \phi^2(y) \\
&\quad - i\lambda^2 \sum_i \int d^4x \phi^2(x) G_{\sigma\sigma}^{21}(x, z) \left(G_{\pi_i\pi_i}^{21}(x, z)\right)^2.
\end{aligned} \tag{113}$$

A similar expression follows also for the lower branch. However, it is sufficient to consider only one of the two branches for the mean-field equation as seen from the general form (71). Applying the relations for the contour Green's functions (32) to (113) and taking the physical solution $\phi^1 \stackrel{\text{!}}{=} \phi^2 \stackrel{\text{!}}{=} \phi$, leads to:

$$\begin{aligned}
D(x) &:= - \left. \frac{\delta\Gamma_2^{\text{b.s.}}}{\delta\phi^1(x)} \right|_{\phi^1=\phi^2=\phi} = - \left. \frac{\delta\Gamma_2^{\text{b.s.}}}{\delta\phi^2(x)} \right|_{\phi^1=\phi^2=\phi} \\
&= -6i\lambda^2 \int d^4y \phi(y) \left[\Theta(x^0 - y^0) \left((iG_{\sigma\sigma}^>(x, y))^3 - (iG_{\sigma\sigma}^<(x, y))^3 \right) \right] \\
&\quad - 2i\lambda^2 \sum_i \int d^4y \phi(y) \left[\Theta(x^0 - y^0) \left(iG_{\sigma\sigma}^>(x, y) \left(iG_{\pi_i\pi_i}^>(x, y) \right)^2 \right. \right. \\
&\quad \quad \quad \left. \left. - iG_{\sigma\sigma}^<(x, y) \left(iG_{\pi_i\pi_i}^<(x, y) \right)^2 \right) \right] \\
&= -6i\lambda^2 \int_{y^0}^{x^0} dy^0 \int d^3\vec{y} \phi(y) \left[\mathcal{M}_{\sigma\sigma}(x, y) + \frac{1}{3} \sum_i \mathcal{M}_{\sigma\pi_i}(x, y) \right],
\end{aligned} \tag{114}$$

where we introduced two kernel functions of the form:

$$\begin{aligned}
\mathcal{M}_{\sigma\sigma}(x, y) &:= (iG_{\sigma\sigma}^>(x, y))^3 - (iG_{\sigma\sigma}^<(x, y))^3, \\
\mathcal{M}_{\sigma\pi_i}(x, y) &:= iG_{\sigma\sigma}^>(x, y) \left(iG_{\pi_i\pi_i}^>(x, y) \right)^2 - iG_{\sigma\sigma}^<(x, y) \left(iG_{\pi_i\pi_i}^<(x, y) \right)^2.
\end{aligned} \tag{115}$$

By considering the limit $y^0 \rightarrow -\infty$ and making use of the relation (75) we rewrite the term (114) for the interaction between the mean-field and hard modes:

$$\begin{aligned}
D(x) &= -6i\lambda^2 \int_{-\infty}^{x^0} dy^0 \int d^3\vec{y} \phi(y) \mathcal{F}_W^{-1} \left[\mathcal{M}_{\sigma\sigma}(x, y) + \frac{1}{3} \sum_i \mathcal{M}_{\sigma\pi_i}(x, y) \right] \\
&= -6i\lambda^2 \int_0^\infty d\Delta t \int \frac{d^4k}{(2\pi)^4} e^{-ik^0\Delta t} e^{i\vec{k}\cdot\vec{x}} \phi(t - \Delta t, \vec{k}) \left[\tilde{\mathcal{M}}_{\sigma\sigma}(X, k) + \frac{1}{3} \sum_i \tilde{\mathcal{M}}_{\sigma\pi_i}(X, k) \right],
\end{aligned} \tag{116}$$

where we introduced a more usual notation with $t := x^0$, $t' := y^0$ and $\Delta t := t - t'$ in the last step, showing explicitly the dependence on the past. Furthermore, we note that a Fourier transformation with respect to k^0 allows us to interpret $\tilde{\mathcal{M}}_{\sigma\sigma}$ and $\tilde{\mathcal{M}}_{\sigma\pi_i}$ as memory kernels, which are explicitly given by Eqs. (A.22) and (A.23).

When the relation (116) is approximated for slowly changing kernel functions with respect to the averaged coordinate X , the one-particle distribution functions $f(t, \vec{x}, \vec{p})$ in Eqs. (A.22), (A.23) can be evaluated at $X \simeq x$. However, one should keep in mind that such an approximation will suffer from causality problems as discussed in Ref. [75]. In comparison to the symmetric kernels of non-zero modes, which are defined in (A.19), the kernels $\tilde{\mathcal{M}}_{\sigma\sigma}$ and $\tilde{\mathcal{M}}_{\sigma\pi_i}$ have qualitatively a similar structure²⁸, but are antisymmetric with respect to k^0 .

With relation (116) the mean-field equation of the order parameter σ becomes (compare with Eq. (71))

$$\partial_\mu \partial^\mu \phi + D(x) + \lambda \left(\phi^2 - v^2 + 3G_{\sigma\sigma}^{11} + \sum_i G_{\pi_i\pi_i}^{11} \right) \phi - f_\pi m_\pi^2 + g \langle \bar{\psi} \psi \rangle = 0, \quad (117)$$

where the terms $G_{\sigma\sigma}^{11} = iG_{\sigma\sigma}^c$ and $G_{\pi_i\pi_i}^{11} = iG_{\pi_i\pi_i}^c$ describe local contributions to the potential, arising from Hartree diagrams. An explicit expression was given in the previous section along with the calculation of the scalar density (see Eqs. (110) and (111)).

For a homogeneous system with initial time t_0 the dissipation term reads

$$D(t) = -6i\lambda^2 \int_0^{t-t_0} d\Delta t \phi(t - \Delta t) \int \frac{dk^0}{(2\pi)} e^{-ik^0\Delta t} \left[\tilde{\mathcal{M}}_{\sigma\sigma}(t, k^0) + \frac{1}{3} \sum_i \tilde{\mathcal{M}}_{\sigma\pi_i}(t, k^0) \right], \quad (118)$$

where the kernels $\tilde{\mathcal{M}}_{\sigma\sigma}(t, k^0)$ and $\tilde{\mathcal{M}}_{\sigma\pi_i}(t, k^0)$ follow directly from the general expressions (A.22), (A.23) with $\vec{k} = 0$ and $X^0 \simeq t$. Since the memory kernels are antisymmetric in k^0 , it is convenient to integrate (118) by parts with respect to the time interval Δt :

$$\begin{aligned} D(t) &= 6\lambda^2 \phi(t - \Delta t) \int \frac{dk^0}{(2\pi)} e^{-ik^0\Delta t} \frac{1}{k^0} \left[\tilde{\mathcal{M}}_{\sigma\sigma}(t, k^0) + \frac{1}{3} \sum_i \tilde{\mathcal{M}}_{\sigma\pi_i}(t, k^0) \right] \Big|_0^{t-t_0} \\ &\quad - 6\lambda^2 \int_0^{t-t_0} d\Delta t \phi'(t - \Delta t) \int \frac{dk^0}{(2\pi)} e^{-ik^0\Delta t} \frac{1}{k^0} \left[\tilde{\mathcal{M}}_{\sigma\sigma}(t, k^0) + \frac{1}{3} \sum_i \tilde{\mathcal{M}}_{\sigma\pi_i}(t, k^0) \right] \\ &= 6\lambda^2 [\Gamma(t, \Delta t = t - t_0) \phi(t_0) - \Gamma(t, \Delta t = 0) \phi(t)] + 6\lambda^2 \int_{t_0}^t dt' \dot{\phi}(t') \Gamma(t, t - t'), \end{aligned} \quad (119)$$

where we introduced a symmetric friction kernel,

$$\Gamma(t, \Delta t) := \int \frac{dk^0}{(2\pi)} e^{-ik^0\Delta t} \frac{1}{k^0} \left[\tilde{\mathcal{M}}_{\sigma\sigma}(t, k^0) + \frac{1}{3} \sum_i \tilde{\mathcal{M}}_{\sigma\pi_i}(t, k^0) \right], \quad (120)$$

to obtain a Langevin-like form (see for example [76, 77, 78]).

The Fourier transformations for the friction kernel (120) and memory kernels (A.20) are numerically evaluated. The pertinent discrete Fourier transform from the energy to time domain introduces an ultraviolet cut-off with respect to the energy k^0 , corresponding to a maximum value of the frequency for the mean-field. In general a sharp cut-off leads to oscillations as well as numerical noise for the Fourier transform. The noise can be significantly reduced by multiplying the memory kernels with a filtering function $S(k^0)$ in the energy domain, continuously suppressing unwanted contributions from high frequencies. In this paper the parametrization for the filtering function is of the form of a Fermi distribution, generating a smooth version of a step function:

$$S(k^0) := \left(\exp\left(\frac{k^0 - \kappa\mu_\phi}{\sigma_\phi}\right) + 1 \right)^{-1}, \quad (121)$$

²⁸This holds true for homogeneous as well as for inhomogeneous systems.

where the product $\kappa\mu_\phi$ defines a typical energy scale beyond which the frequencies are suppressed. The third parameter σ_ϕ denotes then a transition width of the Fermi-like function. In numerical calculations of this paper the parameters are set to $\kappa = 4$, $\mu_\phi := 604$ MeV (standing for the vacuum sigma mass as the relevant estimator of the upper bound for the sigma mass at temperatures below $T \approx 200$ MeV, compare with Fig. 7) and $\sigma_\phi = \mu_\phi/2$.

Illustratively, Fig. 9 shows the memory kernels of the mean field and three explicit momentum modes, thereby the temperature $T \approx 105$ MeV as well as the chemical potential $\mu = 165$ MeV of the system are chosen to be close to the critical point as can also be seen from the position of the peak in the energy domain, moving towards the infrared for decreasing momentum values.

We note, that an effective relaxation time τ for the mean-field can be estimated from the memory kernel by considering the temporal average over the relevant time scale ξ with $\Gamma(t, \Delta t \geq \xi) \approx 0$, leading to $\tau \sim [\xi \langle \Gamma(t, \Delta t) \rangle_{\Delta t < \xi}]^{-1}$. As seen from Fig. 9, the effective relaxation time becomes large near the critical point, emphasizing the requirement for a non-Markovian description in the critical region.

3.9. Linear harmonic approximation of the dissipation term

The physics behind the memory kernels (A.22) and (A.23) becomes more obvious when evaluating the integral (116) in the so-called linear harmonic approximation²⁹,

$$\phi(t - \Delta t, \vec{k}) = \phi(t, \vec{k}) \cos(E_k \Delta t) - \partial_t \phi(t, \vec{k}) \frac{1}{E_k} \sin(E_k \Delta t), \quad (122)$$

which contains much more information about the past in comparison to an instantaneous ansatz for the dynamics of the mean-field as discussed in Ref. [77]. Inserting the expression (122) into the dissipation term (116) requires the evaluation of the following relations:

$$\begin{aligned} C(k^0, E_k) &:= \exp(-ik^0 \Delta t) \cos(E_k \Delta t) \\ &= \frac{1}{2} \left[\exp(i(E_k - k^0) \Delta t) + \exp(-i(E_k + k^0) \Delta t) \right], \\ S(k^0, E_k) &:= \exp(-ik^0 \Delta t) \sin(E_k \Delta t) \\ &= \frac{1}{2i} \left[\exp(i(E_k - k^0) \Delta t) - \exp(-i(E_k + k^0) \Delta t) \right]. \end{aligned} \quad (123)$$

The Fourier transform of a constant function in \mathbb{R}^+ leads to

$$\int_0^\infty \Delta t e^{i(E_k - k^0) \Delta t} = i\mathcal{P} \frac{1}{E_k - k^0} + \pi\delta(E_k - k^0) \quad (124)$$

with \mathcal{P} denoting the Cauchy principal value. Integrating out the Δt -dependence on the past, results then in the following expression:

$$\begin{aligned} \mathcal{I}_{\Delta t} &:= \int_0^\infty d\Delta t e^{-ik^0 \Delta t} \phi(t - \Delta t, \vec{k}) \\ &= \int_0^\infty d\Delta t \left[C(k^0, E_k) \phi(t, \vec{k}) - S(k^0, E_k) \frac{\partial_t \phi(t, \vec{k})}{E_k} \right] \\ &= \left\{ \frac{1}{2} \phi(t, \vec{k}) \left[i\mathcal{P} \frac{1}{E_k - k^0} + \pi\delta(E_k - k^0) - i\mathcal{P} \frac{1}{E_k + k^0} + \pi\delta(E_k + k^0) \right] \right. \\ &\quad \left. - \frac{1}{2i} \frac{\partial_t \phi(t, \vec{k})}{E_k} \left[i\mathcal{P} \frac{1}{E_k - k^0} + \pi\delta(E_k - k^0) + i\mathcal{P} \frac{1}{E_k + k^0} - \pi\delta(E_k + k^0) \right] \right\}. \end{aligned} \quad (125)$$

²⁹The linear harmonic approximation can be understood from considering the differential equation of a simple harmonic oscillator in a field theory.

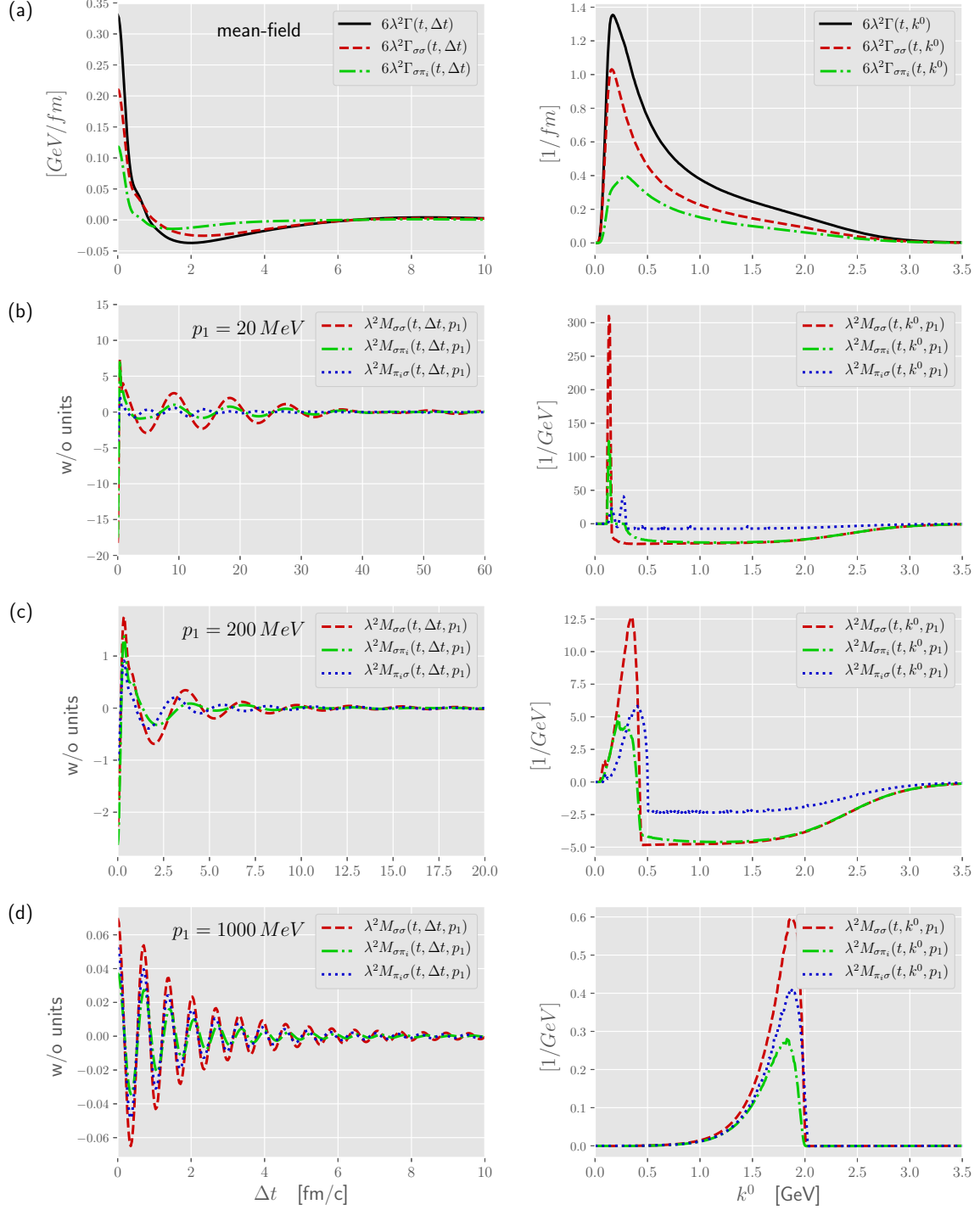


Figure 9: Memory kernels near the critical point ($T \approx 105$ MeV, $\mu = 165$ MeV) for the mean-field as well as three explicit momentum modes in time and energy domains.

With this abbreviation, the general dissipation term (116) can be simplified to

$$D(x) \simeq -6i\lambda^2 \int \frac{d^4k}{(2\pi)^4} e^{i\vec{k}\cdot\vec{x}} \left[\tilde{\mathcal{M}}_{\sigma\sigma}(x, k) + \frac{1}{3} \sum_i \tilde{\mathcal{M}}_{\sigma\pi_i}(x, k) \right] \mathcal{I}_{\Delta t}. \quad (126)$$

From the antisymmetric property of the memory kernels (A.22), (A.23) with respect to k^0 ,

$$\begin{aligned} \tilde{\mathcal{M}}_{\sigma\sigma}(x, k^0, \vec{k}) &= -\tilde{\mathcal{M}}_{\sigma\sigma}(x, -k^0, \vec{k}), \\ \tilde{\mathcal{M}}_{\sigma\pi_i}(x, k^0, \vec{k}) &= -\tilde{\mathcal{M}}_{\sigma\pi_i}(x, -k^0, \vec{k}), \end{aligned} \quad (127)$$

it follows that the on-shell contributions from the δ functions vanish for the ϕ -part of Eq. (125). The same statement holds for the principal values of the $\partial_t\phi$ -part, and one ends up with

$$\begin{aligned} D(x) &\simeq 6\lambda^2 \int \frac{dk^4}{(2\pi)^4} e^{i\vec{k}\cdot\vec{x}} \left[\tilde{\mathcal{M}}_{\sigma\sigma}(x, k) + \frac{1}{3} \sum_i \tilde{\mathcal{M}}_{\sigma\pi_i}(x, k) \right] \phi(t, \vec{k}) \mathcal{P} \frac{1}{E_k - k^0} \\ &+ 6\lambda^2 \int \frac{dk^3}{(2\pi)^3} e^{i\vec{k}\cdot\vec{x}} \left[\tilde{\mathcal{M}}_{\sigma\sigma}(x, E_k, \vec{k}) + \frac{1}{3} \sum_i \tilde{\mathcal{M}}_{\sigma\pi_i}(x, E_k, \vec{k}) \right] \frac{\partial_t \phi(t, \vec{k})}{2E_k}. \end{aligned} \quad (128)$$

For illustration, we explicitly write down the non-Markovian approximation for a homogeneous system,

$$\begin{aligned} D(t) &\simeq 6\lambda^2 \phi(t) \int \frac{dk^0}{(2\pi)} \left[\tilde{\mathcal{M}}_{\sigma\sigma}(t, k^0) + \frac{1}{3} \sum_i \tilde{\mathcal{M}}_{\sigma\pi_i}(t, k^0) \right] \mathcal{P} \frac{1}{E_k - k^0} \\ &+ 6\lambda^2 \dot{\phi}(t) \frac{1}{2E_k} \left[\tilde{\mathcal{M}}_{\sigma\sigma}(t, E_k) + \frac{1}{3} \sum_i \tilde{\mathcal{M}}_{\sigma\pi_i}(t, E_k) \right]. \end{aligned} \quad (129)$$

Thereby, the term with the principal value is an effective mass contribution for the mean-field equation and would require a proper renormalization scheme. However, we expect the resulting shift for the mass spectrum to be small and neglect it in numerical calculations.

3.10. Final set of evolution equations

For homogeneous systems the full set of evolution equations consists of the mean-field equation for the order parameter $\phi := \sigma$,

$$\begin{aligned} \partial_t^2 \phi + D(t) + J(t) &= 0, \\ J(t) &:= \lambda \left(\phi^2 - v^2 + 3G_{\sigma\sigma}^{11} + \sum_i G_{\pi_i\pi_i}^{11} \right) \phi - f_\pi m_\pi^2 + g \langle \bar{\psi} \psi \rangle \end{aligned} \quad (130)$$

with D given by the full non-Markovian Eq. (119) with the divergent mass-contribution (first term) omitted, and of the following evolution equations of Boltzmann type for mesons as well as quarks:

$$\begin{aligned}
\partial_t f^\sigma(t, \vec{p}) &= \mathcal{I}_\sigma^b(t, \vec{p}_1) + \mathcal{I}_\sigma^{b.s.}(t, \vec{p}_1) + \mathcal{I}_\sigma^{f.s.}(t, \vec{p}_1) \\
&= \mathcal{C}_{\sigma\sigma\leftrightarrow\sigma\sigma}^b + \sum_i \mathcal{C}_{\sigma\pi_i\leftrightarrow\sigma\pi_i}^b + \sum_i \mathcal{C}_{\sigma\sigma\leftrightarrow\pi_i\pi_i}^b \\
&\quad + \mathcal{C}_{\sigma\phi\leftrightarrow\sigma\sigma}^{b.s.} + \sum_i \mathcal{C}_{\sigma\phi\leftrightarrow\pi_i\pi_i}^{b.s.} + \mathcal{C}_{\sigma\leftrightarrow\psi\bar{\psi}}^{f.s.}, \\
\partial_t f^{\pi_i}(t, \vec{p}) &= \mathcal{I}_{\pi_i}^b(t, \vec{p}_1) + \mathcal{I}_{\pi_i}^{b.s.}(t, \vec{p}_1) + \mathcal{I}_{\pi_i}^{f.s.}(t, \vec{p}_1) \\
&= \mathcal{C}_{\pi_i\pi_i\leftrightarrow\pi_i\pi_i}^b + \sum_{j\neq i} \mathcal{C}_{\pi_i\pi_j\leftrightarrow\pi_i\pi_j}^b + \sum_{j\neq i} \mathcal{C}_{\pi_i\pi_i\leftrightarrow\pi_j\pi_j}^b + \mathcal{C}_{\pi_i\sigma\leftrightarrow\pi_i\sigma}^b + \mathcal{C}_{\pi_i\pi_i\leftrightarrow\sigma\sigma}^b \\
&\quad + \mathcal{C}_{\pi_i\phi\leftrightarrow\pi_i\sigma}^{b.s.} + \mathcal{C}_{\pi_i\leftrightarrow\psi\bar{\psi}}^{f.s.} \\
\partial_t f^\psi(t, \vec{p}_1) &= \mathcal{I}_\psi^{f.s.}(t, \vec{p}_1) = \mathcal{C}_{\psi\bar{\psi}\leftrightarrow\sigma}^{f.s.} + \sum_i \mathcal{C}_{\psi\bar{\psi}\leftrightarrow\pi_i}^{f.s.} \\
\partial_t f^{\bar{\psi}}(t, \vec{p}_1) &= \mathcal{I}_{\bar{\psi}}^{f.s.}(t, \vec{p}_1) = \mathcal{C}_{\bar{\psi}\psi\leftrightarrow\sigma}^{f.s.} + \sum_i \mathcal{C}_{\bar{\psi}\psi\leftrightarrow\pi_i}^{f.s.},
\end{aligned} \tag{131}$$

where Tab. 2 shows the diagrammatic interpretation of the collision integrals. Their explicit expressions are decomposed with respect to the involved processes in Appendix A.1, leading to Eqs. (A.19), (A.29), (A.30), (A.31).

The non-Markovian mean-field equation (130) is an ordinary integro-differential equation, which can be solved by setting a well-defined initial condition ϕ_0 for the mean-field. In this case the effective mass terms follow then directly from solving the self-consistent relations (109) for general one-particle distribution functions, where the loop integrals are evaluated in accordance with (105), (110) and (111). This procedure requires for instance an improved version of Newton's algorithm for finding minima (respectively roots) of a multidimensional function.

For our study in the following, the evolutions equations (130) can be easily rewritten in an isotropic form by making use of the methods described in Appendix C.1 for bosons and Appendix C.2 for the interaction between bosons and fermions.

4. The chiral phase transition out of equilibrium

The cumulants of conserved quantities are the most promising observables for finding an experimental evidence for the existence of a critical point of the chiral phase transition in QCD. As discussed in the introductory Sec. 1 the cumulant ratios in equilibrium have been studied using various effective models as well as within models derived directly from first principles of QCD [23, 24, 25, 27, 28]. However, the study of the chiral phase transition out of equilibrium with a full spatial dependence is restricted to simplified models, assuming local thermal equilibrium and neglecting for example bosonic, memory and non-Markovian effects [79, 80, 81, 82, 34, 83]. Here, the full set of self-consistent evolution equations of Sec. 3.10³⁰ does not assume local thermal equilibrium and has further advantages by taking also bosonic and memory effects on the level of one-particle distribution functions into account, circumventing thus the impact of stochastic effects as well as the problematic aspect of a finite sample of test particles, which will be discussed in the Sec. 4.2. In its most general form, the numerical solution for the full set of self-consistent evolution equations is computationally highly expensive even for a single simulation run. A study of higher-order cumulants requires many independent runs, resulting in a very large amount of required memory as well as computational time.

Thus, in this paper the focus lies on the dynamical evolution of momentum-dependent cumulants of the initial net-quark density in homogeneous and isotropic systems, allowing to reduce the complexity of the evolution equations of Sec. 3.10 to a feasible level without using further approximations.

Therefore, in the next Sec. 4.1 the derivation procedure is reformulated for the evolution equations of an expanding homogeneous and isotropic system by starting from a Friedmann–Lemaître–Robertson–Walker metric in a spatially

³⁰Note, that the referred set of spatially independent evolution equations can be easily rewritten to a form for non-homogeneous systems.

collision integral	diagram	collision integral	diagram
$C_{\sigma\sigma\leftrightarrow\sigma\sigma}^b.$		$C_{\pi_i\pi_i\leftrightarrow\pi_i\pi_i}^b.$	
$C_{\sigma\pi_i\leftrightarrow\sigma\pi_i}^b.$		$C_{\pi_i\pi_j\leftrightarrow\pi_i\pi_j}^b.$	
$C_{\sigma\sigma\leftrightarrow\pi_i\pi_i}^b.$		$C_{\pi_i\sigma\leftrightarrow\pi_i\sigma}^b.$	
$C_{\sigma\phi\leftrightarrow\sigma\sigma}^{b.s.}$		$C_{\pi_i\pi_i\leftrightarrow\pi_j\pi_j}^b.$	
$C_{\sigma\phi\leftrightarrow\pi_i\pi_i}^{b.s.}$		$C_{\pi_i\pi_i\leftrightarrow\sigma\sigma}^b.$	
$C_{\sigma\leftrightarrow\psi\bar{\psi}}^{f.s.}$		$C_{\pi_i\phi\leftrightarrow\pi_i\sigma}^{b.s.}$	
$C_{\psi\bar{\psi}\leftrightarrow\sigma}^{f.s.}$		$C_{\pi_i\leftrightarrow\psi\bar{\psi}}^{f.s.}$	
$C_{\bar{\psi}\psi\leftrightarrow\sigma}^{f.s.}$		$C_{\psi\bar{\psi}\leftrightarrow\pi_i}^{f.s.}$	
		$C_{\psi\psi\leftrightarrow\pi_i}^{f.s.}$	

Table 2: Collision integrals and their diagrammatic interpretation for the set of evolution equations in (131).

flat geometry. The result is then applied to the set of equations of Sec. (3.10), making it suitable for the study of the dynamical evolution of the net-quark number in expanding geometry, which mimics an expanding spherical domain in a heavy ion collision with a decreasing net-quark density during the expansion process. We also describe the numerical implementation in detail and show that in our approach the net-quark number is conserved to a high level of accuracy within $\sim 0.5 - 1.5 \%$ even for rapidly expanding systems with $v \leq 0.8c$.

In the subsequent Sec. we discuss the initial conditions for the expanding geometry. Being interested in the cumulants of the net-quark number, we introduce two types of statistical ensembles for the initial configurations with a fluctuating net-quark number, which are studied throughout the last section. Thereby, both approaches are based on initial fluctuations of Gaussian type for the total net-quark number, differing in volume and net-quark density fluctuations.

Following the initialization methods, we discuss a crucial advantage of our approach on the level of one-particle distribution functions in comparison to test-particle approaches by showing that a pseudo-stochastic initialization procedure within our framework significantly outperforms naive Monte Carlo methods, which are generally used for test particles.

The final Sec. then shows a broad study of averaged ensemble quantities like the averaged quark chemical potential, the temperature, the order parameter and so forth as a function of the evolving (proper) time. Moreover, we then discuss a possible signature for the experimental confirmation of the chiral phase transition in a heavy-ion collision, by analyzing our results for the cumulant ratios, the rescaled kurtosis, in various momentum ranges, which depend strongly on the trajectories of the statistical ensembles for the initial configuration when passing through the chiral phase transition in the comover region, or passing close to the critical point, or passing through a full first-order phase transition regime.

4.1. Evolution equations in expanding geometry

For deriving evolution equations of an expanding homogeneous and isotropic system it is convenient to start from the Friedmann–Lemaître–Robertson–Walker (FLRW) metric in Cartesian coordinates and vanishing curvature (spatially flat geometry) as described for instance in [84, 85, 86]:

$$ds^2 = dt^2 - a^2(t) (dx_1^2 + dx_2^2 + dx_3^2) \Rightarrow g_{00} = 1, g_{i0} = g_{0i} = 0, g_{ij} = -a^2(t) \delta_{ij}, \quad (132)$$

where $a(t)$ denotes a time-dependent expansion scale as known from cosmological models of the Universe. The Christoffel symbols of the metric (132) can be easily calculated as

$$\Gamma_{\nu\sigma}^\mu = \frac{1}{2} g^{\mu\lambda} (\partial_\nu g_{\sigma\lambda} + \partial_\sigma g_{\nu\lambda} - \partial_\lambda g_{\nu\sigma}) \Rightarrow \Gamma_{ij}^0 = a\dot{a}\delta_{ij}, \Gamma_{0j}^i = \Gamma_{j0}^i = \frac{\dot{a}}{a} \delta_j^i, \Gamma_{jk}^i = 0. \quad (133)$$

One can now rewrite the evolution equations for one-particle distribution functions (131) by taking the expansion via the metric into account. Therefore, we explicitly calculate the general expression of the Liouville operator, defined by the left-hand side of the Boltzmann equation in an arbitrary spacetime geometry. Starting from the covariant expression for the distribution function $f = f(x^\mu, P^\mu)$ and taking its derivative with respect to an affine parameter λ , leads to:

$$\frac{df}{d\lambda} = \frac{\partial f}{\partial x^\mu} \frac{dx^\mu}{d\lambda} + \frac{\partial f}{\partial P^\mu} \frac{dP^\mu}{d\lambda} = P^\mu \frac{\partial f}{\partial x^\mu} - \Gamma_{\nu\sigma}^\mu P^\nu P^\sigma \frac{\partial f}{\partial P^\mu}, \quad (134)$$

where the second equality follows from the geodesic equation, describing particle propagation in curved coordinates,

$$\begin{aligned} \frac{dx^\mu}{d\lambda} &= P^\mu, & \frac{d^2 x^\mu}{d\lambda^2} &= \frac{dP^\mu}{d\lambda} = -\Gamma_{\nu\sigma}^\mu P^\nu P^\sigma \\ & & \Rightarrow \frac{dP^0}{d\lambda} &= -\Gamma_{ij}^0 P^i P^j = -a\dot{a} \vec{P}^2 \\ & & \frac{dP^i}{d\lambda} &= -2\Gamma_{0j}^i P^0 P^j - \Gamma_{jk}^i P^j P^k = -2\frac{\dot{a}}{a} P^0 P^i. \end{aligned} \quad (135)$$

Consequently, the general evolution equation becomes

$$\frac{df}{d\lambda} = P^0 \frac{\partial f}{\partial t} + \vec{P} \cdot \nabla_{\vec{x}} f - 2 \frac{\dot{a}}{a} P^0 P^i \frac{\partial f}{\partial P^i} - a \dot{a} \vec{P}^2 \frac{\partial f}{\partial P^0}. \quad (136)$$

Since we are interested in homogeneous systems, all explicit dependencies on spatial coordinates will be dropped in the following. In analogy to the calculation of Sec. 3.5, it is convenient to integrate out the energy dependence, leading to the relativistic dispersion relation,

$$P^2 = g_{\mu\nu} P^\mu P^\nu = (P^0)^2 - a^2 \vec{P}^2 = m^2, \quad (137)$$

which then allows to introduce the so-called physical or proper momentum $p^i := a P^i \Rightarrow \vec{p}^2 = -g_{ij} P^i P^j$. Furthermore, we obtain a simplified expression by taking into account that the distribution function depends only *implicitly* on the energy $p^0 := P^0 = \sqrt{\vec{p}^2 + m^2}$ in comparison to (136):

$$\frac{df}{d\lambda} = \frac{\partial f}{\partial x^0} \frac{dx^0}{d\lambda} + \frac{\partial f}{\partial P^i} \frac{dP^i}{d\lambda} = P^0 \frac{\partial f}{\partial t} - 2 \frac{\dot{a}}{a} P^0 P^i \frac{\partial f}{\partial P^i}. \quad (138)$$

Making use of $P^i(a, p^i)$ being a function of the time-dependent scale factor a and the proper momentum p^i , we can rewrite the expression (138) in the form

$$\frac{df}{d\lambda} = P^0 \frac{\partial f}{\partial t} + \frac{\partial f}{\partial P^i} \left(\frac{1}{a} \frac{dp^i}{d\lambda} - \frac{1}{a^2} \frac{da}{d\lambda} \frac{dx^0}{d\lambda} p^i \right) = P^0 \frac{\partial f}{\partial t} + \frac{\partial f}{\partial P^i} \left(\frac{1}{a} \frac{dp^i}{d\lambda} - \frac{\dot{a}}{a} P^0 P^i \right) \quad (139)$$

and thus

$$\frac{dp^i}{d\lambda} = \frac{da}{dx^0} \frac{dx^0}{d\lambda} P^i + a \frac{dP^i}{d\lambda} = -\frac{\dot{a}}{a} P^0 P^i. \quad (140)$$

Consequently, the dynamical evolution of the one-particle distribution function can be written in terms of the proper momentum $p^i(a, P^i)$, resulting in

$$\frac{df}{d\lambda} = \frac{\partial f}{\partial x^0} \frac{dx^0}{d\lambda} + \frac{\partial f}{\partial p^i} \frac{dp^i}{d\lambda} = P^0 \frac{\partial f}{\partial t} - \frac{\dot{a}}{a} P^0 P^i \frac{\partial f}{\partial P^i}. \quad (141)$$

After introducing the usual abbreviation $H := \dot{a}/a$, known as Hubble constant, we finally arrive at

$$\left(\frac{\partial}{\partial t} - H p \frac{\partial}{\partial p} \right) f = \mathcal{I}(t, p) \quad \text{with} \quad H p \frac{\partial}{\partial p} = H p^i \frac{\partial}{\partial P^i}, \quad (142)$$

with p^0 being absorbed in the collision integral $\mathcal{I}(t, p)$.

Integrating by parts leads then to the evolution equation of particle densities

$$\int \frac{d^3 \vec{p}}{(2\pi)^3} \left(\frac{\partial f}{\partial t} - H p \frac{\partial f}{\partial p} \right) = \int \frac{d^3 \vec{p}}{(2\pi)^3} \mathcal{I}(t, p) \Rightarrow \dot{n} + 3Hn = \int \frac{d^3 \vec{p}}{(2\pi)^3} \mathcal{I}(t, p). \quad (143)$$

The net number of quarks/baryons $N_{q,\text{net}}$ in an expanding domain with volume $V(t)$ is a strictly conserved quantity, as long as the interaction with other domains is not possible. Therefore, it holds $N_{q,\text{net}} \equiv n_{q,\text{net}} V = \text{const.}$ and one obtains the following relations between the spherical volume V , its radius R and the internal scale factor a :

$$\frac{\dot{V}}{V} - 3H = 0 \quad \Rightarrow \quad \frac{\dot{a}}{a} = \frac{\dot{R}/R_0}{R/R_0}. \quad (144)$$

The general approach with FLRW metric allows to choose between various parametrizations for the radius as a function of time. Thereby, an application to heavy-ion collisions is constrained by physical requirements of a casual

evolution for the expansion³¹. A possible and rather simple parametrization, used in the following, is given by a linear growth of the radius with a constant expansion velocity $v_e < c$,

$$R(t) = R(t_0) + v_e t. \quad (145)$$

The mean-field equation in an expanding homogeneous and isotropic three-dimensional geometry can be described by transforming the d'Alembert operator with respect to the FLRW metric (see for instance [87]):

$$\eta^{\mu\nu} \nabla_\mu \nabla_\nu = \left(\partial_t^2 - \partial_{\vec{x}}^2 \right) \longrightarrow g^{\mu\nu} \nabla_\mu \nabla_\nu = \frac{1}{\sqrt{-g}} \partial_\mu \left(\sqrt{-g} g^{\mu\nu} \partial_\nu \right) = \partial_t^2 + 3H \partial_t - a^2 \partial_{\vec{x}}^2 = \partial_t^2 + 3H \partial_t \quad (146)$$

Here, the damping coefficient $3H$ is directly related to the volume increase in (144). Finally, the mean-field equation (130) becomes

$$\partial_t^2 \phi + E(t) + D(t) + J(t) = 0 \quad \text{with} \quad E(t) := 3H \partial_t \phi \quad (147)$$

with D defined by (129). For expanding geometry the full set of evolution equations consists of the mean-field equation (147) and Eq. (142) for every particle species. Finally, the collision integrals are calculated as in the case without expansion.

The evolution equation for one-particle distribution functions is solved numerically by discretizing Eq. (142) in accordance with the linear-implicit finite difference scheme, meaning that the term including the operator $A := H p \frac{\partial}{\partial p}$ is evaluated at the final time $t_i + \Delta t$, whereas the collision term \mathcal{I} is evaluated at the initial time t_i ,

$$\frac{f_{i+1} - f_i}{\Delta t} = A f_{i+1} + \mathcal{I}_i \quad \Rightarrow \quad f_{i+1} = (\mathbb{1} - \Delta t A)^{-1} (f_i + \Delta t \mathcal{I}_i). \quad (148)$$

The linear-implicit evaluation of the Integro-PDE improves significantly the stability region of the finite difference method (see [88] and references therein). Because of the weighted left-shift operator A , generating a particle flow to the infrared region, the derivative in momentum space is discretized in accordance to the upwind scheme for the first two grid points of the one-particle distribution function $f_{i,j}$ with $j \in \{1, \dots, N\}$. This procedure does not require to specify a boundary condition for the infrared region. The intermediate region is then discretized by applying a central differencing scheme, being an approximation of second order with respect to the momentum interval Δp :

$$A = \frac{H}{\Delta p} \begin{pmatrix} -p^1 & p^1 & 0 \\ -p^2 & 0 & p^2 \\ & \ddots & \\ & -p^{N-1} & 0 & p^{N-1} \\ & 0 & -p^N & p^N \end{pmatrix}, \quad (149)$$

where the last line of the discrete operator in matrix representation is used to specify a boundary condition for the highest momentum on the grid, given here by the backward scheme of the first-order derivative. An alternative boundary condition is given by a vanishing first-order derivative with respect to the absolute value of the momentum $d f / d p|_{p=p^N} = 0$, resulting in a zero line for the last row of the matrix. The mean-field equation (147) is discretized by replacing exact derivatives with corresponding second-order finite differences, leading to the following scheme:

$$\begin{aligned} \frac{\phi_{i+1} - 2\phi_i + \phi_{i-1}}{\Delta t^2} + 3H \frac{\phi_{i+1} - \phi_{i-1}}{2\Delta t} + D_i + J_i &= 0 \\ \Rightarrow \phi_{i+1} &= \left(1 + 3H \frac{\Delta t}{2} \right)^{-1} \left(2\phi_i - \phi_{i-1} \left(1 - 3H \frac{\Delta t}{2} \right) - (D_i + J_i) \Delta t^2 \right). \end{aligned} \quad (150)$$

In the following we are interested in studying fluctuations of the net-quark number in various momentum regions, but requiring that the total quantity has to be conserved. Fig. 10 explicitly shows that the the total net-quark number is indeed conserved to a high accuracy of 0.5% – 1.5% even for large running times $t_{\text{run}} = 12.5 - 100 \text{ fm}/c$. Thereby, test simulations were performed for a wide range of expansion velocities $v_{\text{exp}} = 0.1 - 0.8 c$ as well as initial and final radii. Note, that for the parametrization (145), the running time of a simulation is defined via the relation $t_{\text{run}} = (R(t_f) - R(t_0)) / v_{\text{exp}}$.

³¹This is not required for the expansion of the universe, which can exceed the speed of light.

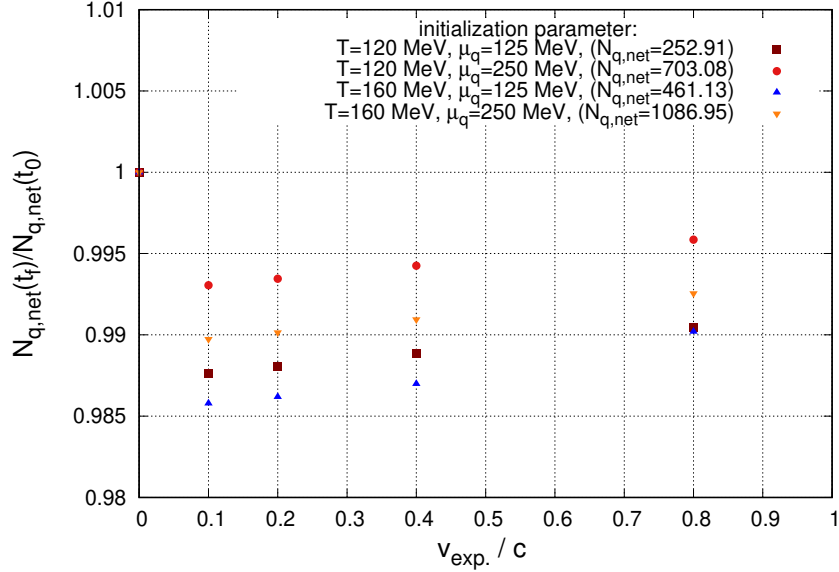


Figure 10: Ratio of the final over the initial net quark number for different initial conditions $T, \mu_q (N_{q,\text{net}})$ and expansion velocities v_{exp} . The initial and final radii of the system are set to $R(t_0) = 5$ fm, respectively $R(t_f) = 15$ fm.

4.2. Initial conditions for expanding geometry

As already discussed in the previous Section, the expansion description in the following models homogeneous and isotropic systems. Therefore, it is required to introduce fluctuating initial conditions for the net-quark number and consider dynamical long-time fluctuations with respect to *different momentum ranges* instead of widely studied long-range fluctuations due to spatial inhomogeneities. In detail, we consider a spherically symmetric bubble/domain with radius R_0 , which is modelled to expand according to the evolution equations of Sec. 4.1. Thereby, the medium inside the bubble is initialized in thermal equilibrium $(T_0, \mu_{q,0})$ and the fluctuations of the initial net quark number are modelled via the Gaussian distribution,

$$N_{q,\text{net}} \sim \mathcal{N}(\langle N_{q,\text{net}} \rangle, \sigma_{q,\text{net}}^2), \quad (151)$$

where $\langle N_{q,\text{net}} \rangle$ denotes the mean of the Gaussian distribution and $\sigma_{q,\text{net}}^2$ its variance. For the thermal choice of $(T_0, \mu_{q,0})$ the mean value of the Gaussian distribution is defined by calculating the net-quark number inside of the spherical domain with $R = R_0$,

$$\langle N_{q,\text{net}} \rangle := n_{q,\text{net}} V = \frac{4}{3} \pi R_0^3 \int \frac{d^3 \vec{p}}{(2\pi)^3} (f_q - f_{\bar{q}}), \quad (152)$$

being a strictly conserved quantity as already discussed in Sec. 4.1. Numerically, the conservation property acts as a necessary condition to ensure a stable and precise result. The standard deviation in our Gaussian description of initial fluctuations in the total number of net quarks is a parameter and will be set to $\sigma_{q,\text{net}} = \langle N_{q,\text{net}} \rangle / 10$ (or also $\sigma_{q,\text{net}} = \langle N_{q,\text{net}} \rangle / 5$), being an arbitrary but reasonable choice of relatively small fluctuations for the net-quark number as one would expect in a fixed-target experiment or in a well defined centrality class of a collider. However, as shown in the following, the absolute value of the standard deviation does not change the qualitative results of the study. As expected naively, the amplitude of net-quark-number fluctuations increases with an increasing value of the standard deviation, without changing significantly the shape of the cumulants and their ratios.

The cumulants of an arbitrary distribution function can be expressed in terms of centralized moments³² $\tilde{m}_k :=$

³²In contradistinction to the moments, the cumulants are pairwise independent quantities of the corresponding distribution function.

$\langle (m - \langle m \rangle)^k \rangle$. In detail, the first six cumulants are given by

$$\begin{aligned}
\kappa_1 &= \langle m \rangle, \\
\kappa_2 &= \tilde{m}_2 \equiv \sigma^2, \\
\kappa_3 &= \tilde{m}_3, \\
\kappa_4 &= \tilde{m}_4 - 3\tilde{m}_2^2, \\
\kappa_5 &= \tilde{m}_5 - 10\tilde{m}_3\tilde{m}_2, \\
\kappa_6 &= \tilde{m}_6 - 15\tilde{m}_4\tilde{m}_2 - 10\tilde{m}_3^2 + 30\tilde{m}_2^3,
\end{aligned} \tag{153}$$

where only the first two are non-zero in the case of a Gaussian distribution function. Note, when later integrating the phase distribution over *all* momenta, only the first two moments should be non-zero. On the other hand, when looking in special momentum classes, this may not be the case and can establish the potential critical fluctuations close to the phase transition region. The other momentum regions can act as an effective particle and heat bath, allowing diffusion into the particular momentum region.

From these moments one can introduce a second class of observables, given by the following ratios of even and odd cumulants:

$$R_{4,2} = \frac{\kappa_4}{\kappa_2}, \quad R_{6,2} = \frac{\kappa_6}{\kappa_2}, \quad R_{3,1} = \frac{\kappa_3}{\kappa_1}, \quad R_{5,1} = \frac{\kappa_5}{\kappa_1}, \tag{154}$$

where $R_{4,2}$ is known as the rescaled excess kurtosis $\kappa\sigma_2$ (see also Sec. 1). Especially, the last type of observables is sensitive to a critical behavior at the phase transition, since all of the ratios in (154) have a non-trivial dependence on the correlation scale³³ and become zero in case of a Gaussian distribution function.

The most natural way of studying fluctuations is to consider a large set of stochastically independent, but equally distributed initial conditions as one also expects for independent heavy ion collisions. From a numerical point of view the initialization procedure can be modeled by Monte Carlo methods, which are suited to generate systems with stochastic initial conditions. Nevertheless, at least simple MC methods are known for having a very slow convergence rate to the exact distribution function³⁴, being the main reason for the usage of so-called quasi-MC or pseudo-stochastic methods, which are more suitable for studying higher order cumulants, especially when the computational time plays a significant role. In our approach, we use a pseudo-stochastic approach for the initialization of independent configurations, which significantly improves the convergence rate to the exact cumulant ratios as discussed in the following.

As already introduced in Eq. (151), the initial probability density of the net quark number is modeled by the Gaussian distribution function,

$$\varrho(N_{q,\text{net}}) = \frac{1}{\sigma_{q,\text{net}} \sqrt{2\pi}} \exp\left(-\frac{(N_{q,\text{net}} - \langle N_{q,\text{net}} \rangle)^2}{2\sigma_{q,\text{net}}^2}\right). \tag{155}$$

Consequently, a numerical simulation requires an initialization procedure of initial configurations with respect to this distribution function. In detail, for a pseudo-stochastic approach it is required to introduce a grid in a range of allowed net-quark numbers. Thereby, a physical choice for heavy-ion systems is restricted by a lower boundary of $N_{q,\text{net}} \geq 0$. Because of symmetry and variance reduction reasons, it is reasonable to set the upper boundary to $N_{q,\text{net}} \leq 2\langle N_{q,\text{net}} \rangle$ for $\sigma_{q,\text{net}} \ll \langle N_{q,\text{net}} \rangle$ and distribute the grid points for different initial configurations within the range of $[0, 2\langle N_{q,\text{net}} \rangle]$. Even so, the convergence rate can be improved by using non-uniform grid points for the initial net-quark number, it is sufficient to discretize the above range with an equidistant spacing of the form $\Delta N_{q,\text{net}} := 2\langle N_{q,\text{net}} \rangle / M$ for $M + 1$ independent initial configurations, leading to the grid points $N_{q,\text{net},k} = k\Delta N_{q,\text{net}}$ with $k \in \{0, \dots, M\}$. This set defines a

³³In the present study the relevant correlation scale is given by the correlation time of net-quark-number fluctuations in different momentum ranges.

³⁴In general, even a small deviation from the exact shape of the distribution function means that its tails cannot be reproduced at all, leading for higher order cumulants to huge uncertainties.

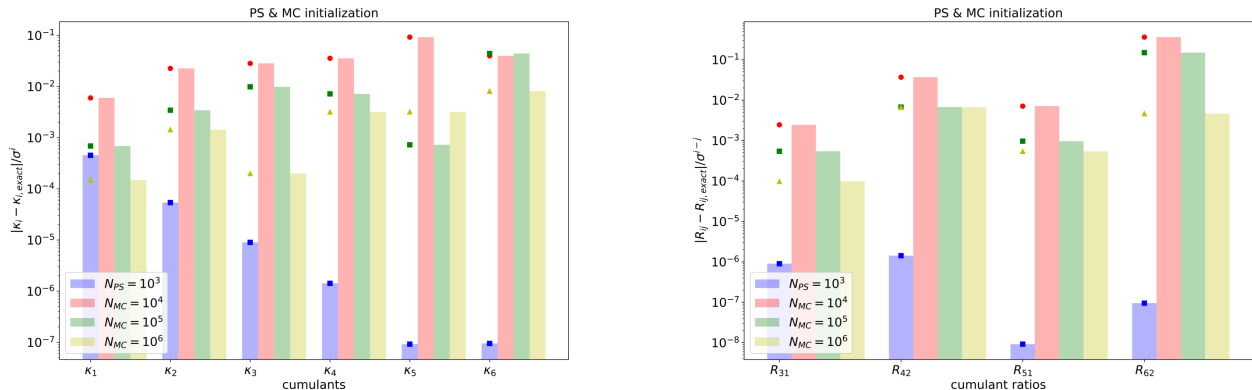


Figure 11: Left: Dimensionless error for cumulants of the total net-quark number for different numbers of independent initial configurations, which are generated/sampled with the pseudo-stochastic as well as MC methods from the Gaussian distribution function (155). Right: The same for the dimensionless error of cumulant ratios.

test sample of initial values for the net quark number. For each value of the test sample only one simulation run has to be performed and the final result for an arbitrary observable \mathbf{O} follows then from calculating the expectation value of the observable with respect to the test sample,

$$\langle \mathbf{O} \rangle = \frac{p_0 \mathbf{O}_0 + p_M \mathbf{O}_M}{2} + \sum_{k=1}^{M-1} p_k \mathbf{O}_k, \quad p_k = \varrho(N_k) / M. \quad (156)$$

Fig. 11 shows a numerical comparison between naive MC sampling for different numbers of initial configurations N_{MC} and pseudo-stochastic (PS) initialization method for N_{PS} grid points as described above. The numerical results are compared with exact values for the distribution function (155) by introducing a dimensionless form of observables from Eqs. (153) and (154)

$$\text{err}_\kappa := \frac{|\kappa_i - \kappa_{i,\text{exact}}|}{(\sigma_{q,\text{net}})^i}, \quad \text{err}_R := \frac{|R_{ij} - R_{ij,\text{exact}}|}{(\sigma_{q,\text{net}})^{i-j}}, \quad (157)$$

where the cumulants κ_i naturally may scale with the standard deviation $\sigma_{q,\text{net}}$ to the power i . Also note that the cumulants $\kappa_{i,\text{exact}} \equiv 0$ for $i > 2$.

Here, the initialization procedure is also compared to a naive MC method as shown in Fig. 11 for different numbers of independent initial configurations. As seen from the comparison, even for very large test samples of MC initializations the pseudo-stochastic method outperforms the naive MC sampling by up to five orders of magnitude for the predefined errors, given by Eq. (157). Note, that a typical simulation run with only one initial configuration requires 1 – 100 hours of computational CPU time, depending on the expansion velocity (see Tab. 3 and Sec. 4.3). Consequently, a simple MC approach is not applicable, since even $N_{MC} = 10^6$ of initial configurations result in a rather poor convergence rate. In the following calculations we restrict the number of independent pseudo-stochastic initial configurations for a single run to $N_{PS} = 100 - 1000$, resulting in a total computational CPU time of $t_{\text{run}} = 10^3 - 10^4$ hours per run.

At this point, we emphasize that our approach, which is based on one-particle distribution functions, has a crucial advantage in comparison to a test particle approach, when studying net-quark-number fluctuations. The pseudo-stochastic initialization procedure ensures not only the correct total number of net quarks on average but also the correct (on average) number of net quarks in an arbitrary sub-range of the momentum space, which is not realized in a test-particle approach even for very high statistics. Particularly, in case of test particles one is restricted to MC methods, making those approaches not suitable for higher-order-cumulant studies of the net-quark number in an arbitrary momentum range since test-particle approaches suffer from the same difficulties as shown in Fig. 11 for every single momentum range.

Before focusing on expanding systems in the next Sec. 4.3, it is required to specify statistical ensembles of initial configurations, which are used in the following. As described above, the initial number of net quarks $N_{q,\text{net}}$ is initialized according to the Gaussian distribution function (155), where $\langle N_{q,\text{net}} \rangle$ is given by the relation (152) with a

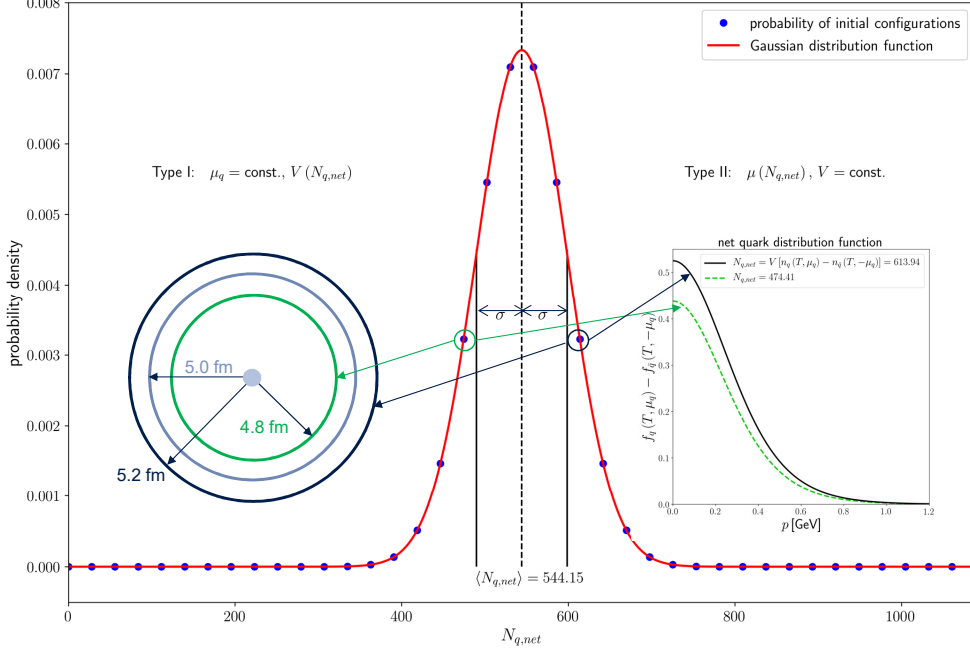


Figure 12: Schematic initialization procedure for two types of initial conditions with respect to a Gaussian distribution function of net quarks. For illustrative reasons, the temperature is set to $T = 150$ MeV and the quark chemical potential to $\mu_q(\langle N_{q,net} \rangle) = 160$ MeV, defining the mean for the Gaussian distribution function $\langle N_{q,net} \rangle = 544.15$. The standard deviation is chosen to be $\sigma_{q,net} = \langle N_{q,net} \rangle / 10 = 54.415$. All averaged observables from numerical calculations are computed with respect to the numerical distribution function of initial configurations, given by the blue points. The net-quark number from a certain initial configuration is transformed into a fluctuation of the radius scale $R(N_{q,net})$ (type I) or into a fluctuation of the chemical potential $\mu_q(N_{q,net})$ (type II) as shown schematically. The effective distribution function of the radius scale as well as the effective distribution function of the chemical potential are shown in Fig. 13. See also Tab. 3 and the text for more details.

certain choice of T and $\mu_q(\langle N_{q,net} \rangle)$. Now, we define two statistical ensembles with a fluctuating net-quark number: The first type is given by holding the physical parameters T , μ_q constant and changing the radius scale R for the size of the initial domain, so that a spherical volume with radius $R(N_{q,net})$ contains the required net quark number $N_{q,net}$ from the Gaussian sampling procedure. Similarly, the second type is given by holding the physical parameters R , T constant and adjusting $\mu_q(N_{q,net})$ in a self-consistent way, so that a spherical volume with radius $R = 5$ fm contains the required net quark number $N_{q,net}$. The type II may be considered to be more close to the experimental setting for various collision centralities. Both initialization procedures are shown schematically in Fig. 12. Furthermore, the general parameters of the corresponding statistical ensembles are summarized in Tab. 3, and Fig. 13 shows the resulting distribution functions for $R(N_{q,net})$ in case of type I and for $\mu_q(N_{q,net})$ in case of type II.

We close this Section with illustrating and demonstrating the purpose of the two types of fluctuations as just described and calculate the cumulant ratios $R_{3,1}$ and $R_{4,2}$ in thermal equilibrium for the quark-meson σ -model as described in Sec. 3: For a test sample of type I (see Tab. 3), fluctuations in momentum space can be expected only for systems out of equilibrium, since the one-particle distribution function of quarks is equal for all independent configurations of a certain choice of T and $\mu_q(\langle N_{q,net} \rangle)$. Hence, the higher-order cumulants have to vanish also in each different and specified momentum window. Therefore, we only show the calculation of cumulant ratios in equilibrium

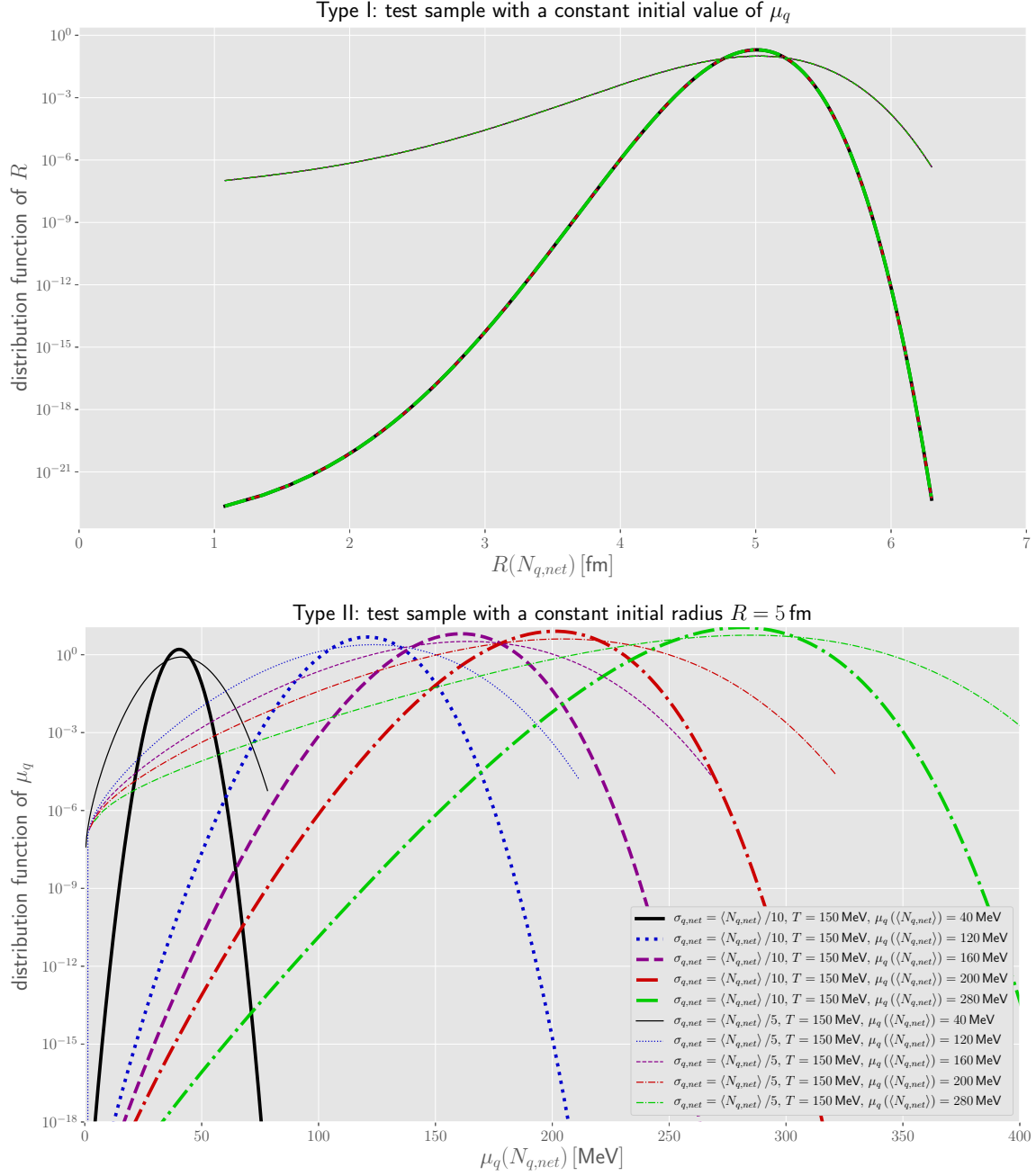


Figure 13: Upper figure: distribution function of the initial radius $R(N_{q,net})$ for the statistical ensemble with initial configuration of type I. Lower figure: distribution function of the quark chemical potential $\mu_q(N_{q,net})$ for the statistical ensemble with initial configuration of type II (compare with Tab. 3 and Fig. 12). Both are shown for $T = 150$ MeV and various values of the quark chemical potential $\mu_q(\langle N_{q,net} \rangle)$ as well as two different values of $\sigma_{q,net}$ (thick lines for $\langle N_{q,net} \rangle / 10$, thin lines for $\langle N_{q,net} \rangle / 5$), denoting the standard deviation of the Gaussian distribution (155).

type	initial condition	$R(\langle N_{q,\text{net}} \rangle)$ [fm]	$R(N_{q,\text{net}})$ [fm]	T	$\mu_q(N_{q,\text{net}})$	v	N_{PS}	$\sigma_{q,\text{net}}$
I	Gaussian	5.0	$\left(\frac{3}{4\pi} \frac{N_{q,\text{net}}}{n_{q,\text{net}}}\right)^{1/3}$	const.	const.	0.05 – 0.8	$10^2 - 10^3$	$\langle N_{q,\text{net}} \rangle / 10$
II	Gaussian	5.0	5.0	const.	variable	0.05 – 0.8	$10^2 - 10^3$	$\langle N_{q,\text{net}} \rangle / 10$

Table 3: Initial parameters for two different types of initial conditions:

I. The first type stands for a fixed combination of the temperature T and chemical potential $\mu_q(\langle N_{q,\text{net}} \rangle)$. Here, the radius of the system is adjusted to match the net quark number from the Gaussian sampling procedure.

II. The second type stands for a fixed combination of the temperature T and initial radius $R_0 = 5$ fm. Here, the chemical potential of quarks $\mu_q(N_{q,\text{net}})$ is adjusted to match the net quark number from the Gaussian sampling procedure, requiring a self-consistent initialization method.

to initial conditions of type II (see Tab. 3), where the net-quark number $N_{q,\text{net}}$ from the sampling procedure defines the chemical potential $\mu_q(N_{q,\text{net}})$ of quarks for a fixed value of T . For each combination of T and $\mu_q(\langle N_{q,\text{net}} \rangle) \Leftrightarrow \langle N_{q,\text{net}} \rangle$, we initialize $N_{PS} = 1000$ of independent initial configurations according to the Gaussian distribution function (155) as described above. Following that, we compute the fluctuations of the net quark number by cumulants and their ratios (see Eqs. (153) and (154)) for different momentum ranges by assuming thermal as well as chemical equilibrium for the quark distribution functions of the quark-meson σ -model. The final result for the cumulant ratios $R_{3,1}$ and $R_{4,2}$ is depicted in Figs. 14 and 15 with respect to T , $\mu_q(\langle N_{q,\text{net}} \rangle)$ as well as five momentum intervals. In both cases the ratios show a critical and even divergent behavior near the phase transition (see the phase diagram in Sec. 3 and also compare to Fig. 16, where the net-quark density is given for various isotherms as function of μ_q). Especially, in the vicinity of the critical point for $\mu_q = 160$ MeV and $T \approx 108$ MeV there is a remarkable sign change in the cumulant ratios. This observation underlines the fact that the cumulant ratios of the net-quark number in momentum space are suitable observables for studying the chiral phase transition within our approach. A careful discussion for these findings of the cumulant ratios we postpone to the next section, when we consider that the physical system expands and cools through the phase diagram.

4.3. Dynamical evolution of the cumulant ratios

After discussing the numerical initialization procedures for the statistical ensembles of types I and II in the previous Section, we now focus on the dynamical evolution of systems with such initial conditions. We start with the dynamical phase diagram in an effective T - μ_q plane, which is obtained from a fit of the numerical quark distribution function $f_q(t, p)$ to the Fermi distribution function, allowing to extract an effective value for the temperature T as well as the chemical potential μ_q . Thereby, the fitting procedure is applied to the (lower) momentum interval $p = 100 - 300$ MeV. The results for T - μ_q trajectories of ensemble averages are shown in Figs. 17 and 18 for $\sigma_{q,\text{net}} = \langle N_{q,\text{net}} \rangle / 10$. On the level of averaged ensemble trajectories there are no significant differences between initial conditions of types I and II. However, on the level of single ensemble trajectories the differences are more pronounced as seen from the boundaries of the one- σ width trajectories (transparent lines with the same color), which show a significant deviation from the averaged trajectories in case of a type II initialization. For type I small deviations can only be observed at high expansion velocities, underlining the fact that the phase transition as well as the thermalization process are determined by the particle density of the system, being constant in case of type I, where the ensemble trajectories differs only with respect to the initial radius scale $R(t_0)$.

Since the averaged trajectories are very similar for both initialization methods, we thus focus on type II for the moment. Fig. 19 shows the dynamical evolution of the averaged net-quark density $\langle n_q \rangle(t)$ (thin lines) as well as the averaged effective quark chemical potential $\langle \mu_q \rangle(t)$ (thick lines). The yellow band stands for the critical region of the net-quark density in equilibrium as calculated near the critical point for $T \approx 108$ MeV and $\mu_q \approx 157$ MeV (compare with Fig. 16). A black cross marks the exact value of the averaged net-quark density, for which the statistical ensemble has an effective averaged quark chemical potential of $\langle \mu_q \rangle \approx 157$ MeV, being represented by a black circle with the equilibrium net-quark density. A large separation between those two points indicates that the averaged quantities of the statistical ensemble deviate significantly from the equilibrium values of the critical point. Indeed, for fast expanding systems with $v \gtrsim 0.4$ one observes strong oscillations of the averaged quantities, and the net-quark density $\langle n_q \rangle(t)$ is even outside of the yellow region, meaning that the system dilutes much faster than it is the case for $v \lesssim 0.2$,

Statistical ensemble of type II

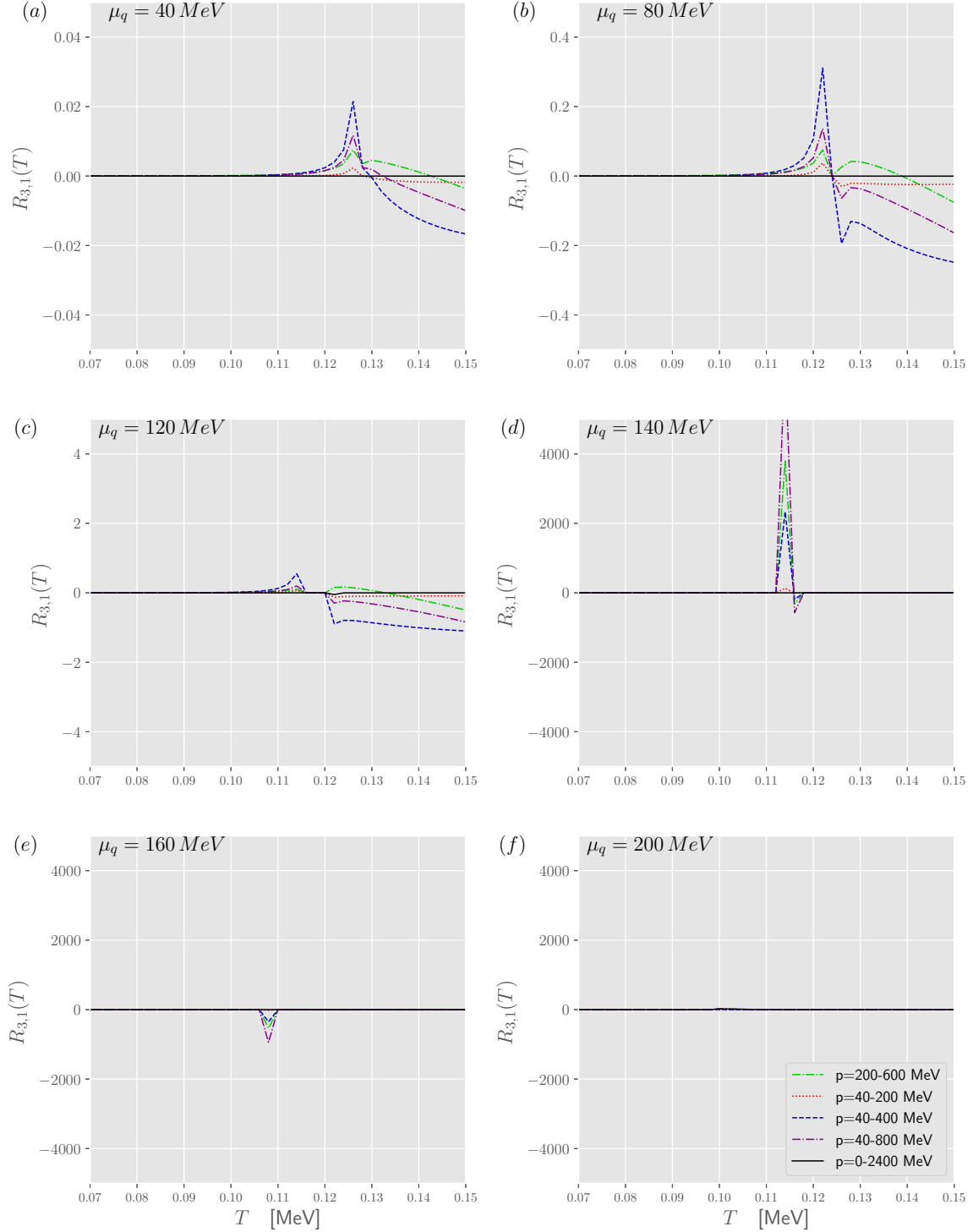


Figure 14: Cumulant ratio $R_{3,1}$ as a function of the temperature T with respect to 5 momentum intervals and 6 different values of the mean quark chemical potential μ_q ($\langle N_{q,\text{net}} \rangle$) in case of the statistical ensemble of type II.

Statistical ensemble of type II

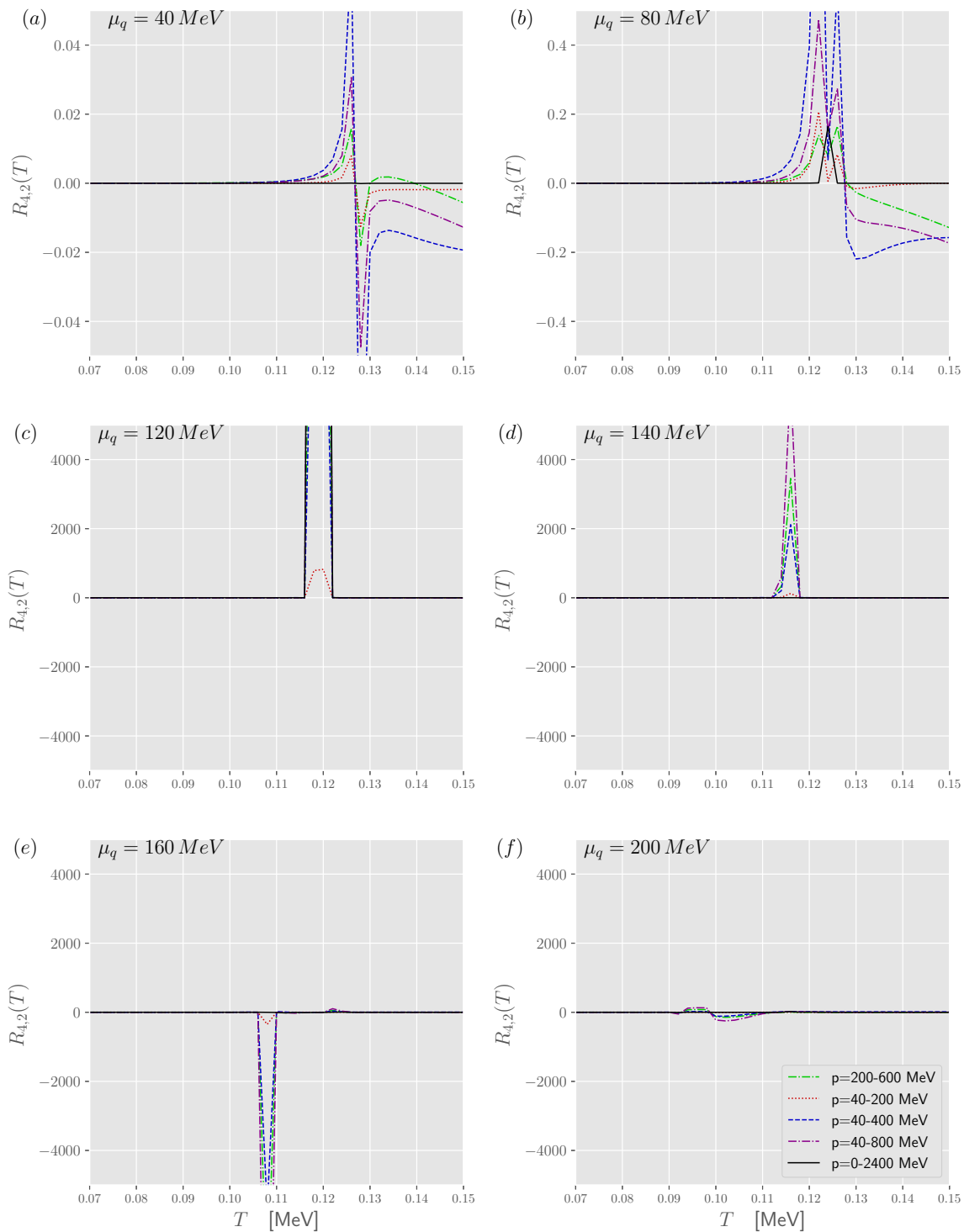


Figure 15: Same as Fig. 14 but for the cumulant ratio $R_{4,2}$.

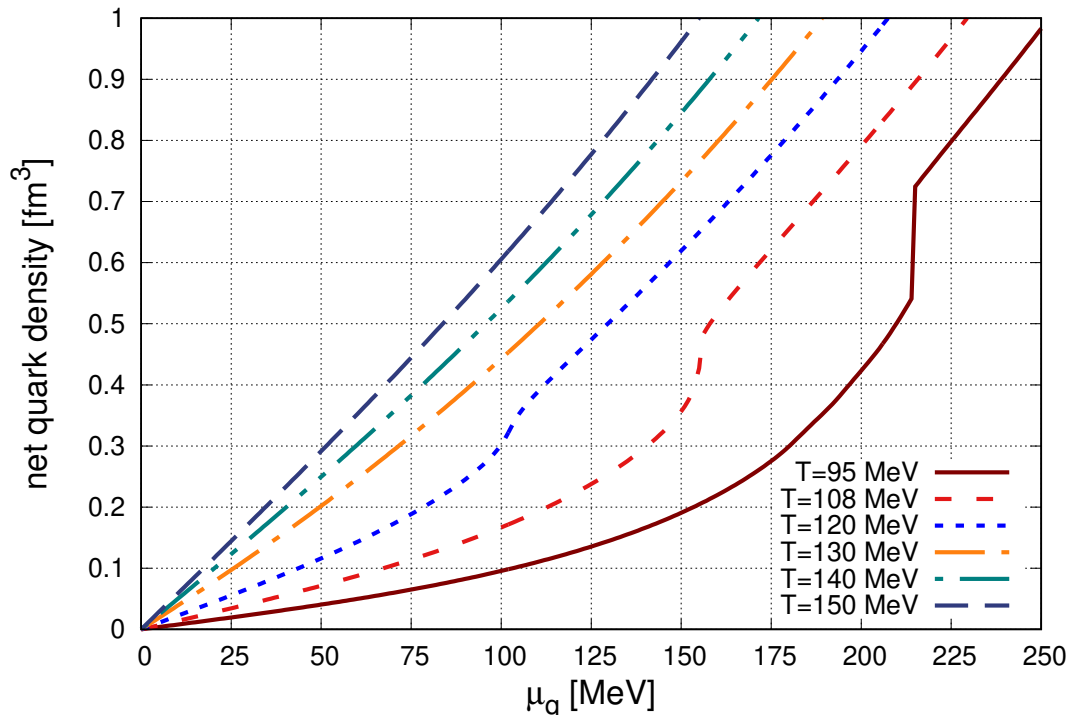


Figure 16: Net-quark density in thermal and chemical equilibrium as a function of the quark chemical potential μ_q , shown for several values of the temperature T .

circumventing the system from passing through the critical point. During the expansion process a similar situation is also observed for the mass evolution of the σ -meson $\langle m_\sigma \rangle(t)$ and of quarks $\langle m_q \rangle(t)$ as shown in Fig. 20. Here, the axis range for quark masses is chosen to be exactly one-half of the axis range for sigma masses. Consequently, a sigma decay to a quark-antiquark pair is only allowed, when the thick curve stays above the corresponding (same color and style) thin curve, defining an important time scale, denoted with $\tau_{\sigma \rightarrow q\bar{q}}$ in the following. Notable is also the minimum of the dynamical sigma mass for the ensemble average, arising at the time scale $\tau_{m_{\sigma, \min}}$ and staying in all cases above 200 MeV, which makes it difficult to distinguish between different orders of the phase transition from averaged quantities.

We now return to the discussion of statistical ensembles of type I with $\sigma_{q, \text{net}} = \langle N_{q, \text{net}} \rangle / 10$ and different initial values of the quark chemical potential $\mu_q = \mu_q(\langle N_{q, \text{net}} \rangle)$. We choose three different initial chemical potentials: (1) $\mu_q(t_0 = 0) = 40 \text{ MeV}$ and thus $\langle N_{q, \text{net}} \rangle = 122.7$, (2) $\mu_q(t_0 = 0) = 160 \text{ MeV}$ and thus $\langle N_{q, \text{net}} \rangle = 544.15$, (3) $\mu_q(t_0 = 0) = 280 \text{ MeV}$ and thus $\langle N_{q, \text{net}} \rangle = 1158.4$. Fig. 21 shows the rescaled cumulant ratio $s_1 \times R_{4,2}$ for various momentum ranges, where the color-marked curves refer to different expansion velocities. Furthermore, the curve thickness refers to different choices of μ_q . Since the results for $R_{4,2}$ vary in absolute values, they are rescaled by the factor $s_1 = 10^5 / \langle N_{q, \text{net}} \rangle^2$, accounting for the increasing net-quark number $\langle N_{q, \text{net}} \rangle$ or the increasing variance $\sigma_{q, \text{net}}$ alongside with an increasing chemical potential μ_q , which leads to the same range of the y-axis for all shown simulation runs. We note, that only in case of the highest net-quark density one observes critical behavior in the range of $\nu t = 2 - 3 \text{ fm}$. However, this time scale is significantly below the typical time scale for nearly vanishing interaction rates (“thermal freezeout”), meaning that this signature of the critical point is not observable at the end of the simulation.

From the thermal calculations of Figs. 14 and 15 and the discussion in this regard, we know, that in thermal and chemical equilibrium the cumulant ratios for our initial distribution function of net quarks are zero for type I fluctuations, and converge to zero for decreasing temperatures for type II fluctuations. In our dynamical simulations without chemical equilibration we now observe significant deviations from zero, which could be used as a weak indication

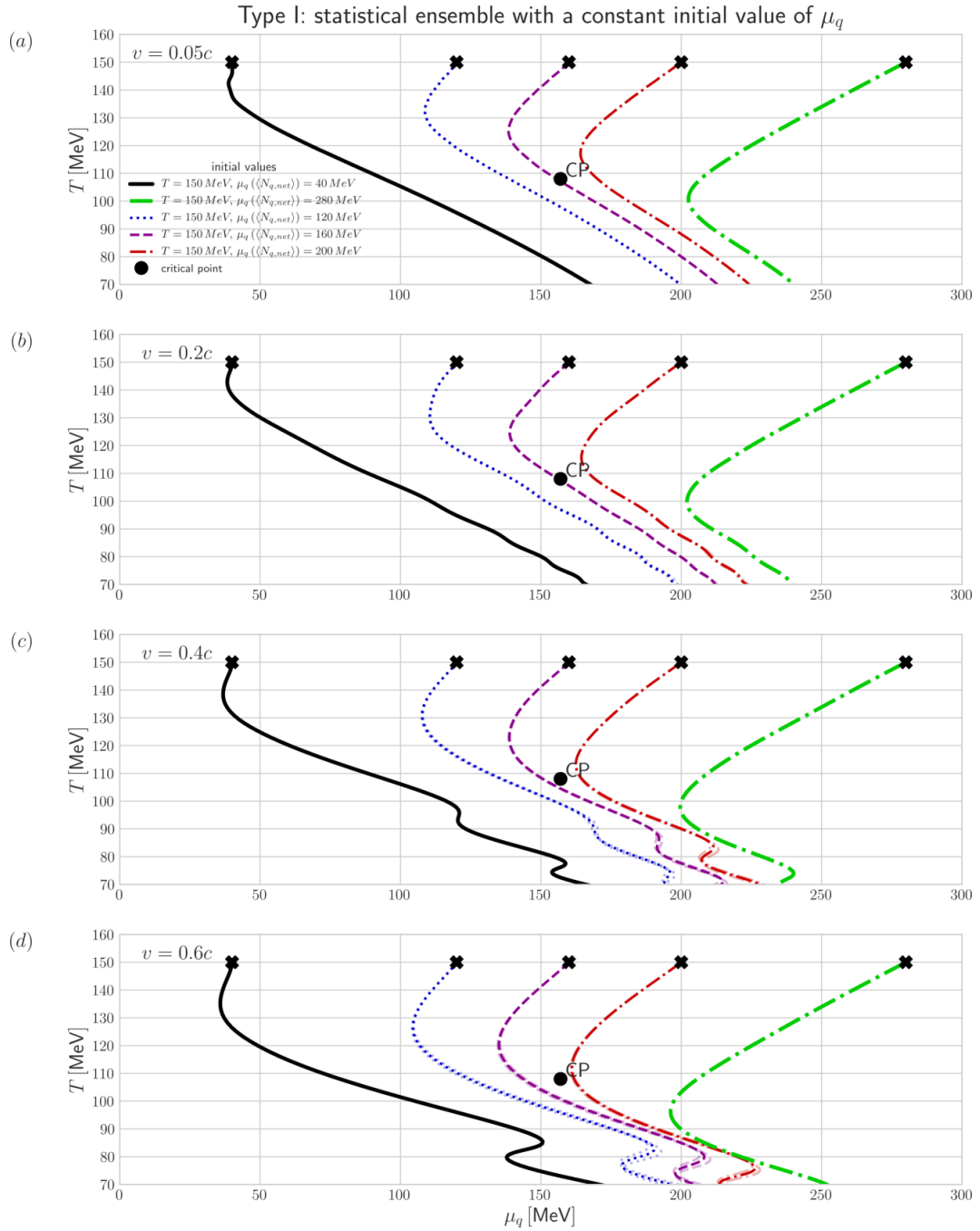


Figure 17: Thick lines are averaged trajectories of initialized statistical ensembles in T - μ_q space. Transparent lines are boundary trajectories of the one- σ width around the mean trajectory with $N_{q,\text{net}} = \langle N_{q,\text{net}} \rangle$.

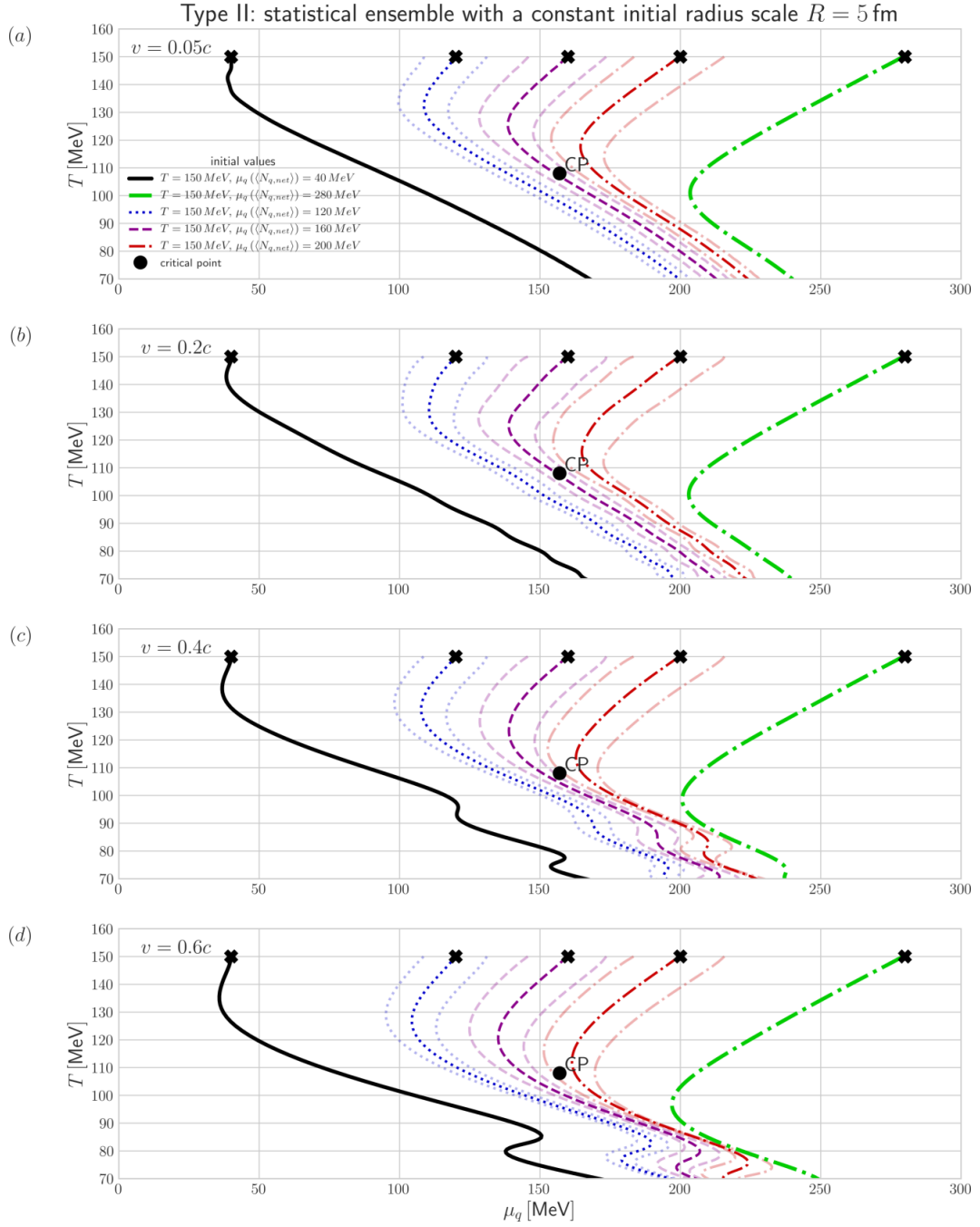


Figure 18: Same as Fig. 17 but for initial condition of type II.

Type II: statistical ensemble with a constant initial radius scale $R = 5$ fm

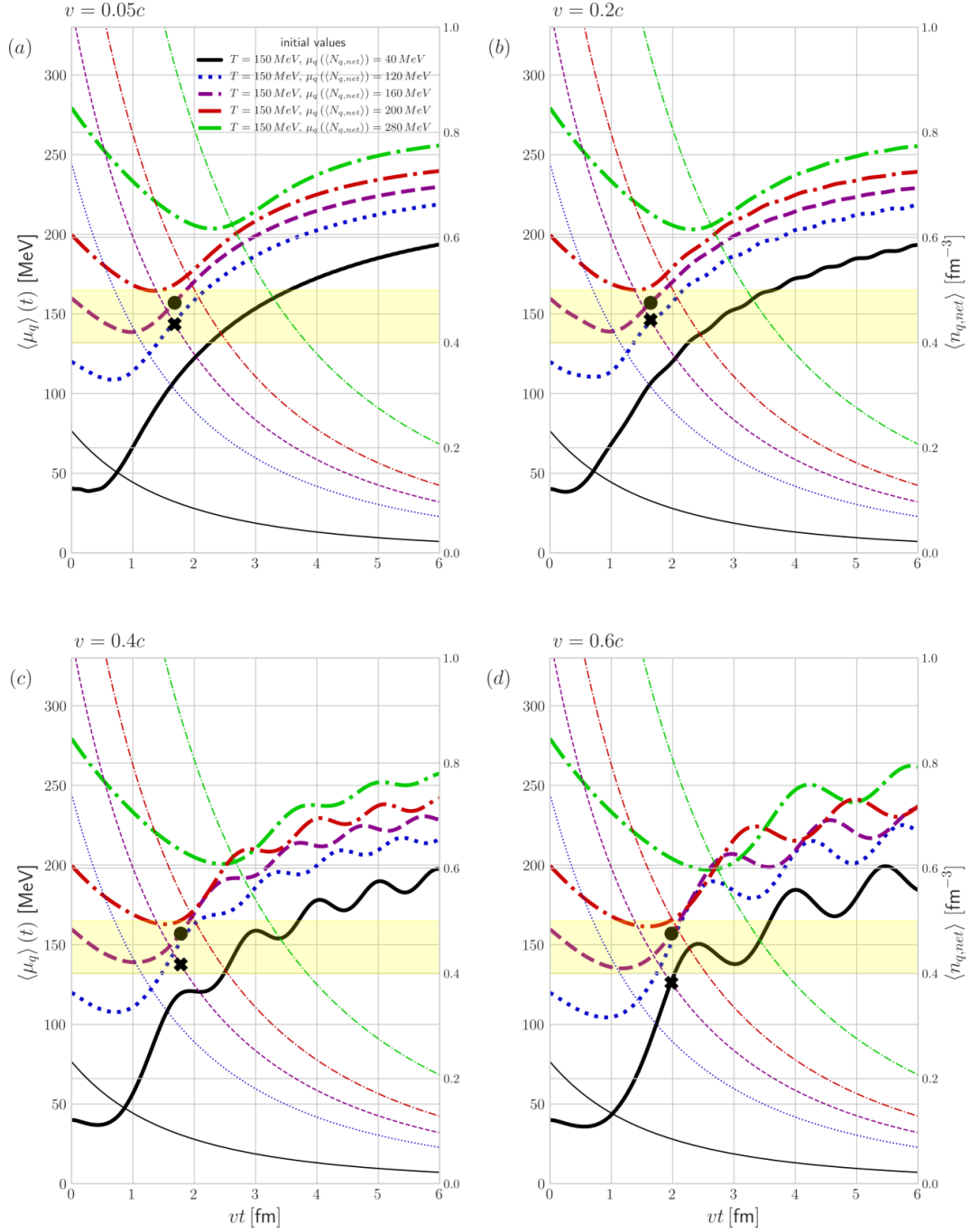


Figure 19: Ensemble average of the effective chemical potential of quarks (thick lines), extracted from a fit to the Fermi distribution function. The averaged net-quark density (thin lines) is calculated directly from numerical realizations of the one-particle distribution functions.

Type II: statistical ensemble with a constant initial radius $R = 5$ fm

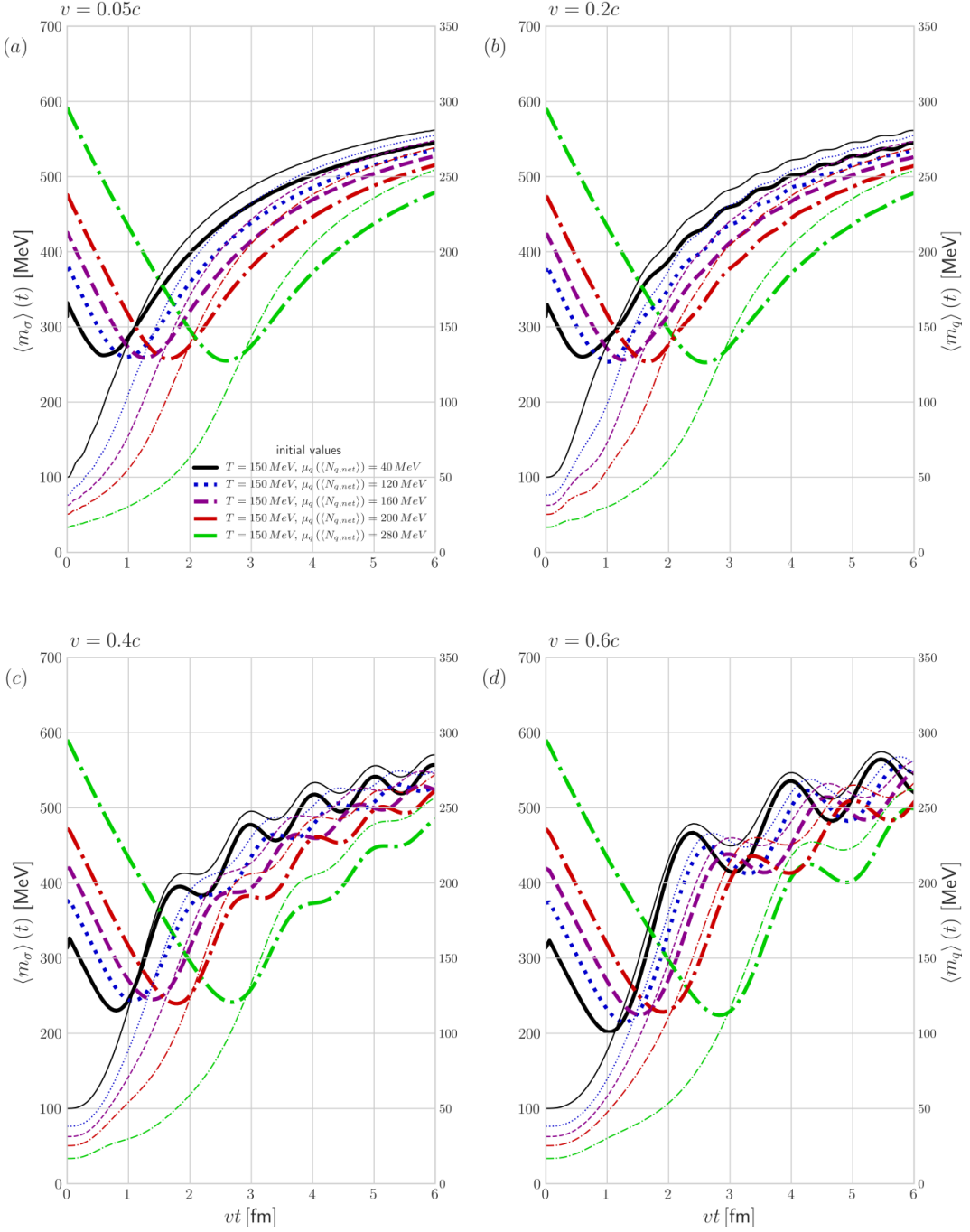


Figure 20: Ensemble average of σ -meson (thick lines) and quark (thin lines) masses. The axis range for quark masses is chosen to be exactly one-half of the axis range for sigma masses. The intersection point between corresponding lines (same color and style) defines a time scale $\tau_{\sigma \rightarrow q\bar{q}}$ for the $q\bar{q}$ -production from sigma decay.

for the phase transition in experiments, when also the cumulant ratios of the baryon number fluctuations deviate significantly from the crossover behavior with a non-trivial dependence on the center-of-momentum energy as well as centrality classes, being indeed observable in experiments (compare our discussion in Sec. 1). However, generally for type I initial conditions the cumulant ratios show only a weak dependence on the expansion velocity, leading to significant oscillations only in the vicinity of the phase transition and at highest net-quark densities. Thereby, the oscillations are stronger pronounced for smaller expansion velocities. Following that, a critical behavior at the phase transition due to simple volume fluctuations of the initial domain is hardly observable at the end of the simulation.

Finally, we consider the rescaled cumulant ratio $s_i R_{4,2}$ for initial configurations of type II, where the rescaling factor s_i with $i \in \{1, 2\}$ accounts for the increasing net-quark number $N_{q,\text{net}}$ as well as for different choices of the standard deviation $\sigma_{q,\text{net}}$. The results are shown in Figs. 22, 23 and 24 for different values of $\mu_q \left(\langle N_{q,\text{net}} \rangle \right)$, which can be referred to the crossover region for $\mu_q = 40 \text{ MeV}$, the critical region of second order for $\mu_q = 160 \text{ MeV}$ and the region of a first order phase transition for $\mu_q = 280 \text{ MeV}$ (compare also with Fig. 18). All calculations are performed for two values of the standard deviation $\sigma_{q,\text{net}}$ for Gaussian-type fluctuations of the net-quark number. Thereby, the cumulant ratios are by an order of magnitude larger in case of $\sigma_{q,\text{net}} = \langle N_{q,\text{net}} \rangle / 5$ (thin lines) compared to $\sigma_{q,\text{net}} = \langle N_{q,\text{net}} \rangle / 10$ (thick lines). Note also, that for the higher value of $\sigma_{q,\text{net}}$ the cumulant ratio $R_{4,2}$ of the total net-quark number (Subfig. (f)) deviates from a vanishing one as expected for a Gaussian distribution function, even though the full range $[0, 2 \langle N_{q,\text{net}} \rangle]$ of the numerical distribution function (155) is given by $10\sigma_{q,\text{net}}$, which again underlines the requirement of an extremely high accuracy for the study of cumulants. However, the qualitative behavior of our results is independent of $\sigma_{q,\text{net}}$ and we should rather focus on details of the dynamical evolution, depending on the expansion velocity.

For all simulations of type II the intermediate time scale of the most pronounced fluctuations is highly correlated to the critical time scales $\tau_{m_{\sigma,\text{min}}}$ (dynamical minimum of the σ -meson mass) and $\tau_{\sigma \rightarrow q\bar{q}}$ ($q\bar{q}$ -production from sigma decay), as discussed above in the context of Fig. 20. Furthermore, as expected intuitively, we observe that the most pronounced fluctuations are formed for the smallest expansion velocity $v = 0.05 c$ (and one may regard as a quasi-adiabatic expansion), since the system stays longer in the critical region, which is also supported by the analysis of the relevant time scales $\tau_{m_{\sigma,\text{min}}}$ as well as $\tau_{\sigma \rightarrow q\bar{q}}$. Following that, our results confirm that the dynamical evolution of the σ -meson mass has a large impact on the fluctuating behavior of the net-quark number in different momentum ranges. However, referring to real experiments the critical effects from intermediate time scales cannot be directly observed and one is restricted to the products of a heavy ion collision, meaning in our case that the final realization at $\nu t \geq 6$ has to be considered, resulting by construction in a final radius scale of $R \geq 11 \text{ fm}$.

All our simulations start with $T = 150 \text{ MeV}$, leading to a time shift of the phase transition to higher values of νt with an increasing initial chemical potential μ_q of the ensemble. Even so, the final fluctuations from the simulation run with $\mu_q = 160 \text{ MeV}$, which is expected to pass through the critical region of second order, show the most interesting behavior. Here, the most pronounced deviations from zero in the *final state* are obtained for intermediate expansion velocities $v = 0.2 - 0.4$, whereas in case of a first order phase transition the final results depend only weakly on the expansion velocity for the most interesting momentum range of $p = 200 - 600 \text{ MeV}$, allowing to distinguish, at least in numerical simulations, between different orders of the phase transition. This indicates non-equilibrium behavior in the critical region of second order due to an increasing relaxation time, which is supported by the fact, that the strongest fluctuations from intermediate time scales $\nu t = 1 - 2 \text{ fm}$ in case of the smallest expansion velocity result in the most suppressed deviations from zero in the final state. In detail, the system requires a longer time to equilibrate and one observes the remnants of the critical behavior at the phase transition, which now depends on the expansion velocity in contrast to type I initial conditions (compare with Fig. 21). Following that, a successful observation of strong fluctuations in cumulant ratios is an interplay between the formation time of fluctuations, which is needed to be as long as possible and the time scale, which is needed to wash out those fluctuations.

We finalize our studies of the cumulant ratios by pointing out, that the absolute value of the cumulant ratio $R_{4,2}$ increases continuously with an increasing net-quark density in systems of type I and II. This effect is significantly reduced by taking the rescaling factors $s_1, s_2 \sim 1 / \langle N_{q,\text{net}} \rangle^2$ into account as discussed before. Nevertheless, an increase of absolute values for $s_i R_{4,2}$ is still observable, which results from non-linear scaling of the net-quark density with respect to the increasing chemical potential μ_q as seen from Fig. 16. Although the fluctuations in an expanding system out of equilibrium are less pronounced compared to the expectations from equilibrium systems (see Figs. 14 and 15), we are able to confirm that a significant deviation from the crossover behavior is observable, when considering higher-

order cumulant ratios of the net-quark number in different momentum ranges, being thus a promising candidate for an experimental signature of the chiral phase transition.

Type I: statistical ensemble with a constant initial value of μ_q

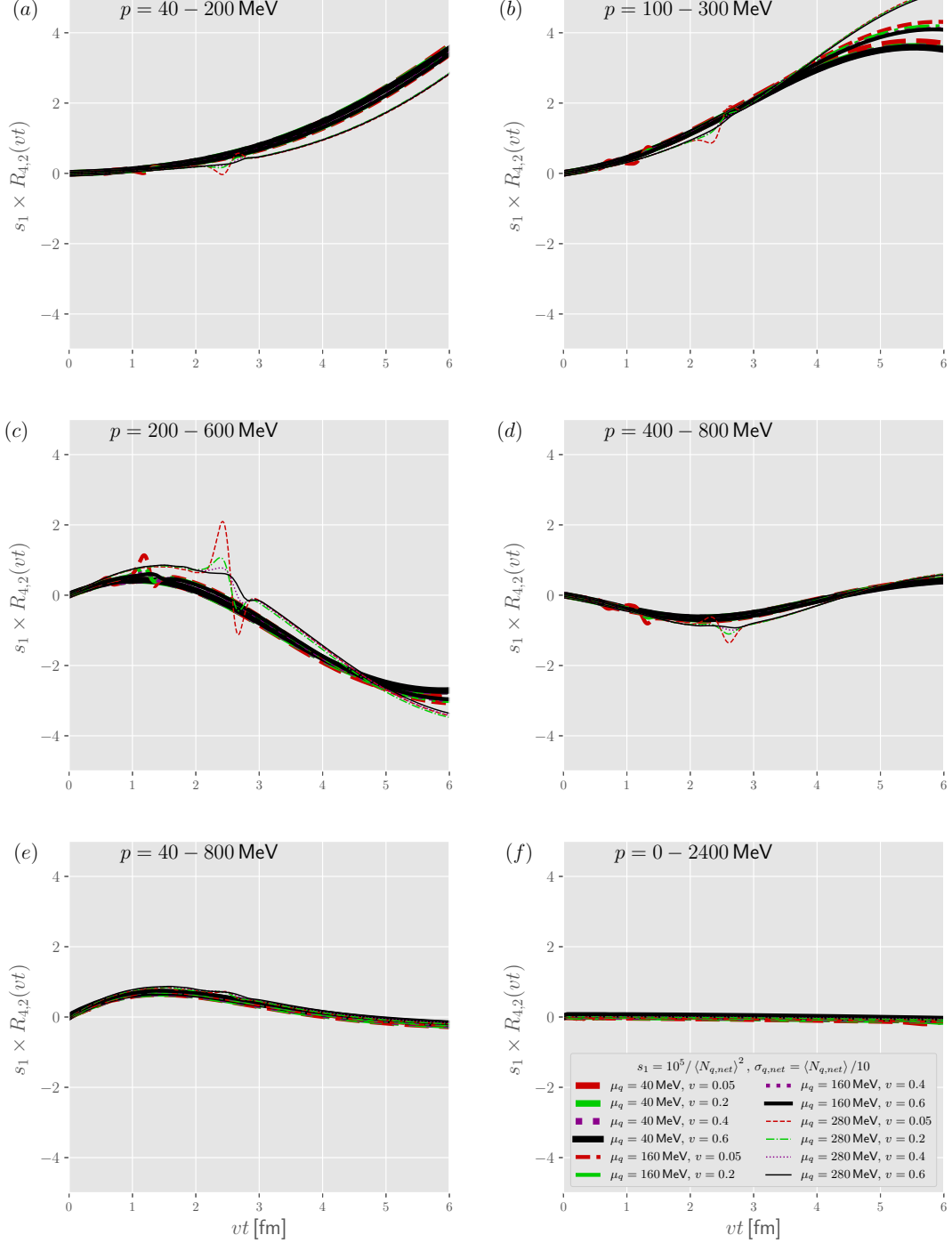


Figure 21: Dynamical evolution of the rescaled cumulant ratio $R_{4,2}$ in different momentum ranges as a function of the growing radius scale $vt =: \Delta R(t)$ in case of the statistical ensemble of type I. Different expansion velocities are shown with different colors and the thickness of curves refer to different values of the quark chemical potential $\mu_q (\langle N_{q,net} \rangle)$.

II: statistical ensemble with a constant initial radius $R = 5$ fm

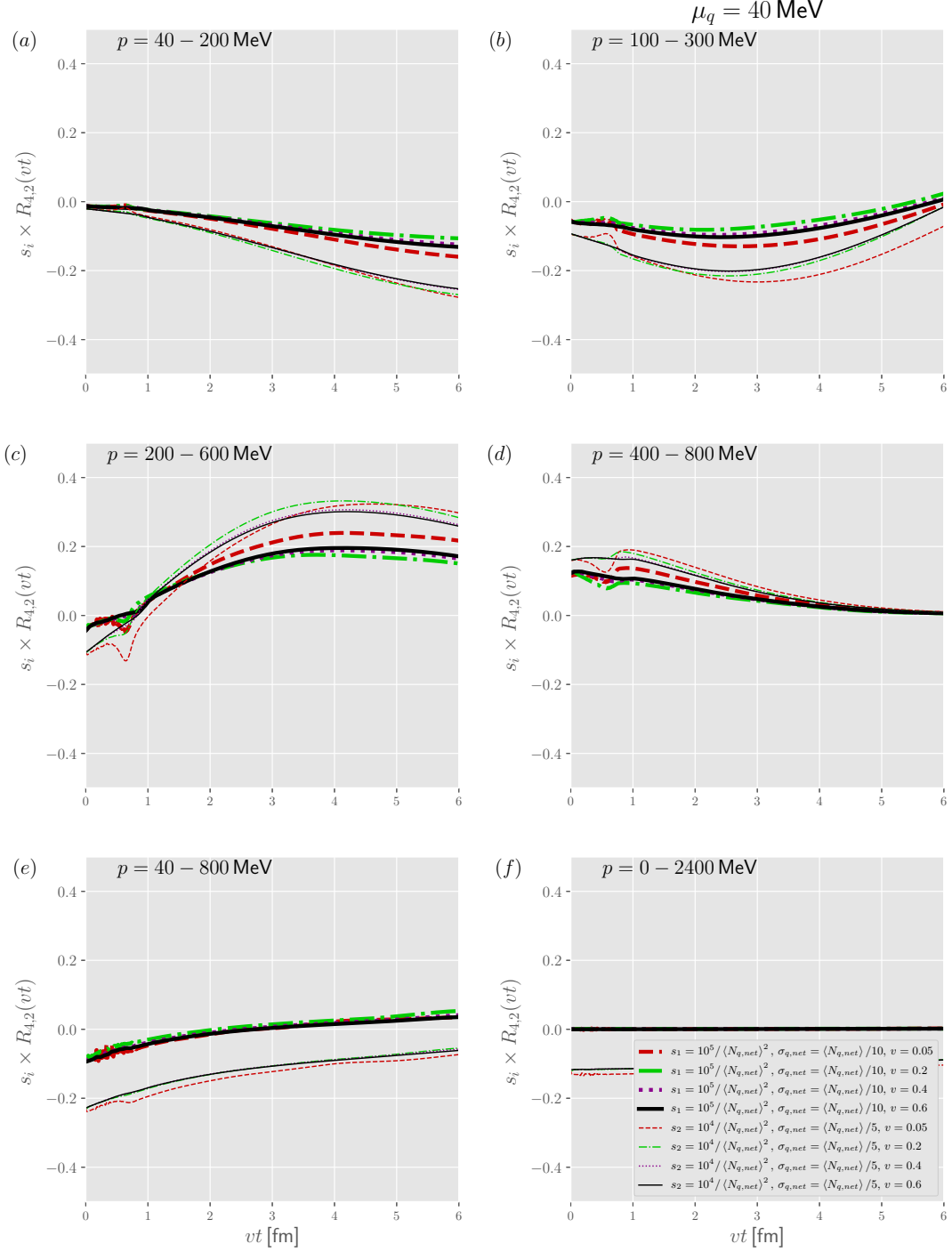


Figure 22: Dynamical evolution of the rescaled cumulant ratio $R_{4,2}$ in different momentum ranges as a function of the growing radius scale $vt =: \Delta R(t)$ in case of the statistical ensemble of type II. Different expansion velocities are shown with different colors and the quark chemical potential of the mean trajectory is set to $\mu_q(\langle N_{q,net} \rangle) = 40$ MeV.

II: statistical ensemble with a constant initial radius $R = 5$ fm

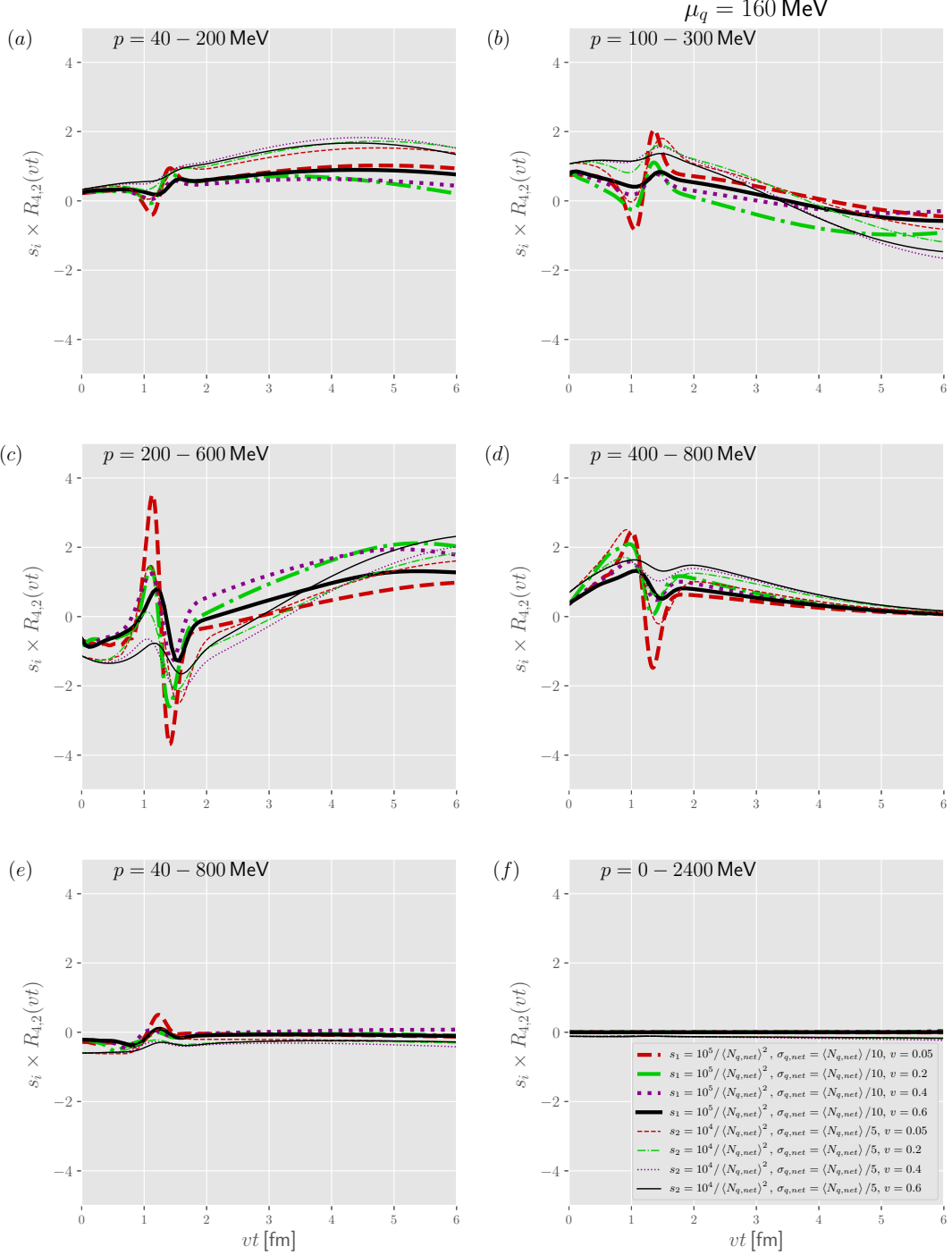


Figure 23: Same as Fig. 22 but for $\mu_q(\langle N_{q,net} \rangle) = 160$ MeV as the quark chemical potential of the mean trajectory.

II: statistical ensemble with a constant initial radius $R = 5$ fm

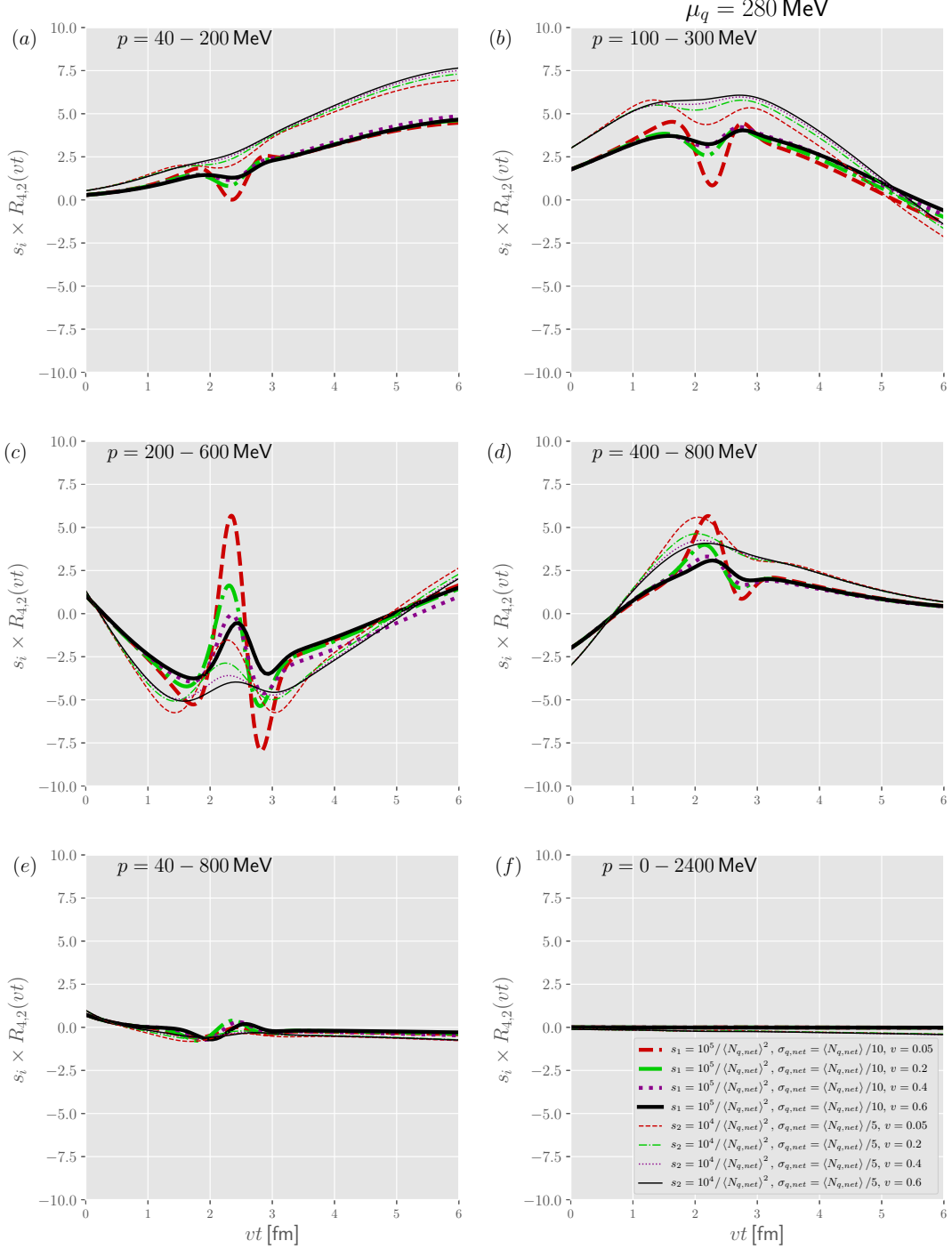


Figure 24: Same as Fig. 22 but for $\mu_q(\langle N_{q,net} \rangle) = 280$ MeV as the quark chemical potential of the mean trajectory.

5. Conclusions and Outlook

In this paper the evolution of net-baryon-number fluctuations in an expanding fireball of strongly interacting matter similar as produced in ultrarelativistic heavy-ion collisions at the Large-Hadron Collider (CERN) or at the Relativistic Heavy Ion Collider (BNL) is investigated. In thermal equilibrium the “grand-canonical fluctuations” of the net-baryon number in different momentum and rapidity ranges of produced hadrons are the most promising observables, indicating phase transitions of the strongly interacting medium. From lattice-QCD calculations it is known that at vanishing net-baryon number ($\mu_B = 0$) both the deconfinement and the chiral transition are smooth cross-over transitions occurring at a “pseudo-critical temperature” of about 155 MeV. From effective models at $\mu_B \neq 0$ one expects a first-order transition line in the T - μ_B phase diagram, ending in a critical point with a second-order phase transition. In thermal equilibrium and in the thermodynamic limit the susceptibilities of conserved quantum numbers, like the net-baryon number, diverge at the critical point and thus are the most promising candidates to observe these different types of phase transitions and maybe constrain the location of the critical point in the phase diagram.

However, the fireball of strongly interacting matter created in heavy-ion collisions is rapidly expanding and cooling, which implies that a realistic theoretical description has to take this off-equilibrium situation as well as the finite volume and lifetime of the fireball into account.

Thus, in this work the restoration of explicitly and spontaneously broken chiral symmetry is studied with respect to the σ field as the order parameter of the chiral symmetry within a linear quark-meson σ model, describing pions, σ -mesons and constituent quarks and anti-quarks. For this system, a set of coupled and self-consistent evolution equations is derived in Sec. 3 by considering a truncation scheme of the underlying two-particle irreducible (2PI) quantum effective action, which still contains the most relevant diagrams, including also dissipation with and without memory effects, arising from the interaction between the slowly changing chiral mean-field and mesonic excitations. Applying a gradient expansion to the exact evolution equations for one- and two-point functions of the quark-meson model, one obtains generalized transport equations, allowing to interpret the full dynamics of two-point functions in terms of mesonic interactions. Thereby, the interaction between soft and hard modes is encoded in a dissipation kernel, leading to memory effects, which become particularly important near the critical point.

In this work a simplified homogeneous and isotropic “Hubble-like” expanding fireball is used to solve the derived set of semiclassical kinetic and mean-field equations, including memory effects in terms of a non-Markovian evolution of the σ field, i.e., the order parameter of chiral symmetry coupled to a set of Boltzmann-Uehling-Uhlenbeck-type transport equations for the phase-space-distribution functions of the σ -mesons, pions, quarks and anti-quarks.

To quantify the fluctuations it is necessary to evaluate the dynamical evolution of the higher-order cumulants of the net-baryon-number distribution and their ratios, which is numerically challenging within the usually employed test-particle Monte Carlo approach. Therefore a numerical integration method for the coupled set of integro-differential equations for two statistical ensembles with initial conditions of Gaussian-type fluctuations of the net-quark number, differing in volume and particle-density fluctuations has been developed.

Simulating the expanding system with different initial conditions and net-baryon densities leads to a dynamical evolution of the medium along different effective trajectories in the phase diagram of the strongly interacting medium, which can stay within the cross-over region as well as run through a first-order phase transition or close to the second-order phase transition at the critical point. Depending on the effective fireball-expansion rate and for trajectories across the first-order-transition line or close to the critical point, larger fluctuations, as quantified by the higher cumulants and cumulant ratios, can build up, but are also damped out again in the later stages. The simulations show that the dynamical evolution of the σ mass thereby has a large impact on the behavior of the net-quark-number fluctuations in different momentum ranges, since these fluctuations are highly correlated to the critical time scale to reach the dynamical minimum of the σ mass during the expansion process. At low expansion rates, i.e., under quite “adiabatic conditions”, the fluctuations of the net-baryon number can be observed in the final cumulant ratios in the range of small and intermediate momenta up to ~ 600 MeV.

From the point of view of observations in heavy-ion collisions the measurable cumulant ratios may be used to distinguish between a dynamical evolution of the fireball with the medium undergoing different types of transition (i.e., cross-over or first- and second-order phase transitions), provided the fireball expansion rate is in an intermediate range, such that on one hand off-equilibrium effects in the vicinity of the first-order-transition line or the critical point become strong but on the other hand, due to the enhanced relaxation times towards the range of low σ masses characterizing this region of the phase diagram, the system stays for a sufficient time close to the transition line or

the critical point. The simulations indeed show that the cumulant ratios in the final state, observable in heavy-ion collisions, are quite sensitive to the fireball-expansion velocity which makes a proper interpretation and quantitative determination of the location of the critical point in the phase diagram, based on a measurement of the cumulants and cumulant ratios of the net-baryon number, challenging.

For a more realistic description of the fireball evolution in heavy-ion collisions an extension of the numerical solution of the set of kinetic equations for anisotropic distribution functions in a (2+1)-dimensional Bjorken-like scenario would be desirable, which however makes a further increase in computational performance necessary.

Acknowledgment

The authors are grateful to the LOEWE Center for Scientific Computing (LOEWE-CSC) at Frankfurt for providing computing resources. We acknowledge support by the Deutsche Forschungsgemeinschaft (DFG, German Research Foundation) through the CRC-TR 211 ‘Strong-interaction matter under extreme conditions’ – project number 315477589 – TRR 211.

Appendix A. Symmetry and multiplicity of diagrams

The multiplicity of a diagram in QFT is directly connected to the number of all possible contractions of two fields, divided by the number of identical contractions. Different diagrams follow from the generating functional by applying derivatives with respect to external sources. However, depending on the theory it becomes a tedious procedure since the multiplicity of diagrams grows extremely fast with the number of vertices. To avoid such calculations one can use simple combinatorial arguments, leading to a formula which simplifies enormously the calculation of higher order diagrams and is applicable to a large class of theories. The basic expression of this formula for O(4) theories³⁵ has the following structure [89, 90]:

$$M = \frac{(cM_v)^n n! n_e!}{(2!)^{s+d} (3!)^t (4!)^f N_v}. \quad (\text{A.1})$$

parameter	description
c	prefactor of the vertex from the expansion of the Lagrangian
M_v	multiplicity of the vertex (product of permutations for equal fields)
n	number of vertices
n_e	number of external lines
s, d, t, f	number of self-, double-, triple- and four-field connections, leaving the diagram unchanged
N_v	number of vertex permutations, leading to the same diagram (vertices are connected to the same lines)

Usually, one defines the symmetry factor S_n of a diagram as a product of the diagrammatic multiplicity with a weight factor w_n , denoting the prefactor from the power series of the generating functional for connected diagrams (as discussed for instance in Sec. 3.2 and Sec. 3.3) with respect to the coupling constant α of the theory:

$$W = \sum_n \frac{1}{n!} (V_\alpha)^n W^{(n)} =: \sum_n (-i\alpha)^n w_n W^{(n)}. \quad (\text{A.2})$$

In case of the Lagrangian (17), there are two expressions of the form V_α . The first one is given by the Yukawa interaction between bosonic $\sigma, \vec{\pi}$ - and fermionic $\psi_i, \bar{\psi}_i$ -fields, whereas the second treats the pure ϕ^4 interaction of

³⁵As seen in the following, the formula (A.1) is also applicable to the Yukawa part of the Lagrangian (17).

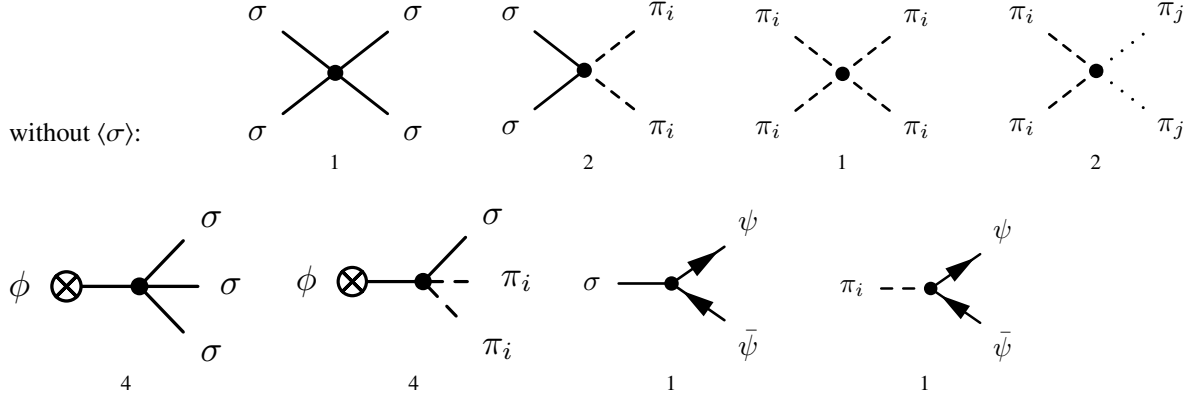


Figure A.25: Relevant vertices for the quantum effective action (66).

σ, π -fields:

$$\begin{aligned} V_g = -ig, \quad w_n = \frac{1}{n!} &\Rightarrow S_n = \frac{1}{n!} M, \\ V_\lambda = \frac{-i\lambda}{4}, \quad w_n = \frac{1}{4^n n!} &\Rightarrow S_n = \frac{1}{4^n n!} M. \end{aligned} \quad (\text{A.3})$$

Now, we apply the formula (A.1) to the truncation of Γ_2 as shown in Fig. 5 and derive the multiplicity factors for all relevant diagrams. The results are summarized in Tab. A.4 and A.5, thereby the different vertices for the $O(N)$ part of the Lagrangian (17) can be extracted from the expansion of the interaction part:

$$V(\sigma, \vec{\pi}) = \frac{\lambda}{4} (\sigma^2 + \vec{\pi}^2 - v^2)^2 = \frac{\lambda}{4} \left(\sigma^4 + 2\sigma^2 \sum_i \pi_i^2 - 2v^2 \sigma^2 + \sum_i \pi_i^4 + 2 \sum_{i,j>i} \pi_i^2 \pi_j^2 - 2v^2 \sum_i \pi_i^2 + v^4 \right). \quad (\text{A.4})$$

From considering individual terms with respect to the transformation $\sigma \rightarrow \sigma + \phi$, where ϕ denotes a finite value for the mean-field part of the σ -field³⁶, one derives all possible bosonic vertices. Furthermore, there are 2 additional vertices, coming from the interaction between bosonic and fermionic fields. Consequently, one obtains for the 2PI quantum effective action 8 relevant vertices (see Sec. 3.3 for more details) with their prefactors given directly by the expansion (A.4), as shown in Fig. A.25.

Appendix A.1. Self-energies and collision integrals

In this chapter we calculate all relevant selfenergies, which arise from the analysis of the diagrams given in Tab. A.4 and A.5.

1. Hartree diagrams (h.)

$$\begin{aligned} \Gamma_2^{\text{h.}} = & -\frac{3}{4}\lambda \int_C d^4x G_{\sigma\sigma}^2(x, x) - \frac{1}{2}\lambda \sum_i \int_C d^4x G_{\sigma\sigma}(x, x) G_{\pi_i\pi_i}(x, x) \\ & - \frac{3}{4}\lambda \sum_i \int_C d^4x G_{\pi_i\pi_i}^2(x, x) - \frac{1}{2}\lambda \sum_{i,j>i} \int_C d^4x G_{\pi_i\pi_i}(x, x) G_{\pi_j\pi_j}(x, x). \end{aligned} \quad (\text{A.5})$$

Using the relations (69) one obtains for the self-energies:

$$\begin{aligned} \Pi_{\sigma\sigma}(x, x) &= -3i\lambda G_{\sigma\sigma}(x, x) - i\lambda \sum_i G_{\pi_i\pi_i}(x, x) \\ \Pi_{\pi_i\pi_i}(x, x) &= -3i\lambda G_{\pi_i\pi_i}(x, x) - i\lambda \sum_{j \neq i} G_{\pi_j\pi_j}(x, x) - i\lambda G_{\sigma\sigma}(x, x). \end{aligned} \quad (\text{A.6})$$

³⁶Analogously, also finite mean-field values for pionic fields can be introduced, but they are not considered in this paper.

type	vertex/diagram/expression	(c, M, n, n_c)	(s, d, t, f, N_c)	M, S
Hartree:				
4 σ -vertex				
Hartree:				
2 σ - 2 π_i -vertex				
Hartree:				
4 π_i -vertex				
Hartree: $i \neq j$				
2 π_i - 2 π_j -vertex				
Sunset:				
$\phi\sigma$ - 2 σ -vertex				
Sunset:				
$\phi\sigma$ - 2 π_i -vertex				

Table A.4: Multiplicities of Hartree and bosonic sunset diagrams.

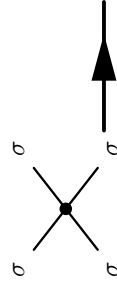
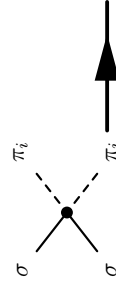
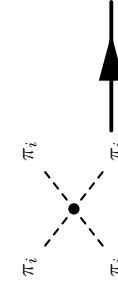
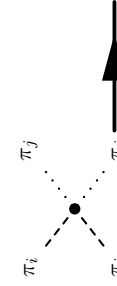
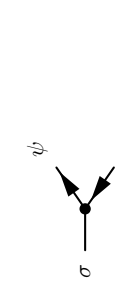

type	vertex/diagram/expression	(c, M_v, n, n_e)	(s, d, t, f, N_V)	M, S
Basketball: 4 σ -vertex	 $\sim \frac{3}{4} i \lambda^2 \int_C \int_C G_{\sigma\sigma}^4$	(1, 4!, 2, 0)	(0, 0, 0, 1, 2)	24, 3/4
Basketball: 2 $\sigma - 2\pi_i$ -vertex	 $\sim \frac{1}{2} i \lambda^2 \sum_i \int_C \int_C G_{\sigma\sigma}^2 G_{\pi_i\pi_i}^2$	(2, 4, 2, 0)	(0, 0, 0, 1, 2)	16, 1/2
Basketball: 4 π_i -vertex	 $\sim \frac{3}{4} i \lambda^2 \sum_i \int_C \int_C G_{\pi_i\pi_i}^4$	(1, 4!, 2, 0)	(0, 0, 0, 1, 2)	24, 3/4
Basketball: $i \neq j$ 2 $\pi_i - 2\pi_j$ -vertex	 $\sim \frac{1}{2} i \lambda^2 \sum_{i,j>i} \int_C \int_C G_{\pi_i\pi_i}^2 G_{\pi_j\pi_j}^2$	(2, 4, 2, 0)	(0, 0, 0, 1, 2)	16, 1/2
Sunset: $\sigma - q\bar{q}$ -vertex	 $\sim -\frac{1}{2} i g^2 \int_C \int_C \text{Tr}[D_{xy} D_{yx}] G_{\sigma\sigma}$	(1, 1, 2, 0)	(0, 0, 0, 0, 2)	1, 1/2
Sunset: $\pi_i - q\bar{q}$ -vertex	 $\sim -\frac{1}{2} i g^2 \sum_i \int_C \int_C \text{Tr}[D_{xy} D_{yx}] G_{\pi_i\pi_i}$	(1, 1, 2, 0)	(0, 0, 0, 0, 2)	1, 1/2

Table A.5: Multiplicities of basketball and fermionic sunset diagrams.

Obviously, the self-energies from Hartree diagrams are local contributions to the full expression of the proper self-energy and can be interpreted as an effective mass (see Sec. 3.6).

2. Bosonic sunset diagrams (b.s.)

$$\begin{aligned}\Gamma_2^{\text{b.s.}} &= 3i\lambda^2 \int_C d^4x \int_C d^4y \phi(x) G_{\sigma\sigma}^3(x, y) \phi(y) \\ &+ i\lambda^2 \sum_i \int_C d^4x \int_C d^4y \phi(x) G_{\sigma\sigma}(x, y) G_{\pi_i\pi_i}^2(x, y) \phi(y).\end{aligned}\quad (\text{A.7})$$

In analogy to (A.6) one obtains for the self-energies:

$$\begin{aligned}i\Pi_{\sigma\sigma}^{<,>}(x, y) &= 18\lambda^2 \phi(x) (iG_{\sigma\sigma}^{<,>}(x, y))^2 \phi(y) + 2\lambda^2 \sum_i \phi(x) (iG_{\pi_i\pi_i}^{<,>}(x, y))^2 \phi(y), \\ i\Pi_{\pi_i\pi_i}^{<,>}(x, y) &= 4\lambda^2 \phi(x) (iG_{\sigma\sigma}^{<,>}(x, y)) (iG_{\pi_i\pi_i}^{<,>}(x, y)) \phi(y).\end{aligned}\quad (\text{A.8})$$

After introducing auxiliary functions over an inner loop,

$$\begin{aligned}\tilde{I}_{G_{\sigma\sigma}^2}^{<,>}(X, k) &:= \int d^4\Delta x e^{ik^\mu \Delta x_\mu} (iG_{\sigma\sigma}^{<,>}(x, y))^2 \\ &= \int \frac{d^4p_3}{(2\pi)^4} i\tilde{G}_{\sigma\sigma}^{<,>}(X, p_3) i\tilde{G}_{\sigma\sigma}^{<,>}(X, k - p_3), \\ \tilde{I}_{G_{\pi_i\pi_i}^2}^{<,>}(X, k) &:= \int d^4\Delta x e^{ik^\mu \Delta x_\mu} (iG_{\pi_i\pi_i}^{<,>}(x, y))^2 \\ &= \int \frac{d^4p_3}{(2\pi)^4} i\tilde{G}_{\pi_i\pi_i}^{<,>}(X, p_3) i\tilde{G}_{\pi_i\pi_i}^{<,>}(X, k - p_3), \\ \tilde{I}_{G_{\sigma\pi_i}^2}^{<,>}(X, k) &:= \int d^4\Delta x e^{ik^\mu \Delta x_\mu} (iG_{\sigma\sigma}^{<,>}(x, y)) (iG_{\pi_i\pi_i}^{<,>}(x, y)) \\ &= \int \frac{d^4p_3}{(2\pi)^4} i\tilde{G}_{\sigma\sigma}^{<,>}(X, p_3) i\tilde{G}_{\pi_i\pi_i}^{<,>}(X, k - p_3),\end{aligned}\quad (\text{A.9})$$

the Wigner transforms of the self-energies become:

$$\begin{aligned}i\tilde{\Pi}_{\sigma\sigma}^{<,>}(X, p_1) &= 18\lambda^2 \int d^4\Delta x e^{ip_1^\mu \Delta x_\mu} \phi(x) (iG_{\sigma\sigma}^{<,>}(x, y))^2 \phi(y) \\ &+ 2\lambda^2 \sum_i \int d^4\Delta x e^{ip_1^\mu \Delta x_\mu} \phi(x) (iG_{\pi_i\pi_i}^{<,>}(x, y))^2 \phi(y) \\ &= 18\lambda^2 \int d^4\Delta x e^{ip_1^\mu \Delta x_\mu} \phi(x) \phi(y) \left[\int \frac{d^4k}{(2\pi)^4} e^{-ik^\mu \Delta x_\mu} \tilde{I}_{G_{\sigma\sigma}^2}^{<,>}(X, k) \right] \\ &+ 2\lambda^2 \sum_i \int d^4\Delta x e^{ip_1^\mu \Delta x_\mu} \phi(x) \phi(y) \left[\int \frac{d^4k}{(2\pi)^4} e^{-ik^\mu \Delta x_\mu} \tilde{I}_{G_{\pi_i\pi_i}^2}^{<,>}(X, k) \right] \\ &= 18\lambda^2 \int d^4\Delta x \phi(x) \phi(x - \Delta x) \left[\int \frac{d^4k}{(2\pi)^4} e^{-i(k-p_1)^\mu \Delta x_\mu} \tilde{I}_{G_{\sigma\sigma}^2}^{<,>}(X, k) \right] \\ &+ 2\lambda^2 \sum_i \int d^4\Delta x \phi(x) \phi(x - \Delta x) \left[\int \frac{d^4k}{(2\pi)^4} e^{-i(k-p_1)^\mu \Delta x_\mu} \tilde{I}_{G_{\pi_i\pi_i}^2}^{<,>}(X, k) \right],\end{aligned}\quad (\text{A.10})$$

$$\begin{aligned}i\tilde{\Pi}_{\pi_i\pi_i}^{<,>}(X, p_1) &= 4\lambda^2 \int d^4\Delta x e^{ip_1^\mu \Delta x_\mu} \phi(x) (iG_{\sigma\sigma}^{<,>}(x, y)) (iG_{\pi_i\pi_i}^{<,>}(x, y)) \phi(y) \\ &= 4\lambda^2 \int d^4\Delta x \phi(x) \phi(x - \Delta x) \left[\int \frac{d^4k}{(2\pi)^4} e^{-i(k-p_1)^\mu \Delta x_\mu} \tilde{I}_{G_{\sigma\pi_i}^2}^{<,>}(X, k) \right].\end{aligned}\quad (\text{A.11})$$

Now, we explicitly calculate the expressions in (A.9) by using the on-shell ansatz for the propagators in Wigner space (96)

$$\begin{aligned}
\tilde{I}_{G_{\sigma\sigma}^2}^<(X, k^0, \vec{k}) &\simeq \frac{\pi}{2} \int \frac{d^3 \vec{p}_3}{(2\pi)^3} \int d^3 \vec{p}_4 \frac{\delta^{(3)}(\vec{k} - \vec{p}_3 - \vec{p}_4)}{E_3^\sigma E_4^\sigma} \\
&\times \left\{ [f_3^\sigma f_4^\sigma] \delta(k^0 - E_3^\sigma - E_4^\sigma) \right. \\
&\quad + [(1 + f_3^\sigma) f_4^\sigma] \delta(k^0 + E_3^\sigma - E_4^\sigma) \\
&\quad + [f_3^\sigma (1 + f_4^\sigma)] \delta(k^0 - E_3^\sigma + E_4^\sigma) \\
&\quad \left. + [(1 + f_3^\sigma)(1 + f_4^\sigma)] \delta(k^0 + E_3^\sigma + E_4^\sigma) \right\},
\end{aligned} \tag{A.12}$$

$$\begin{aligned}
\tilde{I}_{G_{\sigma\sigma}^2}^>(X, k^0, \vec{k}) &\simeq \frac{\pi}{2} \int \frac{d^3 \vec{p}_3}{(2\pi)^3} \int d^3 \vec{p}_4 \frac{\delta^{(3)}(\vec{k} - \vec{p}_3 - \vec{p}_4)}{E_3^\sigma E_4^\sigma} \\
&\times \left\{ [(1 + f_3^\sigma)(1 + f_4^\sigma)] \delta(k^0 - E_3^\sigma - E_4^\sigma) \right. \\
&\quad + [f_3^\sigma (1 + f_4^\sigma)] \delta(k^0 + E_3^\sigma - E_4^\sigma) \\
&\quad + [(1 + f_3^\sigma) f_4^\sigma] \delta(k^0 - E_3^\sigma + E_4^\sigma) \\
&\quad \left. + [f_3^\sigma f_4^\sigma] \delta(k^0 + E_3^\sigma + E_4^\sigma) \right\}.
\end{aligned} \tag{A.13}$$

In analogy one derives similar relations for $\tilde{I}_{G_{\sigma\pi_i}^2}^<$ and $\tilde{I}_{G_{\sigma\pi_i}^2}^>$ by replacing $E_3^\sigma, f_3^\sigma, E_4^\sigma, f_4^\sigma$ with $E_3^{\pi_i}, f_3^{\pi_i}, E_4^{\pi_i}, f_4^{\pi_i}$. Consequently, for the terms $\tilde{I}_{G_{\sigma\pi_i}^2}^<$ and $\tilde{I}_{G_{\sigma\pi_i}^2}^>$ one replaces E_4^σ, f_4^σ with $E_4^{\pi_i}, f_4^{\pi_i}$.

In the following we consider a homogeneous system with mean-fields evaluated at $t := \max(x^0, y^0)$ and $t' := \min(x^0, y^0)$. Taking into account both combinations for $\Delta t := t - t'$ one obtains for the self-energies (A.10), (A.11)

$$\begin{aligned}
i\tilde{\Pi}_{\sigma\sigma}^<>(X^0, p_1) &= 18\lambda^2 \phi(t) \int_0^\infty d\Delta t \phi(t - \Delta t) \left[\int \frac{dk^0}{(2\pi)} e^{-i(k^0 - p_1^0)\Delta t} \tilde{I}_{G_{\sigma\sigma}^2}^<>(X^0, k^0, \vec{p}_1) \right] \\
&\quad + 2\lambda^2 \phi(t) \sum_i \int_0^\infty d\Delta t \phi(t - \Delta t) \left[\int \frac{dk^0}{(2\pi)} e^{-i(k^0 - p_1^0)\Delta t} \tilde{I}_{G_{\pi_i\pi_i}^2}^<>(X^0, k^0, \vec{p}_1) \right] \\
&\quad + 18\lambda^2 \phi(t) \int_0^\infty d\Delta t \phi(t - \Delta t) \left[\int \frac{dk^0}{(2\pi)} e^{-i(p_1^0 - k^0)\Delta t} \tilde{I}_{G_{\sigma\sigma}^2}^<>(X^0, k^0, \vec{p}_1) \right] \\
&\quad + 2\lambda^2 \phi(t) \sum_i \int_0^\infty d\Delta t \phi(t - \Delta t) \left[\int \frac{dk^0}{(2\pi)} e^{-i(p_1^0 - k^0)\Delta t} \tilde{I}_{G_{\pi_i\pi_i}^2}^<>(X^0, k^0, \vec{p}_1) \right],
\end{aligned} \tag{A.14}$$

$$\begin{aligned}
i\tilde{\Pi}_{\pi_i\pi_i}^<>(X^0, p_1) &= 4\lambda^2 \phi(t) \int_0^\infty d\Delta t \phi(t - \Delta t) \left[\int \frac{dk^0}{(2\pi)} e^{-i(k^0 - p_1^0)\Delta t} \tilde{I}_{G_{\sigma\pi_i}^2}^<>(X^0, k^0, \vec{p}_1) \right] \\
&\quad + 4\lambda^2 \phi(t) \int_0^\infty d\Delta t \phi(t - \Delta t) \left[\int \frac{dk^0}{(2\pi)} e^{-i(p_1^0 - k^0)\Delta t} \tilde{I}_{G_{\sigma\pi_i}^2}^<>(X^0, k^0, \vec{p}_1) \right].
\end{aligned} \tag{A.15}$$

Inserting the on-shell approximations (A.12), (A.13) in (A.14), (A.15) and evaluating the integral over k^0 at time $X^0 \simeq t$ for slowly changing one-particle distribution functions as well as substituting the integration variable $k^0 \rightarrow p_1^0 \pm k^0$,

leads to

$$\begin{aligned}
i\tilde{\Pi}_{\sigma\sigma}^{\leq}(t, p_1) &\simeq 9\pi\lambda^2\phi(t) \int_0^\infty d\Delta t \phi(t-\Delta t) \int \frac{dk^0}{(2\pi)} e^{-ik^0\Delta t} \\
&\times \left[\int \frac{d^3\vec{p}_3}{(2\pi)^3} \int d^3\vec{p}_4 \frac{\delta^{(3)}(\vec{p}_1 - \vec{p}_3 - \vec{p}_4)}{E_3^\sigma E_4^\sigma} \right. \\
&\quad \times \left\{ [f_3^\sigma f_4^\sigma] \delta(k^0 + E_1^\sigma - E_3^\sigma - E_4^\sigma) \right. \\
&\quad + [(1 + f_3^\sigma) f_4^\sigma] \delta(k^0 + E_1^\sigma + E_3^\sigma - E_4^\sigma) \\
&\quad + [f_3^\sigma (1 + f_4^\sigma)] \delta(k^0 + E_1^\sigma - E_3^\sigma + E_4^\sigma) \\
&\quad + [(1 + f_3^\sigma)(1 + f_4^\sigma)] \delta(k^0 + E_1^\sigma + E_3^\sigma + E_4^\sigma) \\
&\quad + [f_3^\sigma f_4^\sigma] \delta(k^0 - E_1^\sigma + E_3^\sigma + E_4^\sigma) \\
&\quad + [(1 + f_3^\sigma) f_4^\sigma] \delta(k^0 - E_1^\sigma - E_3^\sigma + E_4^\sigma) \\
&\quad + [f_3^\sigma (1 + f_4^\sigma)] \delta(k^0 - E_1^\sigma + E_3^\sigma - E_4^\sigma) \\
&\quad \left. \left. + [(1 + f_3^\sigma)(1 + f_4^\sigma)] \delta(k^0 - E_1^\sigma - E_3^\sigma - E_4^\sigma) \right\} \right] \\
&+ \pi\lambda^2\phi(t) \sum_i \int_0^\infty d\Delta t \phi(t-\Delta t) \int \frac{dk^0}{(2\pi)} e^{-ik^0\Delta t} \\
&\times \left[\int \frac{d^3\vec{p}_3}{(2\pi)^3} \int d^3\vec{p}_4 \frac{\delta^{(3)}(\vec{p}_1 - \vec{p}_3 - \vec{p}_4)}{E_3^{\pi_i} E_4^{\pi_i}} \right. \\
&\quad \times \left\{ [f_3^{\pi_i} f_4^{\pi_i}] \delta(k^0 + E_1^\sigma - E_3^{\pi_i} - E_4^{\pi_i}) \right. \\
&\quad + [(1 + f_3^{\pi_i}) f_4^{\pi_i}] \delta(k^0 + E_1^\sigma + E_3^{\pi_i} - E_4^{\pi_i}) \\
&\quad + [f_3^{\pi_i} (1 + f_4^{\pi_i})] \delta(k^0 + E_1^\sigma - E_3^{\pi_i} + E_4^{\pi_i}) \\
&\quad + [(1 + f_3^{\pi_i})(1 + f_4^{\pi_i})] \delta(k^0 + E_1^\sigma + E_3^{\pi_i} + E_4^{\pi_i}) \\
&\quad + [f_3^{\pi_i} f_4^{\pi_i}] \delta(k^0 - E_1^\sigma + E_3^{\pi_i} + E_4^{\pi_i}) \\
&\quad + [(1 + f_3^{\pi_i}) f_4^{\pi_i}] \delta(k^0 - E_1^\sigma - E_3^{\pi_i} + E_4^{\pi_i}) \\
&\quad + [f_3^{\pi_i} (1 + f_4^{\pi_i})] \delta(k^0 - E_1^\sigma + E_3^{\pi_i} - E_4^{\pi_i}) \\
&\quad \left. \left. + [(1 + f_3^{\pi_i})(1 + f_4^{\pi_i})] \delta(k^0 - E_1^\sigma - E_3^{\pi_i} - E_4^{\pi_i}) \right\} \right], \tag{A.16}
\end{aligned}$$

$$\begin{aligned}
i\tilde{\Pi}_{\sigma\sigma}^{\geq}(t, p_1) &\simeq 9\pi\lambda^2\phi(t) \int_0^\infty d\Delta t \phi(t-\Delta t) \int \frac{dk^0}{(2\pi)} e^{-ik^0\Delta t} \\
&\times \left[\int \frac{d^3\vec{p}_3}{(2\pi)^3} \int d^3\vec{p}_4 \frac{\delta^{(3)}(\vec{p}_1 - \vec{p}_3 - \vec{p}_4)}{E_3^\sigma E_4^\sigma} \right. \\
&\quad \times \left\{ [(1+f_3^\sigma)(1+f_4^\sigma)] \delta(k^0 + E_1^\sigma - E_3^\sigma - E_4^\sigma) \right. \\
&\quad + [f_3^\sigma(1+f_4^\sigma)] \delta(k^0 + E_1^\sigma + E_3^\sigma - E_4^\sigma) \\
&\quad + [(1+f_3^\sigma)f_4^\sigma] \delta(k^0 + E_1^\sigma - E_3^\sigma + E_4^\sigma) \\
&\quad + [f_3^\sigma f_4^\sigma] \delta(k^0 + E_1^\sigma + E_3^\sigma + E_4^\sigma) \\
&\quad + [(1+f_3^\sigma)(1+f_4^\sigma)] \delta(k^0 - E_1^\sigma + E_3^\sigma + E_4^\sigma) \\
&\quad + [f_3^\sigma(1+f_4^\sigma)] \delta(k^0 - E_1^\sigma - E_3^\sigma + E_4^\sigma) \\
&\quad + [(1+f_3^\sigma)f_4^\sigma] \delta(k^0 - E_1^\sigma + E_3^\sigma - E_4^\sigma) \\
&\quad \left. \left. + [f_3^\sigma f_4^\sigma] \delta(k^0 - E_1^\sigma - E_3^\sigma - E_4^\sigma) \right\} \right. \\
&+ \pi\lambda^2\phi(t) \sum_i \int_0^\infty d\Delta t \phi(t-\Delta t) \int \frac{dk^0}{(2\pi)} e^{-ik^0\Delta t} \\
&\times \left[\int \frac{d^3\vec{p}_3}{(2\pi)^3} \int d^3\vec{p}_4 \frac{\delta^{(3)}(\vec{p}_1 - \vec{p}_3 - \vec{p}_4)}{E_3^{\pi_i} E_4^{\pi_i}} \right. \\
&\quad \times \left\{ [(1+f_3^{\pi_i})(1+f_4^{\pi_i})] \delta(k^0 + E_1^\sigma - E_3^{\pi_i} - E_4^{\pi_i}) \right. \\
&\quad + [f_3^{\pi_i}(1+f_4^{\pi_i})] \delta(k^0 + E_1^\sigma + E_3^{\pi_i} - E_4^{\pi_i}) \\
&\quad + [(1+f_3^{\pi_i})f_4^{\pi_i}] \delta(k^0 + E_1^\sigma - E_3^{\pi_i} + E_4^{\pi_i}) \\
&\quad + [f_3^{\pi_i} f_4^{\pi_i}] \delta(k^0 + E_1^\sigma + E_3^{\pi_i} + E_4^{\pi_i}) \\
&\quad + [(1+f_3^{\pi_i})(1+f_4^{\pi_i})] \delta(k^0 - E_1^\sigma + E_3^{\pi_i} + E_4^{\pi_i}) \\
&\quad + [f_3^{\pi_i}(1+f_4^{\pi_i})] \delta(k^0 - E_1^\sigma - E_3^{\pi_i} + E_4^{\pi_i}) \\
&\quad + [(1+f_3^{\pi_i})f_4^{\pi_i}] \delta(k^0 - E_1^\sigma + E_3^{\pi_i} - E_4^{\pi_i}) \\
&\quad \left. \left. + [f_3^{\pi_i} f_4^{\pi_i}] \delta(k^0 - E_1^\sigma - E_3^{\pi_i} - E_4^{\pi_i}) \right\} \right], \tag{A.17}
\end{aligned}$$

In analogy to (A.16) and (A.17) one derives the self-energies $i\tilde{\Pi}_{\pi_i\pi_i}^{\langle,\rangle}$ by replacing $\tilde{I}_{G_{\sigma\sigma}^2}^{\langle,\rangle}$ and $\tilde{I}_{G_{\pi_i\pi_i}^2}^{\langle,\rangle}$ with the terms $\tilde{I}_{G_{\sigma\pi_i}^2}^{\langle,\rangle}$. The self-energies define the scattering-in and -out rates for the momentum mode p_1 . By combining in- as well as out-rates and including the external propagator, one obtains the contributions for the collision integral due to time-

dependent interactions with the mean-field mode

$$\begin{aligned}
\mathcal{I}_{\sigma}^{b.s.}(t, \vec{p}_1) &= \frac{1}{2E_1^{\sigma}} \left((1 + f_1^{\sigma}) i\tilde{\Pi}_{\sigma\sigma}^{\leftarrow}(t, p_1) - f_1^{\sigma} i\tilde{\Pi}_{\sigma\sigma}^{\rightarrow}(t, p_1) \right) \\
&= \frac{9}{2} \pi \lambda^2 \phi(t) \int_0^{\infty} d\Delta t \phi(t - \Delta t) \int \frac{dk^0}{(2\pi)} e^{-ik^0 \Delta t} \\
&\quad \times \left[\int \frac{d^3 \vec{p}_3}{(2\pi)^3} \int d^3 \vec{p}_4 \frac{\delta^{(3)}(\vec{p}_1 - \vec{p}_3 - \vec{p}_4)}{E_1^{\sigma} E_3^{\sigma} E_4^{\sigma}} \right. \\
&\quad \times \left\{ \left[(1 + f_1^{\sigma}) f_3^{\sigma} f_4^{\sigma} - f_1^{\sigma} (1 + f_3^{\sigma})(1 + f_4^{\sigma}) \right] \delta(k^0 + E_1^{\sigma} - E_3^{\sigma} - E_4^{\sigma}) \right. \\
&\quad + \left[(1 + f_1^{\sigma})(1 + f_3^{\sigma}) f_4^{\sigma} - f_1^{\sigma} f_3^{\sigma} (1 + f_4^{\sigma}) \right] \delta(k^0 + E_1^{\sigma} + E_3^{\sigma} - E_4^{\sigma}) \\
&\quad + \left[(1 + f_1^{\sigma}) f_3^{\sigma} (1 + f_4^{\sigma}) - f_1^{\sigma} (1 + f_3^{\sigma}) f_4^{\sigma} \right] \delta(k^0 + E_1^{\sigma} - E_3^{\sigma} + E_4^{\sigma}) \\
&\quad + \left[(1 + f_1^{\sigma})(1 + f_3^{\sigma})(1 + f_4^{\sigma}) - f_1^{\sigma} f_3^{\sigma} f_4^{\sigma} \right] \delta(k^0 + E_1^{\sigma} + E_3^{\sigma} + E_4^{\sigma}) \\
&\quad + \left[(1 + f_1^{\sigma}) f_3^{\sigma} f_4^{\sigma} - f_1^{\sigma} (1 + f_3^{\sigma})(1 + f_4^{\sigma}) \right] \delta(k^0 - E_1^{\sigma} + E_3^{\sigma} + E_4^{\sigma}) \\
&\quad + \left[(1 + f_1^{\sigma})(1 + f_3^{\sigma}) f_4^{\sigma} - f_1^{\sigma} f_3^{\sigma} (1 + f_4^{\sigma}) \right] \delta(k^0 - E_1^{\sigma} - E_3^{\sigma} + E_4^{\sigma}) \\
&\quad + \left[(1 + f_1^{\sigma}) f_3^{\sigma} (1 + f_4^{\sigma}) - f_1^{\sigma} (1 + f_3^{\sigma}) f_4^{\sigma} \right] \delta(k^0 - E_1^{\sigma} + E_3^{\sigma} - E_4^{\sigma}) \\
&\quad \left. \left. + \left[(1 + f_1^{\sigma})(1 + f_3^{\sigma})(1 + f_4^{\sigma}) - f_1^{\sigma} f_3^{\sigma} f_4^{\sigma} \right] \delta(k^0 - E_1^{\sigma} - E_3^{\sigma} - E_4^{\sigma}) \right\} \right] \\
&\quad + \frac{1}{2} \pi \lambda^2 \phi(t) \sum_i \int_0^{\infty} d\Delta t \phi(t - \Delta t) \int \frac{dk^0}{(2\pi)} e^{-ik^0 \Delta t} \\
&\quad \times \left[\int \frac{d^3 \vec{p}_3}{(2\pi)^3} \int d^3 \vec{p}_4 \frac{\delta^{(3)}(\vec{p}_1 - \vec{p}_3 - \vec{p}_4)}{E_1^{\sigma} E_3^{\pi_i} E_4^{\pi_i}} \right. \\
&\quad \times \left\{ \left[(1 + f_1^{\sigma}) f_3^{\pi_i} f_4^{\pi_i} - f_1^{\sigma} (1 + f_3^{\pi_i})(1 + f_4^{\pi_i}) \right] \delta(k^0 + E_1^{\sigma} - E_3^{\pi_i} - E_4^{\pi_i}) \right. \\
&\quad + \left[(1 + f_1^{\sigma})(1 + f_3^{\pi_i}) f_4^{\pi_i} - f_1^{\sigma} f_3^{\pi_i} (1 + f_4^{\pi_i}) \right] \delta(k^0 + E_1^{\sigma} + E_3^{\pi_i} - E_4^{\pi_i}) \\
&\quad + \left[(1 + f_1^{\sigma}) f_3^{\pi_i} (1 + f_4^{\pi_i}) - f_1^{\sigma} (1 + f_3^{\pi_i}) f_4^{\pi_i} \right] \delta(k^0 + E_1^{\sigma} - E_3^{\pi_i} + E_4^{\pi_i}) \\
&\quad + \left[(1 + f_1^{\sigma})(1 + f_3^{\pi_i})(1 + f_4^{\pi_i}) - f_1^{\sigma} f_3^{\pi_i} f_4^{\pi_i} \right] \delta(k^0 + E_1^{\sigma} + E_3^{\pi_i} + E_4^{\pi_i}) \\
&\quad + \left[(1 + f_1^{\sigma}) f_3^{\pi_i} f_4^{\pi_i} - f_1^{\sigma} (1 + f_3^{\pi_i})(1 + f_4^{\pi_i}) \right] \delta(k^0 - E_1^{\sigma} + E_3^{\pi_i} + E_4^{\pi_i}) \\
&\quad + \left[(1 + f_1^{\sigma})(1 + f_3^{\pi_i}) f_4^{\pi_i} - f_1^{\sigma} f_3^{\pi_i} (1 + f_4^{\pi_i}) \right] \delta(k^0 - E_1^{\sigma} - E_3^{\pi_i} + E_4^{\pi_i}) \\
&\quad + \left[(1 + f_1^{\sigma}) f_3^{\pi_i} (1 + f_4^{\pi_i}) - f_1^{\sigma} (1 + f_3^{\pi_i}) f_4^{\pi_i} \right] \delta(k^0 - E_1^{\sigma} + E_3^{\pi_i} - E_4^{\pi_i}) \\
&\quad \left. \left. + \left[(1 + f_1^{\sigma})(1 + f_3^{\pi_i})(1 + f_4^{\pi_i}) - f_1^{\sigma} f_3^{\pi_i} f_4^{\pi_i} \right] \delta(k^0 - E_1^{\sigma} - E_3^{\pi_i} - E_4^{\pi_i}) \right\} \right]
\end{aligned} \tag{A.18}$$

$$\begin{aligned}
\mathcal{I}_\sigma^{b.s.}(t, \vec{p}_1) &:= \mathcal{C}_{\sigma\phi\leftrightarrow\sigma\sigma}^{b.s.} + \sum_i \mathcal{C}_{\sigma\phi\leftrightarrow\pi_i\pi_i}^{b.s.} \\
&:= \frac{9}{2}\pi\lambda^2\phi(t) \int_0^\infty d\Delta t \phi(t-\Delta t) \int \frac{dk^0}{(2\pi)} e^{-ik^0\Delta t} \mathcal{M}_{\sigma\sigma}(t, k^0, p_1) \\
&\quad + \frac{1}{2}\pi\lambda^2\phi(t) \sum_i \int_0^\infty d\Delta t \phi(t-\Delta t) \int \frac{dk^0}{(2\pi)} e^{-ik^0\Delta t} \mathcal{M}_{\sigma\pi_i}(t, k^0, p_1), \tag{A.19}
\end{aligned}$$

$$\begin{aligned}
\mathcal{I}_{\pi_i}^{b.s.}(t, \vec{p}_1) &:= \mathcal{C}_{\pi_i\phi\leftrightarrow\pi_i\sigma}^{b.s.} \\
&:= \pi\lambda^2\phi(t) \int_0^\infty d\Delta t \phi(t-\Delta t) \int \frac{dk^0}{(2\pi)} e^{-ik^0\Delta t} \mathcal{M}_{\pi_i\sigma}(t, k^0, p_1),
\end{aligned}$$

where the calculation for pions is analogous to that of σ modes. $\mathcal{M}_{\sigma\sigma}(t, k^0, p_1)$, $\mathcal{M}_{\sigma\pi_i}(t, k^0, p_1)$ and $\mathcal{M}_{\pi_i\sigma}(t, k^0, p_1)$ define memory kernels with respect to Δt via the Fourier transform:

$$\begin{aligned}
\mathcal{M}_{\sigma\sigma}(t, \Delta t, p_1) &:= \int \frac{dk^0}{(2\pi)} e^{-ik^0\Delta t} \mathcal{M}_{\sigma\sigma}(t, k^0, p_1), \\
\mathcal{M}_{\sigma\pi_i}(t, \Delta t, p_1) &:= \int \frac{dk^0}{(2\pi)} e^{-ik^0\Delta t} \mathcal{M}_{\sigma\pi_i}(t, k^0, p_1), \\
\mathcal{M}_{\pi_i\sigma}(t, \Delta t, p_1) &:= \int \frac{dk^0}{(2\pi)} e^{-ik^0\Delta t} \mathcal{M}_{\pi_i\sigma}(t, k^0, p_1). \tag{A.20}
\end{aligned}$$

Obviously, we recover contributions in (A.18) which do not conserve the particle number and therefore should be essential for the chemical equilibration. However, an inclusion of such inelastic processes requires a proper renormalization, since they contain a divergent part and we decide not to consider those contributions in our first study.

In numerical simulations one has different possibilities for computing the collision integrals (A.19), either by explicitly evaluating the kernel functions $\mathcal{M}_{\sigma\sigma}(t, k^0, p_1)$, $\mathcal{M}_{\sigma\pi_i}(t, k^0, p_1)$, $\mathcal{M}_{\pi_i\sigma}(t, k^0, p_1)$ and taking the Fourier transform or directly by making use of the symmetry with respect to k^0 and integrating out the energy δ -function. By doing the latter, the integration over the antisymmetric and complex part vanishes, leading to a time integration which contains a cosine. Such behavior is known from oscillatory systems and a pure time integration with cosine as argument converges to a delta like function³⁷ for large time differences:

$$\lim_{t-t_0 \rightarrow \infty} \int_0^{t-t_0} d\Delta t \cos(k^0\Delta t) = \lim_{t-t_0 \rightarrow \infty} \frac{1}{k^0} \sin(k^0(t-t_0)) \simeq \pi\delta(k^0). \tag{A.21}$$

Therefore, we note that a local time approximation with $\phi(t-\Delta t) \simeq \phi(t)$ leads to a simple on-shell gradient expression for the sunset diagram and cannot account for important dissipation phenomena from the mean-field to hard modes of the same particle species.

Due to detailed balance also the mean-field equation contains memory kernels, which are defined in Sec. 3.8. By making use of the decomposition (96) for the Green's functions, applying the on-shell ansatz (100) for the spectral function in Wigner space and combining that with relations (A.12), (A.13) results in the following form for the kernels

³⁷In a strict sense a sequence of sinc functions does not converge to a delta function because of negative contributions. Nevertheless, an integral over such a sequence with an arbitrary test function has the same properties as known for a delta function.

of the mean-field equation:

$$\begin{aligned}
\tilde{\mathcal{M}}_{\sigma\sigma}(X, k) &= \int d^4\Delta x e^{ik^\mu\Delta x_\mu} \left[(iG_{\sigma\sigma}^>(x, y))^3 - (iG_{\sigma\sigma}^<(x, y))^3 \right] \\
&=: \left(\tilde{\mathcal{I}}_{G_{\sigma\sigma}}^> * \tilde{\mathcal{I}}_{G_{\sigma\sigma}^2}^> \right)(X, k) - \left(\tilde{\mathcal{I}}_{G_{\sigma\sigma}}^< * \tilde{\mathcal{I}}_{G_{\sigma\sigma}^2}^< \right)(X, k) \\
&= \int \frac{d^4p_1}{(2\pi)^4} \left[i\tilde{G}^>(X, p_1) \tilde{\mathcal{I}}_{G_{\sigma\sigma}^2}^>(X, k - p_1) - i\tilde{G}^<(X, p_1) \tilde{\mathcal{I}}_{G_{\sigma\sigma}^2}^<(X, k - p_1) \right] \\
&\simeq \frac{\pi}{4} \int \frac{d\vec{p}_1}{(2\pi)^3} \int \frac{d\vec{p}_3}{(2\pi)^3} \int d\vec{p}_4 \frac{\delta^{(3)}(\vec{k} + \vec{p}_1 - \vec{p}_3 - \vec{p}_4)}{E_1^\sigma E_3^\sigma E_4^\sigma} \\
&\quad \times \left\{ \left[f_1^\sigma (1 + f_3^\sigma) (1 + f_4^\sigma) - (1 + f_1^\sigma) f_3^\sigma f_4^\sigma \right] \delta(k^0 + E_1^\sigma - E_3^\sigma - E_4^\sigma) \right. \\
&\quad + \left[f_1^\sigma f_3^\sigma (1 + f_4^\sigma) - (1 + f_1^\sigma) (1 + f_3^\sigma) f_4^\sigma \right] \delta(k^0 + E_1^\sigma + E_3^\sigma - E_4^\sigma) \\
&\quad + \left[f_1^\sigma (1 + f_3^\sigma) f_4^\sigma - (1 + f_1^\sigma) f_3^\sigma (1 + f_4^\sigma) \right] \delta(k^0 + E_1^\sigma - E_3^\sigma + E_4^\sigma) \\
&\quad + \left[f_1^\sigma f_3^\sigma f_4^\sigma - (1 + f_1^\sigma) (1 + f_3^\sigma) (1 + f_4^\sigma) \right] \delta(k^0 + E_1^\sigma + E_3^\sigma + E_4^\sigma) \\
&\quad + \left[(1 + f_1^\sigma) f_3^\sigma f_4^\sigma - f_1^\sigma (1 + f_3^\sigma) (1 + f_4^\sigma) \right] \delta(k^0 - E_1^\sigma + E_3^\sigma + E_4^\sigma) \\
&\quad + \left[(1 + f_1^\sigma) (1 + f_3^\sigma) f_4^\sigma - f_1^\sigma f_3^\sigma (1 + f_4^\sigma) \right] \delta(k^0 - E_1^\sigma - E_3^\sigma + E_4^\sigma) \\
&\quad + \left[(1 + f_1^\sigma) f_3^\sigma (1 + f_4^\sigma) - f_1^\sigma (1 + f_3^\sigma) f_4^\sigma \right] \delta(k^0 - E_1^\sigma + E_3^\sigma - E_4^\sigma) \\
&\quad \left. + \left[(1 + f_1^\sigma) (1 + f_3^\sigma) (1 + f_4^\sigma) - f_1^\sigma f_3^\sigma f_4^\sigma \right] \delta(k^0 - E_1^\sigma - E_3^\sigma - E_4^\sigma) \right\}
\end{aligned} \tag{A.22}$$

$$\begin{aligned}
\tilde{\mathcal{M}}_{\sigma\pi_i}(X, k) &\simeq \frac{\pi}{4} \int \frac{d\vec{p}_1}{(2\pi)^3} \int \frac{d\vec{p}_3}{(2\pi)^3} \int d\vec{p}_4 \frac{\delta^{(3)}(\vec{k} + \vec{p}_1 - \vec{p}_3 - \vec{p}_4)}{E_1^\sigma E_3^{\pi_i} E_4^{\pi_i}} \\
&\quad \times \left\{ \left[f_1^\sigma (1 + f_3^{\pi_i}) (1 + f_4^{\pi_i}) - (1 + f_1^\sigma) f_3^{\pi_i} f_4^{\pi_i} \right] \delta(k^0 + E_1^\sigma - E_3^{\pi_i} - E_4^{\pi_i}) \right. \\
&\quad + \left[f_1^\sigma f_3^{\pi_i} (1 + f_4^{\pi_i}) - (1 + f_1^\sigma) (1 + f_3^{\pi_i}) f_4^{\pi_i} \right] \delta(k^0 + E_1^\sigma + E_3^{\pi_i} - E_4^{\pi_i}) \\
&\quad + \left[f_1^\sigma (1 + f_3^{\pi_i}) f_4^{\pi_i} - (1 + f_1^\sigma) f_3^{\pi_i} (1 + f_4^{\pi_i}) \right] \delta(k^0 + E_1^\sigma - E_3^{\pi_i} + E_4^{\pi_i}) \\
&\quad + \left[f_1^\sigma f_3^{\pi_i} f_4^{\pi_i} - (1 + f_1^\sigma) (1 + f_3^{\pi_i}) (1 + f_4^{\pi_i}) \right] \delta(k^0 + E_1^\sigma + E_3^{\pi_i} + E_4^{\pi_i}) \\
&\quad + \left[(1 + f_1^\sigma) f_3^{\pi_i} f_4^{\pi_i} - f_1^\sigma (1 + f_3^{\pi_i}) (1 + f_4^{\pi_i}) \right] \delta(k^0 - E_1^\sigma + E_3^{\pi_i} + E_4^{\pi_i}) \\
&\quad + \left[(1 + f_1^\sigma) (1 + f_3^{\pi_i}) f_4^{\pi_i} - f_1^\sigma f_3^{\pi_i} (1 + f_4^{\pi_i}) \right] \delta(k^0 - E_1^\sigma - E_3^{\pi_i} + E_4^{\pi_i}) \\
&\quad + \left[(1 + f_1^\sigma) f_3^{\pi_i} (1 + f_4^{\pi_i}) - f_1^\sigma (1 + f_3^{\pi_i}) f_4^{\pi_i} \right] \delta(k^0 - E_1^\sigma + E_3^{\pi_i} - E_4^{\pi_i}) \\
&\quad \left. + \left[(1 + f_1^\sigma) (1 + f_3^{\pi_i}) (1 + f_4^{\pi_i}) - f_1^\sigma f_3^{\pi_i} f_4^{\pi_i} \right] \delta(k^0 - E_1^\sigma - E_3^{\pi_i} - E_4^{\pi_i}) \right\}.
\end{aligned} \tag{A.23}$$

3. Basketball diagrams (b.)

$$\begin{aligned}
\Gamma_2^b &= \frac{3}{4} i\lambda^2 \int_C d^4x \int_C d^4y G_{\sigma\sigma}^4(x, y) + \frac{3}{4} i\lambda^2 \sum_i \int_C d^4x \int_C d^4y G_{\pi_i\pi_i}^4(x, y) \\
&\quad + \frac{1}{2} i\lambda^2 \sum_i \int_C d^4x \int_C d^4y G_{\sigma\sigma}^2(x, y) G_{\pi_i\pi_i}^2(x, y) \\
&\quad + \frac{1}{2} i\lambda^2 \sum_{i,j>i} \int_C d^4x \int_C d^4y G_{\pi_i\pi_i}^2(x, y) G_{\pi_j\pi_j}^2(x, y).
\end{aligned} \tag{A.24}$$

In analogy to (A.8) one obtains for the self-energies:

$$\begin{aligned}
i\Pi_{\sigma\sigma}^{<>}(x, y) &= 6\lambda^2 (iG_{\sigma\sigma}^{<>}(x, y))^3 + 2\lambda^2 \sum_i (iG_{\sigma\sigma}^{<>}(x, y)) (iG_{\pi_i\pi_i}^{<>}(x, y))^2 \\
i\Pi_{\pi_i\pi_i}^{<>}(x, y) &= 6\lambda^2 (iG_{\pi_i\pi_i}^{<>}(x, y))^3 \\
&\quad + 2\lambda^2 (iG_{\pi_i\pi_i}^{<>}(x, y)) \left[(iG_{\sigma\sigma}^{<>}(x, y))^2 + \sum_{j \neq i} (iG_{\pi_j\pi_j}^{<>}(x, y))^2 \right].
\end{aligned} \tag{A.25}$$

With the auxiliary functions (A.9), it follows for the Wigner transforms:

$$\begin{aligned}
i\tilde{\Pi}_{\sigma\sigma}^{<>}(X, p_1) &= 6\lambda^2 \left(i\tilde{G}_{\sigma\sigma}^{<>} * \tilde{I}_{G_{\sigma\sigma}^2}^{<>} \right) (X, p_1) + 2\lambda^2 \sum_i \left(i\tilde{G}_{\sigma\sigma}^{<>} * \tilde{I}_{G_{\pi_i\pi_i}^2}^{<>} \right) (X, p_1), \\
i\tilde{\Pi}_{\pi_i\pi_i}^{<>}(X, p_1) &= 6\lambda^2 \left(i\tilde{G}_{\pi_i\pi_i}^{<>} * \tilde{I}_{G_{\pi_i\pi_i}^2}^{<>} \right) (X, p_1) \\
&\quad + 2\lambda^2 \left(i\tilde{G}_{\pi_i\pi_i}^{<>} * \left[\tilde{I}_{G_{\sigma\sigma}^2}^{<>} + \sum_{j \neq i} \tilde{I}_{G_{\pi_j\pi_j}^2}^{<>} \right] \right) (X, p_1).
\end{aligned} \tag{A.26}$$

Inserting the on-shell ansatz for the propagators in Wigner space (96) leads then to the following gain and loss contributions (compare also with (A.12)):

$$\begin{aligned}
\left(i\tilde{G}_{\sigma\sigma}^{<} * \tilde{I}_{G_{\sigma\sigma}^2}^{<} \right) (X, p_1) &= \frac{\pi}{4} \int \frac{d^3 \vec{p}_2}{(2\pi)^3} \int \frac{d^3 \vec{p}_3}{(2\pi)^3} \int d^3 \vec{p}_4 \frac{\delta^{(3)}(\vec{p}_1 - \vec{p}_2 - \vec{p}_3 + \vec{p}_4)}{E_2^\sigma E_3^\sigma E_4^\sigma} \\
&\quad \times \left\{ \left[(1 + f_2^\sigma) f_3^\sigma f_4^\sigma \right] \delta(E_1 + E_2 - E_3 - E_4) \right. \\
&\quad \quad + \left[f_2^\sigma (1 + f_3^\sigma) f_4^\sigma \right] \delta(E_1 - E_2 + E_3 - E_4) \\
&\quad \quad \left. + \left[f_2^\sigma f_3^\sigma (1 + f_4^\sigma) \right] \delta(E_1 - E_2 - E_3 + E_4) \right\},
\end{aligned} \tag{A.27}$$

$$\begin{aligned}
\left(i\tilde{G}_{\sigma\sigma}^{>} * \tilde{I}_{G_{\sigma\sigma}^2}^{>} \right) (X, p_1) &= \frac{\pi}{4} \int \frac{d^3 \vec{p}_2}{(2\pi)^3} \int \frac{d^3 \vec{p}_3}{(2\pi)^3} \int d^3 \vec{p}_4 \frac{\delta^{(3)}(\vec{p}_1 - \vec{p}_2 - \vec{p}_3 + \vec{p}_4)}{E_2^\sigma E_3^\sigma E_4^\sigma} \\
&\quad \times \left\{ \left[f_2^\sigma (1 + f_3^\sigma) (1 + f_4^\sigma) \right] \delta(E_1 + E_2 - E_3 - E_4) \right. \\
&\quad \quad + \left[(1 + f_2^\sigma) f_3^\sigma (1 + f_4^\sigma) \right] \delta(E_1 - E_2 + E_3 - E_4) \\
&\quad \quad \left. + \left[(1 + f_2^\sigma) (1 + f_3^\sigma) f_4^\sigma \right] \delta(E_1 - E_2 - E_3 + E_4) \right\},
\end{aligned} \tag{A.28}$$

where we neglected all energy conserving δ -functions, which cannot be fulfilled on-shell.

In analogy one derives similar expressions for $\left(i\tilde{G}_{\sigma\sigma}^{<} * \tilde{I}_{G_{\pi_i\pi_i}^2}^{<} \right)$ and $\left(i\tilde{G}_{\sigma\sigma}^{>} * \tilde{I}_{G_{\pi_i\pi_i}^2}^{>} \right)$ by replacing $E_3^\sigma, f_3^\sigma, E_4^\sigma, f_4^\sigma$ with $E_3^{\pi_i}, f_3^{\pi_i}, E_4^{\pi_i}, f_4^{\pi_i}$. Consequently, for the terms $\left(i\tilde{G}_{\pi_i\pi_i}^{<} * \tilde{I}_{G_{\sigma\sigma}^2}^{<} \right)$ and $\left(i\tilde{G}_{\pi_i\pi_i}^{>} * \tilde{I}_{G_{\sigma\sigma}^2}^{>} \right)$ one replaces E_2^σ, f_2^σ with $E_2^{\pi_i}, f_2^{\pi_i}$. Finally, terms of the form $\left(i\tilde{G}_{\pi_i\pi_i}^{<} * \tilde{I}_{G_{\pi_i\pi_i}^2}^{<} \right)$, $\left(i\tilde{G}_{\pi_i\pi_i}^{>} * \tilde{I}_{G_{\pi_i\pi_i}^2}^{>} \right)$, $\left(i\tilde{G}_{\pi_i\pi_i}^{<} * \tilde{I}_{G_{\pi_j\pi_j}^2}^{<} \right)$ as well as $\left(i\tilde{G}_{\pi_i\pi_i}^{>} * \tilde{I}_{G_{\pi_j\pi_j}^2}^{>} \right)$ contain only π_i and π_j as upper indices, but have the same structure like equations (A.27), (A.28).

Combining in- as well as out-rates and summing up identical contributions leads to the collision integrals of elastic

scatterings between mesons:

$$\begin{aligned}
\mathcal{I}_\sigma^b(t, \vec{p}_1) &= \frac{1}{2E_1^\sigma} \left((1 + f_1^\sigma) i\tilde{\Pi}_{\sigma\sigma}^<(t, p_1) - f_1^\sigma i\tilde{\Pi}_{\sigma\sigma}^>(t, p_1) \right) \\
&=: \mathcal{C}_{\sigma\sigma \leftrightarrow \sigma\sigma}^b + \sum_i \mathcal{C}_{\sigma\pi_i \leftrightarrow \sigma\pi_i}^b + \sum_i \mathcal{C}_{\sigma\sigma \leftrightarrow \pi_i\pi_i}^b, \\
\mathcal{I}_{\pi_i}^b(t, \vec{p}_1) &= \frac{1}{2E_1^{\pi_i}} \left((1 + f_1^{\pi_i}) i\tilde{\Pi}_{\pi_i\pi_i}^<(t, p_1) - f_1^{\pi_i} i\tilde{\Pi}_{\pi_i\pi_i}^>(t, p_1) \right) \\
&=: \mathcal{C}_{\pi_i\pi_i \leftrightarrow \pi_i\pi_i}^b + \sum_{j \neq i} \mathcal{C}_{\pi_i\pi_j \leftrightarrow \pi_i\pi_j}^b + \sum_{j \neq i} \mathcal{C}_{\pi_i\pi_i \leftrightarrow \pi_j\pi_j}^b + \mathcal{C}_{\pi_i\sigma \leftrightarrow \pi_i\sigma}^b + \mathcal{C}_{\pi_i\pi_i \leftrightarrow \sigma\sigma}^b,
\end{aligned} \tag{A.29}$$

where the following decomposition with respect to different processes is applied:

$$\begin{aligned}
\mathcal{C}_{\sigma\sigma \leftrightarrow \sigma\sigma}^b &:= \frac{9}{4} \pi \lambda^2 \int \frac{d^3 \vec{p}_2}{(2\pi)^3} \int \frac{d^3 \vec{p}_3}{(2\pi)^3} \int d^3 \vec{p}_4 \frac{\delta^{(3)}(\vec{p}_1 + \vec{p}_2 - \vec{p}_3 - \vec{p}_4)}{E_1^\sigma E_2^\sigma E_3^\sigma E_4^\sigma} \\
&\quad \times \left\{ \left[(1 + f_1^\sigma)(1 + f_2^\sigma) f_3^\sigma f_4^\sigma - f_1^\sigma f_2^\sigma (1 + f_3^\sigma)(1 + f_4^\sigma) \right] \delta(E_1^\sigma + E_2^\sigma - E_3^\sigma - E_4^\sigma) \right\}, \\
\mathcal{C}_{\sigma\pi_i \leftrightarrow \sigma\pi_i}^b &:= \frac{2}{4} \pi \lambda^2 \int \frac{d^3 \vec{p}_2}{(2\pi)^3} \int \frac{d^3 \vec{p}_3}{(2\pi)^3} \int d^3 \vec{p}_4 \frac{\delta^{(3)}(\vec{p}_1 + \vec{p}_2 - \vec{p}_3 - \vec{p}_4)}{E_1^\sigma E_2^{\pi_i} E_3^\sigma E_4^{\pi_i}} \\
&\quad \times \left\{ \left[(1 + f_1^\sigma)(1 + f_2^{\pi_i}) f_3^\sigma f_4^{\pi_i} - f_1^\sigma f_2^{\pi_i} (1 + f_3^\sigma)(1 + f_4^{\pi_i}) \right] \delta(E_1^\sigma + E_2^{\pi_i} - E_3^\sigma - E_4^{\pi_i}) \right\}, \\
\mathcal{C}_{\sigma\sigma \leftrightarrow \pi_i\pi_i}^b &:= \frac{1}{4} \pi \lambda^2 \int \frac{d^3 \vec{p}_2}{(2\pi)^3} \int \frac{d^3 \vec{p}_3}{(2\pi)^3} \int d^3 \vec{p}_4 \frac{\delta^{(3)}(\vec{p}_1 + \vec{p}_2 - \vec{p}_3 - \vec{p}_4)}{E_1^\sigma E_2^\sigma E_3^{\pi_i} E_4^{\pi_i}} \\
&\quad \times \left\{ \left[(1 + f_1^\sigma)(1 + f_2^\sigma) f_3^{\pi_i} f_4^{\pi_i} - f_1^\sigma f_2^\sigma (1 + f_3^{\pi_i})(1 + f_4^{\pi_i}) \right] \delta(E_1^\sigma + E_2^\sigma - E_3^{\pi_i} - E_4^{\pi_i}) \right\}, \\
\mathcal{C}_{\pi_i\pi_i \leftrightarrow \pi_i\pi_i}^b &:= \frac{9}{4} \pi \lambda^2 \int \frac{d^3 \vec{p}_2}{(2\pi)^3} \int \frac{d^3 \vec{p}_3}{(2\pi)^3} \int d^3 \vec{p}_4 \frac{\delta^{(3)}(\vec{p}_1 + \vec{p}_2 - \vec{p}_3 - \vec{p}_4)}{E_1^{\pi_i} E_2^{\pi_i} E_3^{\pi_i} E_4^{\pi_i}} \\
&\quad \times \left\{ \left[(1 + f_1^{\pi_i})(1 + f_2^{\pi_i}) f_3^{\pi_i} f_4^{\pi_i} - f_1^{\pi_i} f_2^{\pi_i} (1 + f_3^{\pi_i})(1 + f_4^{\pi_i}) \right] \delta(E_1^{\pi_i} + E_2^{\pi_i} - E_3^{\pi_i} - E_4^{\pi_i}) \right\} \\
\mathcal{C}_{\pi_i\pi_j \leftrightarrow \pi_i\pi_j}^b &:= \frac{2}{4} \pi \lambda^2 \int \frac{d^3 \vec{p}_2}{(2\pi)^3} \int \frac{d^3 \vec{p}_3}{(2\pi)^3} \int d^3 \vec{p}_4 \frac{\delta^{(3)}(\vec{p}_1 + \vec{p}_2 - \vec{p}_3 - \vec{p}_4)}{E_1^{\pi_i} E_2^{\pi_j} E_3^{\pi_i} E_4^{\pi_j}} \\
&\quad \times \left\{ \left[(1 + f_1^{\pi_i})(1 + f_2^{\pi_j}) f_3^{\pi_i} f_4^{\pi_j} - f_1^{\pi_i} f_2^{\pi_j} (1 + f_3^{\pi_i})(1 + f_4^{\pi_j}) \right] \delta(E_1^{\pi_i} + E_2^{\pi_j} - E_3^{\pi_i} - E_4^{\pi_j}) \right\} \\
\mathcal{C}_{\pi_i\pi_i \leftrightarrow \pi_j\pi_j}^b &:= \frac{1}{4} \pi \lambda^2 \int \frac{d^3 \vec{p}_2}{(2\pi)^3} \int \frac{d^3 \vec{p}_3}{(2\pi)^3} \int d^3 \vec{p}_4 \frac{\delta^{(3)}(\vec{p}_1 + \vec{p}_2 - \vec{p}_3 - \vec{p}_4)}{E_1^{\pi_i} E_2^{\pi_i} E_3^{\pi_j} E_4^{\pi_j}} \\
&\quad \times \left\{ \left[(1 + f_1^{\pi_i})(1 + f_2^{\pi_i}) f_3^{\pi_j} f_4^{\pi_j} - f_1^{\pi_i} f_2^{\pi_i} (1 + f_3^{\pi_j})(1 + f_4^{\pi_j}) \right] \delta(E_1^{\pi_i} + E_2^{\pi_i} - E_3^{\pi_j} - E_4^{\pi_j}) \right\},
\end{aligned} \tag{A.30}$$

$$\begin{aligned}
C_{\pi_i\sigma\leftrightarrow\pi_i\sigma}^b &:= \frac{2}{4}\pi\lambda^2 \int \frac{d^3\vec{p}_2}{(2\pi)^3} \int \frac{d^3\vec{p}_3}{(2\pi)^3} \int d^3\vec{p}_4 \frac{\delta^{(3)}(\vec{p}_1 + \vec{p}_2 - \vec{p}_3 - \vec{p}_4)}{E_1^{\pi_i} E_2^\sigma E_3^{\pi_i} E_4^\sigma} \\
&\quad \times \left\{ \left[(1 + f_1^{\pi_i})(1 + f_2^\sigma) f_3^{\pi_i} f_4^\sigma \right. \right. \\
&\quad \left. \left. - f_1^{\pi_i} f_2^\sigma (1 + f_3^{\pi_i})(1 + f_4^\sigma) \right] \delta(E_1^{\pi_i} + E_2^\sigma - E_3^{\pi_i} - E_4^\sigma) \right\}, \\
C_{\pi_i\pi_i\leftrightarrow\sigma\sigma}^b &:= \frac{1}{4}\pi\lambda^2 \int \frac{d^3\vec{p}_2}{(2\pi)^3} \int \frac{d^3\vec{p}_3}{(2\pi)^3} \int d^3\vec{p}_4 \frac{\delta^{(3)}(\vec{p}_1 + \vec{p}_2 - \vec{p}_3 - \vec{p}_4)}{E_1^{\pi_i} E_2^{\pi_i} E_3^\sigma E_4^\sigma} \\
&\quad \times \left\{ \left[(1 + f_1^{\pi_i})(1 + f_2^{\pi_i}) f_3^\sigma f_4^\sigma \right. \right. \\
&\quad \left. \left. - f_1^{\pi_i} f_2^{\pi_i} (1 + f_3^\sigma)(1 + f_4^\sigma) \right] \delta(E_1^{\pi_i} + E_2^{\pi_i} - E_3^\sigma - E_4^\sigma) \right\}.
\end{aligned} \tag{A.31}$$

Note: since the collision integrals (A.30), (A.31) for elastic scatterings have locally (in space) the same form for homogeneous and inhomogeneous systems, we skip the possible dependence on the position vector \vec{x} .

4. Fermionic sunset diagrams (f.s.)

$$\begin{aligned}
\Gamma_2^{\text{f.s.}} &= -\frac{1}{2}ig^2 \int_C d^4x \int_C d^4y \text{Tr} [D(x, y) D(y, x)] G_{\sigma\sigma}(x, y) \\
&\quad - \frac{1}{2}ig^2 \sum_i \int_C d^4x \int_C d^4y \text{Tr} [D(x, y) D(y, x)] G_{\pi_i\pi_i}(x, y).
\end{aligned} \tag{A.32}$$

In analogy to (A.8) one obtains for the self-energies

$$\begin{aligned}
i\Pi_{\sigma\sigma}^{<,>}(x, y) &= -g^2 \text{Tr} [iD^{<,>}(x, y) iD^{>,<}(y, x)], \\
i\Pi_{\pi_i\pi_i}^{<,>}(x, y) &= -g^2 \text{Tr} [iD^{<,>}(x, y) iD^{>,<}(y, x)].
\end{aligned} \tag{A.33}$$

Consequently, for the Wigner transforms it follows

$$\begin{aligned}
i\tilde{\Pi}_{\sigma\sigma}^{<,>}(X, p_1) &= -g^2 \text{Tr} (i\tilde{D}^{<,>} * i\tilde{D}^{>,<})(X, p_1), \\
i\tilde{\Pi}_{\pi_i\pi_i}^{<,>}(X, p_1) &= -g^2 \text{Tr} (i\tilde{D}^{<,>} * i\tilde{D}^{>,<})(X, p_1).
\end{aligned} \tag{A.34}$$

Since the expressions for sigma and pions have identical structure, it is suitable to skip the mesonic index in the following.

Inserting the on-shell ansatz for the propagators in Wigner space (see Eqs. (97), (100)) results in (analogous calculation for $i\tilde{\Pi}^{<}(X, p_1)$):

$$\begin{aligned}
i\tilde{\Pi}^{>}(X, p_1) &= \pi^2 g^2 \int \frac{d^4p_2}{(2\pi)^4} \frac{\text{Tr} \left[(\gamma^\mu (p_{1,\mu} + p_{2,\mu}) + M_\psi) (\gamma^\nu p_{2,\nu} + M_\psi) \right]}{E^\psi(X, p_1 + p_2) E^\psi(X, p_2)} \\
&\quad \times \left[\delta(p_1^0 + p_2^0 - E^\psi(X, p_1 + p_2)) - \delta(p_1^0 + p_2^0 + E^\psi(X, p_1 + p_2)) \right] \\
&\quad \times \left[\delta(p_2^0 - E^\psi(X, p_2)) - \delta(p_2^0 + E^\psi(X, p_2)) \right] \\
&\quad \times N_\psi^>(X, p_1 + p_2) N_\psi^<(X, p_2).
\end{aligned} \tag{A.35}$$

After evaluating the trace over Dirac and flavor indices,

$$\begin{aligned}
&\text{Tr} \left[(\gamma^\mu (p_{1,\mu} + p_{2,\mu}) + M_\psi) (\gamma^\nu p_{2,\nu} + M_\psi) \right] \\
&= \text{Tr} \left[\gamma^\mu \gamma^\nu (p_{1,\mu} + p_{2,\mu}) p_{2,\nu} + M_\psi^2 \right] = 4d_\psi (\eta^{\mu\nu} (p_{1,\mu} + p_{2,\mu}) p_{2,\nu} + M_\psi^2) \\
&= 4d_\psi \left((p_1^\nu + p_2^\nu) p_{2,\nu} + M_\psi^2 \right) = 4d_\psi \left((p_1^0 + p_2^0) p_{2,0} - (\vec{p}_1 + \vec{p}_2) \cdot \vec{p}_2 + M_\psi^2 \right),
\end{aligned} \tag{A.36}$$

the relevant self-energies with $p_1^0 \geq 0$ become:

$$\begin{aligned}
i\tilde{\Pi}^>(X, p_1) &= 2\pi g^2 d_\psi \int \frac{d^3 \vec{p}_2}{(2\pi)^3} \frac{p_1^0 E_{\vec{p}_2}^{\bar{\psi}} - \vec{p}_1 \cdot \vec{p}_2 - 2M_\psi^2}{E_{\vec{p}_1 - \vec{p}_2}^\psi E_{\vec{p}_2}^{\bar{\psi}}} \\
&\quad \times \delta(p_1^0 - E_{\vec{p}_1 - \vec{p}_2}^\psi - E_{\vec{p}_2}^{\bar{\psi}}) (1 - f^\psi(\vec{p}_1 - \vec{p}_2)) (1 - f^{\bar{\psi}}(\vec{p}_2)), \\
i\tilde{\Pi}^<(X, p_1) &= 2\pi g^2 d_\psi \int \frac{d^3 p_2}{(2\pi)^3} \frac{p_1^0 E_{\vec{p}_2}^{\bar{\psi}} - \vec{p}_1 \cdot \vec{p}_2 - 2M_\psi^2}{E_{\vec{p}_1 - \vec{p}_2}^\psi E_{\vec{p}_2}^{\bar{\psi}}} \\
&\quad \times \delta(p_1^0 - E_{\vec{p}_1 - \vec{p}_2}^\psi - E_{\vec{p}_2}^{\bar{\psi}}) f^\psi(\vec{p}_1 - \vec{p}_2) f^{\bar{\psi}}(\vec{p}_2),
\end{aligned} \tag{A.37}$$

where all energy conserving δ -functions were neglected, which cannot be fulfilled on-shell.

Combining in- as well as out-rates and including the external propagators, leads to the collision integrals of elastic scatterings between mesons and quarks:

$$\begin{aligned}
C_{\sigma \leftrightarrow \psi \bar{\psi}}^{f.s.} &:= \pi g^2 d_\psi \int \frac{d^3 \vec{p}_2}{(2\pi)^3} \int d^3 \vec{p}_3 \frac{\delta^{(3)}(\vec{p}_1 - \vec{p}_2 - \vec{p}_3)}{E_1^\sigma} \left(1 - \frac{\vec{p}_2 \cdot \vec{p}_3}{E_2^{\bar{\psi}} E_3^\psi} - \frac{M_\psi^2}{E_2^{\bar{\psi}} E_3^\psi} \right) \\
&\quad \times \left\{ \left[(1 + f_1^\sigma) f_2^{\bar{\psi}} f_3^\psi - f_1^\sigma (1 - f_2^{\bar{\psi}}) (1 - f_3^\psi) \right] \delta(E_1^\sigma - E_2^{\bar{\psi}} - E_3^\psi) \right\}, \\
C_{\pi_i \leftrightarrow \psi \bar{\psi}}^{f.s.} &:= \pi g^2 d_\psi \int \frac{d^3 \vec{p}_2}{(2\pi)^3} \int d^3 \vec{p}_3 \frac{\delta^{(3)}(\vec{p}_1 - \vec{p}_2 - \vec{p}_3)}{E_1^{\pi_i}} \left(1 - \frac{\vec{p}_2 \cdot \vec{p}_3}{E_2^{\bar{\psi}} E_3^\psi} - \frac{M_\psi^2}{E_2^{\bar{\psi}} E_3^\psi} \right) \\
&\quad \times \left\{ \left[(1 + f_1^{\pi_i}) f_2^{\bar{\psi}} f_3^\psi - f_1^{\pi_i} (1 - f_2^{\bar{\psi}}) (1 - f_3^\psi) \right] \delta(E_1^{\pi_i} - E_2^{\bar{\psi}} - E_3^\psi) \right\}.
\end{aligned} \tag{A.38}$$

Instead of an explicit and tedious calculation for the collision integrals of quarks, we make use of detailed balance, leading directly to the following expressions:

$$\begin{aligned}
\mathcal{I}_\psi^{f.s.}(t, \vec{p}_1) &:= C_{\psi \bar{\psi} \leftrightarrow \sigma}^{f.s.} + \sum_i C_{\psi \bar{\psi} \leftrightarrow \pi_i}^{f.s.}, \\
C_{\psi \bar{\psi} \leftrightarrow \sigma}^{f.s.} &:= \pi g^2 \int \frac{d^3 \vec{p}_2}{(2\pi)^3} \int d^3 \vec{p}_3 \frac{\delta^{(3)}(\vec{p}_1 + \vec{p}_2 - \vec{p}_3)}{E_3^\sigma} \left(1 - \frac{\vec{p}_1 \cdot \vec{p}_2}{E_1^\psi E_2^{\bar{\psi}}} - \frac{M_\psi^2}{E_1^\psi E_2^{\bar{\psi}}} \right) \\
&\quad \times \left\{ \left[(1 - f_1^\psi) (1 - f_2^{\bar{\psi}}) f_3^\sigma - f_1^\psi f_2^{\bar{\psi}} (1 + f_3^\sigma) \right] \delta(E_1^\psi + E_2^{\bar{\psi}} - E_3^\sigma) \right\}, \\
C_{\psi \bar{\psi} \leftrightarrow \pi_i}^{f.s.} &:= \pi g^2 \int \frac{d^3 \vec{p}_2}{(2\pi)^3} \int d^3 \vec{p}_3 \frac{\delta^{(3)}(\vec{p}_1 + \vec{p}_2 - \vec{p}_3)}{E_1^{\pi_i}} \left(1 - \frac{\vec{p}_1 \cdot \vec{p}_2}{E_1^\psi E_2^{\bar{\psi}}} - \frac{M_\psi^2}{E_1^\psi E_2^{\bar{\psi}}} \right) \\
&\quad \times \left\{ \left[(1 - f_1^\psi) (1 - f_2^{\bar{\psi}}) f_3^{\pi_i} - f_1^\psi f_2^{\bar{\psi}} (1 + f_3^{\pi_i}) \right] \delta(E_1^\psi + E_2^{\bar{\psi}} - E_3^{\pi_i}) \right\},
\end{aligned} \tag{A.39}$$

Consequently, the collision integral for anti-quarks $\mathcal{I}_{\bar{\psi}}^{f.s.}(t, \vec{p}_1)$ follows by exchanging fermionic field indices $\psi \leftrightarrow \bar{\psi}$.

Appendix B. Thermodynamic calculations within the imaginary time formalism

Appendix B.1. Bosonic loop integrals

As already discussed in Sec. 3.6 the propagators of a system in equilibrium depend only on the relative space-time difference, allowing to perform all relevant calculations in momentum space. Additionally, by focusing only on

momentum independent mass terms from local part of the self-energy (see propagator relations 104), one obtains

$$\begin{aligned} \frac{i}{2} \text{Tr} \ln [G_{\varphi_a \varphi_a}^{-1}] &= \frac{i}{2} \int_x \int_k \ln [G_{\varphi_a \varphi_a}^{-1}(k)] = \frac{i}{2} V \sum_n \int \frac{d^3 \vec{k}}{(2\pi)^3} \ln [-i(k_n^2 - M_{\varphi_a}^2)] \\ &= \frac{i}{2} V \sum_n \int \frac{d^3 \vec{k}}{(2\pi)^3} \ln (k_n^2 - M_{\varphi_a}^2) \end{aligned} \quad (\text{B.1})$$

The sum over bosonic Matsubara frequencies can be evaluated by applying following steps (see also Ref. [50]):

$$\begin{aligned} f(E_{\varphi_a}) &:= \sum_n \ln [i(-k_n^2 + M_{\varphi_a}^2)] = \sum_n \ln \left[i \left(\frac{4\pi^2 n^2}{\beta^2} + E_{\varphi_a}^2 \right) \right], \\ \frac{\partial f}{\partial E_{\varphi_a}} &= \sum_n \frac{2E_{\varphi_a}}{\frac{4\pi^2 n^2}{\beta^2} + E_{\varphi_a}^2} = \beta \left(2 \sum_{n=1}^{\infty} \frac{\left(\frac{\beta E_{\varphi_a}}{2}\right)}{\pi^2 n^2 + \left(\frac{\beta E_{\varphi_a}}{2}\right)^2} + \frac{1}{\left(\frac{\beta E_{\varphi_a}}{2}\right)} \right) \\ &= \beta \coth \left(\frac{\beta E_{\varphi_a}}{2} \right) = 2\beta \left(\frac{1}{2} + \frac{1}{e^{\beta E_{\varphi_a}} - 1} \right) \\ &\Rightarrow f(E_{\varphi_a}) = 2\beta \left(\frac{E_{\varphi_a}}{2} + \frac{1}{\beta} \ln [1 - e^{-\beta E_{\varphi_a}}] \right) + \text{const.} \end{aligned} \quad (\text{B.2})$$

Neglecting energy independent terms results for Eq. (B.1) in:

$$\frac{i}{2} \text{Tr} \ln [G_{\varphi_a \varphi_a}^{-1}] = \frac{i}{2} \beta V \int \frac{d^3 \vec{k}}{(2\pi)^3} E_{\varphi_a} + iV \int \frac{d^3 \vec{k}}{(2\pi)^3} \ln [1 - e^{-\beta E_{\varphi_a}}], \quad (\text{B.3})$$

where the first term requires a proper renormalization.

Within the Hartree approximation and imaginary time formalism, the simple loop integral becomes:

$$\begin{aligned} G_{\varphi_a \varphi_a} &= \int_k G_{\varphi_a \varphi_a}(k) = \frac{1}{-i\beta} \sum_n \int \frac{d^3 \vec{k}}{(2\pi)^3} \frac{i}{(k_n^2 - M_{\varphi_a}^2)} \\ &= \frac{1}{\beta} \sum_n \int \frac{d^3 \vec{k}}{(2\pi)^3} \frac{1}{\left(\frac{4\pi^2 n^2}{\beta^2} + E^2\right)} = \frac{\beta}{4} \sum_n \int \frac{d^3 \vec{k}}{(2\pi)^3} \frac{1}{\left(\frac{\beta E_{\varphi_a}}{2}\right)^2 + \pi^2 n^2} \\ &= \frac{\beta}{4} \int \frac{d^3 \vec{k}}{(2\pi)^3} \frac{1}{\left(\frac{\beta E_{\varphi_a}}{2}\right)} \coth \left(\frac{\beta E_{\varphi_a}}{2} \right) \\ &= \frac{1}{2} \int \frac{d^3 \vec{k}}{(2\pi)^3} \frac{1}{E_{\varphi_a}} + \int \frac{d^3 \vec{k}}{(2\pi)^3} \frac{1}{E_{\varphi_a}} \frac{1}{e^{\beta E_{\varphi_a}} - 1}, \end{aligned} \quad (\text{B.4})$$

leading obviously to the same result as already known from Eq. (110), when the one-particle distribution function is replaced by the Bose distribution.

Appendix B.2. Fermionic loop integrals

The logarithmic term for fermionic propagators has the following form:

$$\begin{aligned}
i \text{Tr} \ln [D_{\psi_i \psi_i}^{-1}] &= i \int_x \int_k \ln \left[-i \det_{Dirac} (\mathbf{k} - M_{\psi_i}) \right] \\
&= i d_{\psi_i} V \sum_n \int \frac{d^3 \vec{k}}{(2\pi)^3} \ln \left[i (-k_n^2 + M_{\psi_i}^2) \right] \\
&= i d_{\psi_i} V \sum_n \int \frac{d^3 \vec{k}}{(2\pi)^3} \ln \left[i \left(\frac{(2n+1)^2 \pi^2}{\beta^2} + E_{\psi_i}^2 \right) \right], \\
&= \frac{i}{2} V \sum_n \int \frac{d^3 \vec{p}}{(2\pi)^3} \ln (k_n^2 - M_{\varphi_a}^2)
\end{aligned} \tag{B.5}$$

where $d_{\psi_i} = N_c N_s = 6$ denotes the degeneracy factor of a fermionic flavor ψ_i with $N_c = 3$ colors and $N_s = 2$ spin states.

In analogy to (B.2) the sum over fermionic Matsubara frequencies can be evaluated by applying following steps (see also Ref. [50]):

$$\begin{aligned}
f(E_{\psi_i}) &:= \sum_n \ln \left[i \left(\frac{(2n+1)^2 \pi^2}{\beta^2} + E_{\psi_i}^2 \right) \right], \\
\frac{\partial f}{\partial E_{\psi_i}} &= \sum_n \frac{2E_{\psi_i}}{\frac{(2n+1)^2 \pi^2}{\beta^2} + E_{\psi_i}^2} = 2\beta \sum_n \frac{\beta E_{\psi_i}}{(2n+1)^2 \pi^2 + (\beta E_{\psi_i})^2} \\
&= 2\beta \left(\frac{1}{2} + \frac{1}{e^{\beta E_{\psi_i}} + 1} \right) \\
&\Rightarrow f(E_{\psi_i}) = 2\beta \left(\frac{E_{\psi_i}}{2} + \frac{1}{\beta} \ln [1 + e^{-\beta E_{\psi_i}}] \right) + \text{const.}
\end{aligned} \tag{B.6}$$

By introducing energy shifts due to the quark chemical potential μ_ψ and neglecting energy independent terms, leads for Eq. (B.5) to the following result:

$$\begin{aligned}
i \text{Tr} \ln [D_{\psi_i \psi_i}^{-1}] &= i\beta d_{\psi_i} V \int \frac{d^3 \vec{k}}{(2\pi)^3} E_{\psi_i} \\
&\quad + i d_{\psi_i} V \int \frac{d^3 \vec{k}}{(2\pi)^3} \left(\ln [1 + e^{-\beta(E_{\psi_i} - \mu_{\psi_i})}] + \ln [1 + e^{-\beta(E_{\psi_i} + \mu_{\psi_i})}] \right).
\end{aligned} \tag{B.7}$$

Within the Hartree approximation and imaginary time formalism, the simple loop integral becomes

$$\begin{aligned}
D_{\psi_a \varphi_a} &= \int_k G_{\varphi_a \varphi_a}(k) = \frac{1}{-i\beta} \sum_n \int \frac{d^3 \vec{k}}{(2\pi)^3} \frac{i}{(k_n^2 - M_{\varphi_a}^2)} \\
&= \frac{1}{\beta} \sum_n \int \frac{d^3 \vec{k}}{(2\pi)^3} \frac{1}{\left(\frac{4\pi^2 n^2}{\beta^2} + E^2 \right)} = \frac{\beta}{4} \sum_n \int \frac{d^3 \vec{k}}{(2\pi)^3} \frac{1}{\left(\frac{\beta E_{\varphi_a}}{2} \right)^2 + \pi^2 n^2} \\
&= \frac{\beta}{4} \int \frac{d^3 \vec{k}}{(2\pi)^3} \frac{1}{\left(\frac{\beta E_{\varphi_a}}{2} \right)} \coth \left(\frac{\beta E_{\varphi_a}}{2} \right) \\
&= \frac{1}{2} \int \frac{d^3 \vec{k}}{(2\pi)^3} \frac{1}{E_{\varphi_a}} + \int \frac{d^3 \vec{k}}{(2\pi)^3} \frac{1}{E_{\varphi_a}} \frac{1}{e^{\beta E_{\varphi_a}} - 1},
\end{aligned} \tag{B.8}$$

leading obviously to the same result as already known from Eq. (111), when the one-particle distribution function is replaced by the Bose distribution.

Appendix C. Isotropic Boltzmann equations

Appendix C.1. Isotropic collisions between scalar bosons

In the case of a ϕ^4 -interaction with a constant matrix element one can integrate out the angular dependence of a general Boltzmann-Uehling-Uhlenbeck equation,

$$\begin{aligned} \partial_t f(t, \vec{p}_1) &= \frac{1}{2E_1} \int \frac{d^3 \vec{p}_2}{(2\pi)^3 2E_2} \int \frac{d^3 \vec{p}_3}{(2\pi)^3 2E_3} \int \frac{d^3 \vec{p}_4}{(2\pi)^3 2E_4} \\ &\times (2\pi)^4 \delta^{(4)}(P_1 + P_2 - P_3 - P_4) \frac{|\mathcal{M}_{12 \rightarrow 34}|^2}{v} \\ &\times [(1 + f_1)(1 + f_2) f_3 f_4 - f_1 f_2 (1 + f_3)(1 + f_4)], \end{aligned} \quad (\text{C.1})$$

by simply using the Fourier transform of the momentum conserving δ -function

$$\begin{aligned} (2\pi)^3 \delta^{(3)}(\vec{p}) &= \int_{\mathbb{R}^3} d^3 q \exp(-i \vec{p} \cdot \vec{q}) \\ &= \int_0^\infty dq q^2 \int_0^{2\pi} d\varphi \int_0^\pi d\vartheta_q \sin \vartheta_q \exp[-i pq \cos \vartheta_q] \\ &= \int_0^\infty dq q^2 \left[\frac{4\pi}{pq} \sin(pq) \right], \end{aligned} \quad (\text{C.2})$$

leading to the isotropic form

$$\begin{aligned} \partial_t f_1 \sim &\int_0^\infty dp_2 \int_0^\infty dp_3 \int_0^\infty dp_4 \int_0^\infty dq \frac{p_2 p_3 p_4}{E_1 E_2 E_3 E_4} \delta(E_1 + E_2 - E_3 - E_4) \\ &\times \frac{\sin(p_1 q) \sin(p_2 q) \sin(p_3 q) \sin(p_4 q)}{p_1 q^2} [(1 + f_1)(1 + f_2) f_3 f_4 - f_1 f_2 (1 + f_3)(1 + f_4)]. \end{aligned} \quad (\text{C.3})$$

Defining an auxiliary function which depends on the involved momenta

$$\mathcal{F}_{1,2 \leftrightarrow 3,4}^{p_1} = \int_0^\infty dq \frac{\sin(p_1 q) \sin(p_2 q) \sin(p_3 q) \sin(p_4 q)}{p_1 q^2}, \quad (\text{C.4})$$

and integrating out the q -dependence leads to

$$\begin{aligned} \mathcal{F}_{1,2 \leftrightarrow 3,4}^{p_1=0} &= \frac{\pi}{8} \left[\text{sign}(p_2 + p_3 - p_4) - \text{sign}(p_2 - p_3 - p_4) \right. \\ &\quad \left. + \text{sign}(p_2 - p_3 + p_4) - \text{sign}(p_2 + p_3 + p_4) \right], \end{aligned} \quad (\text{C.5})$$

$$\begin{aligned} \mathcal{F}_{1,2 \leftrightarrow 3,4}^{p_1>0} &= \frac{\pi}{16 p_1} \left[|p_1 - p_2 - p_3 - p_4| - |p_1 + p_2 - p_3 - p_4| \right. \\ &\quad - |p_1 - p_2 + p_3 - p_4| + |p_1 + p_2 + p_3 - p_4| \\ &\quad - |p_1 - p_2 - p_3 + p_4| + |p_1 + p_2 - p_3 + p_4| \\ &\quad \left. + |p_1 - p_2 + p_3 + p_4| - |p_1 + p_2 + p_3 + p_4| \right], \end{aligned} \quad (\text{C.6})$$

where the form of $\mathcal{F}_{1,2 \leftrightarrow 3,4}^{p_1}$ depends especially on the incoming momentum p_1 . The remaining energy conserving δ -function is used to reduce the dimension of the integral by writing

$$\delta(E_1 + E_2 - E_3 - E_4) = \frac{E_4}{p_4} \delta(p_4 - \tilde{p}_4). \quad (\text{C.7})$$

Here \tilde{p}_4 is given via energy-momentum conservation with the relativistic dispersion relation

$$\tilde{p}_4 = \sqrt{(E_1 + E_2 - E_3)^2 - m_4^2}. \quad (\text{C.8})$$

Finally, one ends up with the following expression for the isotropic Boltzmann equation

$$\begin{aligned} \partial_t f_1 \sim & \int_0^\infty dp_2 \int_0^\infty dp_3 \frac{p_2 p_3}{E_1 E_2 E_3} \theta(\tilde{p}_4^2) \mathcal{F}_{1,2 \leftrightarrow 3,4}^{p_1} \\ & \times [(1 + f_1)(1 + f_2)f_3 f_4 - f_1 f_2(1 + f_3)(1 + f_4)], \end{aligned} \quad (\text{C.9})$$

where the θ -function ensures that $\tilde{p}_4^2 \geq 0$.

In analogy to (C.4) one can define the auxiliary functions

$$\begin{aligned} \mathcal{F}_{1,2 \leftrightarrow 3,4}^{p_2=0} &= \int_0^\infty dq \frac{\sin(p_1 q) \sin(p_3 q) \sin(p_4 q)}{p_1 q}, \\ \mathcal{F}_{1,2 \leftrightarrow 3,4}^{p_3=0} &= \int_0^\infty dq \frac{\sin(p_1 q) \sin(p_2 q) \sin(p_4 q)}{p_1 q}, \\ \mathcal{F}_{1,2 \leftrightarrow 3,4}^{p_4=0} &= \int_0^\infty dq \frac{\sin(p_1 q) \sin(p_2 q) \sin(p_3 q)}{p_1 q}, \end{aligned} \quad (\text{C.10})$$

allowing for the description of condensation and mean-field dynamics in isotropic systems, when one of the internal modes has zero momentum.

Appendix C.2. Isotropic collisions between scalar bosons and fermions

Compared to relations of Sec. Appendix C.1, the isotropic integrations for fermions are carried out along similar lines. The main difference arises from the scalar product of fermionic momenta (compare with Eqs. (A.38) and (A.39)). Writing the scalar product between the fermions in spherical coordinates leads to

$$\begin{aligned} \vec{p}_2 \cdot \vec{p}_3 = & p_2 p_3 \left[\sin(\vartheta_2) \sin(\vartheta_3) \cos(\varphi_2) \cos(\varphi_3) \right. \\ & \left. + \sin(\vartheta_2) \sin(\vartheta_3) \sin(\varphi_2) \sin(\varphi_3) + \cos(\vartheta_2) \cos(\vartheta_3) \right]. \end{aligned} \quad (\text{C.11})$$

Without loss of generality, the integration over the inner momenta \vec{p}_2 and \vec{p}_3 can be performed by choosing the z -axis in direction of the auxiliary vector \vec{q} , which is used for the Fourier transform of the momentum conserving δ -function (see Eq. (C.2)). For the energy conserving δ -function it follows

$$\delta(E_1^{\varphi_a} - E_2^{\tilde{\psi}} - E_3^{\psi}) = \frac{E_2^{\tilde{\psi}}}{p_2} \delta(p_2 - \tilde{p}_2), \quad \tilde{p}_2 := \sqrt{(E_1^{\varphi_a} - E_3^{\psi})^2 - M_\psi^2}. \quad (\text{C.12})$$

In case of fermions, it is convenient to introduce some additional auxiliary functions and analytically integrate out the dependence on the vector \vec{q} :

$$\begin{aligned} \mathcal{F}_{1 \leftrightarrow 2,3}^{1,p_1} &= \int_0^\infty dq \frac{\sin(p_1 q) \sin(p_2 q) \sin(p_3 q)}{p_1 q} \\ &= \frac{\pi}{8 p_1} \left[\text{sign}(p_1 + p_2 - p_3) - \text{sign}(p_1 - p_2 - p_3) \right. \\ &\quad \left. + \text{sign}(p_1 - p_2 + p_3) - \text{sign}(p_1 + p_2 + p_3) \right], \\ \mathcal{F}_{1 \leftrightarrow 2,3}^{2,p_1} &= \int_0^\infty dq \frac{\sin(p_1 q) \sin(p_2 q) \sin(p_3 q)}{p_1 q^3} \\ &= \frac{\pi}{16 p_1} \left[(p_1 + p_2 + p_3)^2 \text{sign}(p_1 + p_2 + p_3) \right. \\ &\quad \left. + (p_2 + p_3 - p_1)^2 \text{sign}(p_1 - p_2 - p_3) \right. \\ &\quad \left. - (p_1 + p_2 - p_3)^2 \text{sign}(p_1 + p_2 - p_3) \right. \\ &\quad \left. - (p_1 - p_2 + p_3)^2 \text{sign}(p_1 - p_2 + p_3) \right], \end{aligned}$$

$$\begin{aligned}
\mathcal{F}_{1\leftrightarrow 2,3}^{3,p_1} &= \int_0^\infty dq \frac{\sin(p_1 q) \sin(p_2 q) \cos(p_3 q)}{p_1 q^2} \\
&= \frac{\pi}{8p_1} \left[p_1 + p_2 + p_3 + |p_1 + p_2 - p_3| \right. \\
&\quad \left. - |p_1 - p_2 + p_3| - |p_2 + p_3 - p_1| \right], \\
\mathcal{F}_{1\leftrightarrow 2,3}^{4,p_1} &= \int_0^\infty dq \frac{\sin(p_1 q) \cos(p_2 q) \sin(p_3 q)}{p_1 q^2} \\
&= \frac{\pi}{8p_1} \left[p_1 + p_2 + p_3 + |p_1 - p_2 + p_3| \right. \\
&\quad \left. - |p_1 + p_2 - p_3| - |p_2 + p_3 - p_1| \right], \\
\mathcal{F}_{1\leftrightarrow 2,3}^{5,p_1} &= \int_0^\infty dq \frac{\sin(p_1 q) \cos(p_2 q) \cos(p_3 q)}{p_1 q} \\
&= \frac{\pi}{8p_1} \left[\text{sign}(p_1 - p_2 - p_3) + \text{sign}(p_1 + p_2 - p_3) \right. \\
&\quad \left. + \text{sign}(p_1 - p_2 + p_3) + \text{sign}(p_1 + p_2 + p_3) \right].
\end{aligned} \tag{C.13}$$

Finally, one arrives at the following form for the collision integrals:

$$\begin{aligned}
\partial_t f_1^{\varphi_a} &\sim \int dp_3 \left[\left(\frac{p_3 E_2^{\bar{\psi}}}{E_1^{\varphi_a}} - \frac{p_3 M_\psi^2}{E_1^{\varphi_a} E_3^{\psi}} \right) \mathcal{F}_{1\leftrightarrow 2,3}^{1,p_1} + \frac{p_3}{E_1^{\varphi_a} E_3^{\psi}} \mathcal{F}_{1\leftrightarrow 2,3}^{2,p_1} \right. \\
&\quad \left. - \frac{p_3^2}{E_1^{\varphi_a} E_3^{\psi}} \mathcal{F}_{1\leftrightarrow 2,3}^{3,p_1} - \frac{p_2 p_3}{E_1^{\varphi_a} E_3^{\psi}} \mathcal{F}_{1\leftrightarrow 2,3}^{4,p_1} + \frac{p_2 p_3^2}{E_1^{\varphi_a} E_3^{\psi}} \mathcal{F}_{1\leftrightarrow 2,3}^{5,p_1} \right] \theta(\tilde{p}_2^2) \\
&\quad \times \left[(1 + f_1^{\varphi_a}) f_2^{\bar{\psi}} f_3^{\psi} - f_1^{\varphi_a} (1 - f_2^{\bar{\psi}}) (1 - f_3^{\psi}) \right],
\end{aligned} \tag{C.14}$$

$$\begin{aligned}
\partial_t f_1^{\psi} &\sim \int dp_3 \left[\left(\frac{p_3^2 E_2^{\bar{\psi}}}{p_1 E_3^{\varphi_a}} - \frac{p_3^2 M_\psi^2}{p_1 E_1^{\psi} E_3^{\varphi_a}} \right) \mathcal{F}_{1\leftrightarrow 2,3}^{1,p_3} + \frac{p_3^2}{p_1 E_1^{\psi} E_3^{\varphi_a}} \mathcal{F}_{1\leftrightarrow 2,3}^{2,p_3} \right. \\
&\quad \left. - \frac{p_3^2}{E_1^{\psi} E_3^{\varphi_a}} \mathcal{F}_{1\leftrightarrow 2,3}^{3,p_3} - \frac{p_2 p_3^2}{p_1 E_1^{\psi} E_3^{\varphi_a}} \mathcal{F}_{1\leftrightarrow 2,3}^{4,p_3} + \frac{p_2 p_3^2}{E_1^{\psi} E_3^{\varphi_a}} \mathcal{F}_{1\leftrightarrow 2,3}^{5,p_3} \right] \theta(\tilde{p}_2^2) \\
&\quad \times \left[(1 - f_2^{\psi}) (1 - f_2^{\bar{\psi}}) f_3^{\varphi_a} - f_1^{\psi} f_2^{\bar{\psi}} (1 + f_3^{\varphi_a}) \right],
\end{aligned} \tag{C.15}$$

where the auxiliary functions with the index p_3 are obtained by exchanging and renaming the momentum p_1 of the boson with p_3 of the fermion in (C.13). The expression for $\partial_t f_1^{\bar{\psi}}$ follows analogously to Eq. (C.15).

References

- [1] I. A. et al., Nuclear Physics A 757 (2005) 1 , first Three Years of Operation of RHIC, URL <https://doi.org/10.1016/j.nuclphysa.2005.02.130>.
- [2] Z. Fodor and S. Katz, Physics Letters B 534 (2002) 87 , URL [https://doi.org/10.1016/S0370-2693\(02\)01583-6](https://doi.org/10.1016/S0370-2693(02)01583-6).
- [3] Y. Aoki, G. Endrodi, Z. Fodor, S. D. Katz, and K. K. Szabo, Nature 443 (2006) 675, URL <https://dx.doi.org/10.1038/nature05120>.
- [4] H.-T. Ding, F. Karsch, and S. Mukherjee, *Thermodynamics of Strong-Interaction Matter from Lattice QCD* (World Scientific, 2016), 1–65, URL https://dx.doi.org/10.1142/9789814663717_0001.
- [5] Y. Nambu and G. Jona-Lasinio, Phys. Rev. 122 (1961) 345, URL <https://dx.doi.org/10.1103/PhysRev.122.345>.
- [6] Y. Nambu and G. Jona-Lasinio, Phys. Rev. 124 (1961) 246, URL <https://dx.doi.org/10.1103/PhysRev.124.246>.
- [7] D. U. Jungnickel and C. Wetterich, Phys. Rev. D 53 (1996) 5142.
- [8] J. Berges, D.-U. Jungnickel, and C. Wetterich, International Journal of Modern Physics A 18 (2003) 3189, URL <https://dx.doi.org/10.1142/S0217751X03014034>.
- [9] C. Ratti, M. A. Thaler, and W. Weise, Phys. Rev. D 73 (2006) 014019, URL <https://dx.doi.org/10.1103/PhysRevD.73.014019>.
- [10] S. Rößner, C. Ratti, and W. Weise, Phys. Rev. D 75 (2007) 034007, URL <https://dx.doi.org/10.1103/PhysRevD.75.034007>.
- [11] B.-J. Schaefer, J. M. Pawłowski, and J. Wambach, Phys. Rev. D 76 (2007) 074023, URL <https://dx.doi.org/10.1103/PhysRevD.76.074023>.
- [12] T. K. Herbst, J. M. Pawłowski, and B.-J. Schaefer, Physics Letters B 696 (2011) 58 , URL <https://doi.org/10.1016/j.physletb.2010.12.003>.
- [13] A. Masayuki and Y. Koichi, Nuclear Physics A 504 (1989) 668 , URL [https://doi.org/10.1016/0375-9474\(89\)90002-X](https://doi.org/10.1016/0375-9474(89)90002-X).
- [14] M. A. Halasz, A. D. Jackson, R. E. Shrock, M. A. Stephanov, and J. J. M. Verbaarschot, Phys. Rev. D 58 (1998) 096007, URL <https://dx.doi.org/10.1103/PhysRevD.58.096007>.
- [15] F. Wilczek, International Journal of Modern Physics A 07 (1992) 3911, URL <https://dx.doi.org/10.1142/S0217751X92001757>.
- [16] B.-J. Schaefer and J. Wambach, Phys. Rev. D 75 (2007) 085015, URL <https://dx.doi.org/10.1103/PhysRevD.75.085015>.
- [17] M. Asakawa, M. Kitazawa, and B. Müller, Phys. Rev. C 101 (2020) 034913, URL <https://dx.doi.org/10.1103/PhysRevC.101.034913>.
- [18] M. Stephanov, K. Rajagopal, and E. Shuryak, Phys. Rev. D 60 (1999) 114028, URL <https://dx.doi.org/10.1103/PhysRevD.60.114028>.
- [19] M. Asakawa, U. Heinz, and B. Müller, Phys. Rev. Lett. 85 (2000) 2072, URL <https://dx.doi.org/10.1103/PhysRevLett.85.2072>.
- [20] M. A. Stephanov, Phys. Rev. Lett. 102 (2009) 032301, URL <https://dx.doi.org/10.1103/PhysRevLett.102.032301>.
- [21] M. Asakawa, S. Ejiri, and M. Kitazawa, Phys. Rev. Lett. 103 (2009) 262301, URL <https://dx.doi.org/10.1103/PhysRevLett.103.262301>.
- [22] C. Athanasiou, K. Rajagopal, and M. Stephanov, Phys. Rev. D 82 (2010) 074008, URL <https://dx.doi.org/10.1103/PhysRevD.82.074008>.
- [23] C. Wetterich, Physics Letters B 301 (1993) 90 , URL [https://doi.org/10.1016/0370-2693\(93\)90726-X](https://doi.org/10.1016/0370-2693(93)90726-X).
- [24] T. R. Morris, International Journal of Modern Physics A 09 (1994) 2411, URL <https://dx.doi.org/10.1142/S0217751X94000972>.
- [25] J. Berges, N. Tetradis, and C. Wetterich, Physics Reports 363 (2002) 223 , renormalization group theory in the new millennium. IV, URL [https://doi.org/10.1016/S0370-1573\(01\)00098-9](https://doi.org/10.1016/S0370-1573(01)00098-9).
- [26] V. Skokov, B. Friman, and K. Redlich, Phys. Rev. C 83 (2011) 054904, URL <https://dx.doi.org/10.1103/PhysRevC.83.054904>.
- [27] C. R. Allton, S. Ejiri, S. J. Hands, O. Kaczmarek, F. Karsch, E. Laermann, C. Schmidt, and L. Scorzato, Phys. Rev. D 66 (2002) 074507, URL <https://dx.doi.org/10.1103/PhysRevD.66.074507>.
- [28] A. Bazavov, H.-T. Ding, P. Hegde, O. Kaczmarek, F. Karsch, E. Laermann, Y. Maezawa, S. Mukherjee, H. Ohno, P. Petreczky, H. Sandmeyer, P. Steinbrecher, C. Schmidt, S. Sharma, W. Soeldner, and M. Wagner, Phys. Rev. D 95 (2017) 054504, URL <https://dx.doi.org/10.1103/PhysRevD.95.054504>.
- [29] M. M. e. a. Aggarwal (STAR Collaboration), Phys. Rev. Lett. 105 (2010) 022302, URL <https://dx.doi.org/10.1103/PhysRevLett.105.022302>.
- [30] X. Luo, Nuclear Physics A 956 (2016) 75 , URL <https://doi.org/10.1016/j.nuclphysa.2016.03.025>.
- [31] S. He, X. Luo, Y. Nara, S. Esumi, and N. Xu, Physics Letters B 762 (2016) 296 , URL <https://doi.org/10.1016/j.physletb.2016.09.053>.
- [32] M. A. Stephanov, Phys. Rev. Lett. 107 (2011) 052301, URL <https://dx.doi.org/10.1103/PhysRevLett.107.052301>.
- [33] A. Meistrenko, C. Wesp, H. van Hees, and C. Greiner, J. Phys. Conf. Ser. 503 (2014) 012003, URL <https://dx.doi.org/10.1088/1742-6596/503/1/012003>.
- [34] C. Wesp, H. van Hees, A. Meistrenko, and C. Greiner, Eur. Phys. J. A 54 (2018) 24, URL <https://dx.doi.org/10.1140/epja/i2018-12464-y>.
- [35] L. Shen, J. Berges, J. M. Pawłowski, and A. Rothkopf, Phys. Rev. D 102 (2020) 016012, URL <https://doi.org/10.1103/PhysRevD.102.016012>.
- [36] J. F. Donoghue, E. Golowich, and B. R. Holstein, *Dynamics of the Standard Model* (Cambridge University press, 1992).
- [37] V. Koch, International Journal of Modern Physics E 06 (1997) 203, URL <https://dx.doi.org/10.1142/S0218301397000147>.
- [38] C. Patrignani et al. (Particle Data Group), Chin. Phys. C 40 (2016) 100001, URL <https://dx.doi.org/10.1088/1674-1137/40/10/100001>.
- [39] M. Gell-Mann, R. J. Oakes, and B. Renner, Phys. Rev. 175 (1968) 2195, URL <https://dx.doi.org/10.1103/PhysRev.175.2195>.
- [40] J. Goldstone, A. Salam, and S. Weinberg, Phys. Rev. 127 (1962) 965, URL <https://dx.doi.org/10.1103/PhysRev.127.965>.
- [41] O. Scavenius, A. Mócsy, I. N. Mishustin, and D. H. Rischke, Phys. Rev. C 64 (2001) 045202, URL <https://dx.doi.org/10.1103/PhysRevC.64.045202>.

- [42] H. van Hees, C. Wesp, A. Meistrenko, and C. Greiner, *Acta Phys. Polon. Supp.* 7 (2014) 59, URL <https://dx.doi.org/10.5506/APhysPolBSupp.7.59>.
- [43] C. Wesp, H. van Hees, A. Meistrenko, and C. Greiner, *Phys. Rev. E* 91 (2015) 043302, URL <https://dx.doi.org/10.1103/PhysRevE.91.043302>.
- [44] C. Greiner, C. Wesp, H. van Hees, and A. Meistrenko, *J. Phys. Conf. Ser.* 636 (2015) 012007, URL <https://dx.doi.org/10.1088/1742-6596/636/1/012007>.
- [45] C. Wesp, *Dynamical simulation of a linear sigma model near the chiral phase transition*, Ph.D. thesis, Goethe-Universität Frankfurt (2015).
- [46] J. Schwinger, *Journal of Mathematical Physics* 2 (1961) 407, URL <https://dx.doi.org/10.1063/1.1703727>.
- [47] L. V. Keldysh, *Zh. Eksp. Teor. Fiz.* 47 (1964) 1515, URL <http://www.jetp.ac.ru/cgi-bin/e/index/e/20/4/p1018?a=list>.
- [48] D. V. S. Michael E. Peskin, *An introduction to quantum field theory*, *Frontiers in Physics* (Addison-Wesley Pub. Co, 1995).
- [49] T. Matsubara, *Progress of Theoretical Physics* 14 (1955) 351, URL <https://dx.doi.org/10.1143/PTP.14.351>.
- [50] L. Dolan and R. Jackiw, *Phys. Rev. D* 9 (1974) 3320, URL <https://dx.doi.org/10.1103/PhysRevD.9.3320>.
- [51] J. Berges, *AIP Conference Proceedings* 739 (2004) 3, URL <https://dx.doi.org/10.1063/1.1843591>.
- [52] F. Gelis, *Z. Phys. C* 70 (1996) 321, URL <https://dx.doi.org/10.1007/s002880050109>.
- [53] F. Gelis, *Phys. Lett. B* 455 (1999) 205, hep-ph/9901263, URL [https://dx.doi.org/10.1016/S0370-2693\(99\)00460-8](https://dx.doi.org/10.1016/S0370-2693(99)00460-8).
- [54] R. Jackiw, *Phys. Rev. D* 9 (1974) 1686, URL <https://dx.doi.org/10.1103/PhysRevD.9.1686>.
- [55] H. van Hees, *Renormierung selbstkonsistenter Näherungen in der Quantenfeldtheorie bei endlichen Temperaturen*, Ph.D. thesis, Technische Universität Darmstadt (2000).
- [56] J. M. Cornwall, R. Jackiw, and E. Tomboulis, *Phys. Rev. D* 10 (1974) 2428, URL <https://dx.doi.org/10.1103/PhysRevD.10.2428>.
- [57] G. Amelino-Camelia and S.-Y. Pi, *Phys. Rev. D* 47 (1993) 2356, URL <https://dx.doi.org/10.1103/PhysRevD.47.2356>.
- [58] H. van Hees and J. Knoll, *Phys. Rev. D* 65 (2001) 025010, URL <https://dx.doi.org/10.1103/PhysRevD.65.025010>.
- [59] H. van Hees and J. Knoll, *Phys. Rev. D* 65 (2002) 105005, URL <https://dx.doi.org/10.1103/PhysRevD.65.105005>.
- [60] G. Baym, *Phys. Rev.* 127 (1962) 1391, URL <https://dx.doi.org/10.1103/PhysRev.127.1391>.
- [61] Y. Ivanov, J. Knoll, and D. Voskresensky, *Nuclear Physics A* 657 (1999) 413, URL [https://dx.doi.org/10.1016/S0375-9474\(99\)00313-9](https://dx.doi.org/10.1016/S0375-9474(99)00313-9).
- [62] Y. Ivanov, J. Knoll, and D. Voskresensky, *Nuclear Physics A* 672 (2000) 313, URL [https://dx.doi.org/10.1016/S0375-9474\(99\)00559-X](https://dx.doi.org/10.1016/S0375-9474(99)00559-X).
- [63] J. Knoll, Y. Ivanov, and D. Voskresensky, *Annals of Physics* 293 (2001) 126, URL <http://dx.doi.org/10.1006/aphy.2001.6185>.
- [64] Y. B. Ivanov, J. Knoll, and D. N. Voskresensky, *Physics of Atomic Nuclei* 66 (2003) 1902, URL <https://dx.doi.org/10.1134/1.1619502>.
- [65] G. Baym and G. Grinstein, *Phys. Rev. D* 15 (1977) 2897, URL <https://dx.doi.org/10.1103/PhysRevD.15.2897>.
- [66] H. van Hees and J. Knoll, *Phys. Rev. D* 66 (2002) 025028, URL <https://dx.doi.org/10.1103/PhysRevD.66.025028>.
- [67] A. Pilaftsis and D. Teresi, *Nuclear Physics B* 874 (2013) 594, URL <https://doi.org/10.1016/j.nuclphysb.2013.06.004>.
- [68] J. Maciejko, *An Introduction to Non-equilibrium Many-Body Theory* (Springer, Lecture Notes, 2007).
- [69] J. Rammer, *Quantum Field Theory of Non-equilibrium States* (Cambridge University Press, 2007).
- [70] S. Juchem, W. Cassing, and C. Greiner, *Nucl. Phys. A* 743 (2004) 92, URL <https://dx.doi.org/10.1016/j.nuclphysa.2004.07.010>.
- [71] S. Juchem, W. Cassing, and C. Greiner, *Phys. Rev. D* 69 (2004) 025006, URL <https://dx.doi.org/10.1103/PhysRevD.69.025006>.
- [72] D. H. Rischke, *Phys. Rev. C* 58 (1998) 2331, URL <https://dx.doi.org/10.1103/PhysRevC.58.2331>.
- [73] J. T. Lenaghan and D. H. Rischke, *J. Phys. G* 26 (2000) 431, URL <https://dx.doi.org/10.1088/0954-3899/26/4/309>.
- [74] J.-P. Blaizot, E. Iancu, and U. Reinosa, *Phys. Lett. B* 568 (2003) 160, URL <https://doi.org/10.1016/j.physletb.2003.06.008>.
- [75] B. Schenke and C. Greiner, *Phys. Rev. C* 73 (2006) 034909, URL <https://dx.doi.org/10.1103/PhysRevC.73.034909>.
- [76] C. Greiner and S. Leupold, *Ann. Phys.* 270 (1998) 328, URL <https://dx.doi.org/10.1006/aphy.1998.5849>.
- [77] C. Greiner and B. Müller, *Phys. Rev. D* 55 (1997) 1026, URL <https://dx.doi.org/10.1103/PhysRevD.55.1026>.
- [78] Z. Xu and C. Greiner, *Phys. Rev. D* 62 (2000) 036012, URL <https://dx.doi.org/10.1103/PhysRevD.62.036012>.
- [79] C. Herold, M. Nahrgang, I. Mishustin, and M. Bleicher, *Phys. Rev. C* 87 (2013) 014907, URL <https://dx.doi.org/10.1103/PhysRevC.87.014907>.
- [80] M. Nahrgang and C. Herold, *Eur. Phys. J. A* 52 (2016) 240, URL <https://dx.doi.org/10.1140/epja/i2016-16240-9>.
- [81] C. Herold, M. Nahrgang, Y. Yan, and C. Kobdaj, *Phys. Rev. C* 93 (2016) 021902, URL <https://dx.doi.org/10.1103/PhysRevC.93.021902>.
- [82] M. Nahrgang, M. Bluhm, T. Schaefer, and S. A. Bass, *Phys. Rev. D* 99 (2019) 116015, URL <https://dx.doi.org/10.1103/PhysRevD.99.116015>.
- [83] M. Kitazawa, G. Pihan, N. Touroux, M. Bluhm, and M. Nahrgang, *Nucl. Phys. A* 1005 (2021) 121797, URL <https://doi.org/10.1016/j.nuclphysa.2020.121797>.
- [84] D. Bazow, G. S. Denicol, U. Heinz, M. Martinez, and J. Noronha, *Phys. Rev. Lett.* 116 (2016) 022301, URL <https://dx.doi.org/10.1103/PhysRevLett.116.022301>.
- [85] D. Bazow, G. S. Denicol, U. Heinz, M. Martinez, and J. Noronha, *Physical Review D* 94 (2016), URL <https://dx.doi.org/10.1103/PhysRevD.94.125006>.
- [86] J. Bernstein, *Kinetic Theory in the Expanding Universe (Cambridge Monographs on Mathematical Physics)* (Cambridge University Press, 1988).
- [87] H. Goenner, *Einführung in die Kosmologie* (Spektrum Akademischer Verlag, 1994).
- [88] G. J. L. et al., *An Introduction to Computational Stochastic PDEs*, *Cambridge Texts in Applied Mathematics* (Cambridge University Press, 2014), 1 ed.
- [89] H. Kleinert, A. Pelster, B. Kastening, and M. Bachmann, *Phys. Rev. E* 62 (2000) 1537, URL <https://dx.doi.org/10.1103/PhysRevE.62.1537>.

[90] H. Kleinert, *Particles and quantum fields* (World Scientific Pub Co Inc, 2016).